

UNIVERSITY OF NAIROBI  
LIBRARY

THIS COPY MAY BE PLACED IN  
UNIVERSITY LIBRARY

//  
MULTI-ELEMENTAL ENERGY DISPERSIVE X-RAY FLUORESCENCE  
ANALYSIS OF KERIO VALLEY FLUORITE ORES AND MRIMA HILL  
SOIL SEDIMENTS //

MANGALA, MICHAEL JOSIAH  
B.Sc. (Hons)

A thesis submitted in partial fulfilment of the degree  
of Master of Science in the University of Nairobi.

1987.

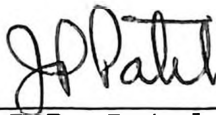
This thesis is my original work and has not been presented for a degree in any other University.

THIS THESIS IS THE PROPERTY OF THE UNIVERSITY OF..... AND A COPY MAY BE PLACED IN UNIVERSITY LIBRARY.



Mangala, Michael Josiah

This thesis has been submitted for examination with my approval as University Supervisor.



Dr. J.P. Patel  
Senior Lecturer,  
Department of Physics.

COPY HAS BEEN DEPOSITED IN  
UNIVERSITY LIBRARY,

ACKNOWLEDGEMENT

I wish to express my gratitude to Dr. J.P. Patel for supervising the research, advice, and initiatives. Special thanks to Prof. Barbra Holynska, I.A.E.A. expert, for usual discussions.

Many thanks to Prof. J. Otieno Malo, Chairman, Physics Department, and Prof. Musuva, Dean, Faculty of Engineering for making available the facilities for research at the University. I also thank the National Council for Science & Technology and the University of Nairobi for awarding me the fellowship and the necessary support towards this project study. I also wish to express my indebtedness to the Ministry of Transport and Communications, Materials Branch for releasing me from duties and providing me with the necessary support even at the time when it was not possible for me physically to undertake on this research project.

To Chief Materials Engineer, Mr. J.H.G. Wambura, your assistance will always remain memorable. Lastly, I am grateful to my wife for the patience, moral support and inspiration given during the course of the work and in which time we were blessed with Flo.

ABSTRACT

A total of fifty three radioactive fluorite samples from Kerio valley and Mrima Hill were analysed using Energy Dispersive X-ray Fluorescence (EDXRF) method. The excitation source used was Cadmium 109 and a silicon-lithium drifted (Si(Li)) detector.

A Quantitative analytical approach based on Fundamental Parameter method has been used in the analysis of these samples.

Concentrations of uranium, thorium and other elements of probable economic values are also reported.

Frequency histograms for elemental distributions in these samples are also presented. A correlation matrix of uranium and thorium with the associated elements is also established.

In order to illustrate the accuracy of EDXRF method, analysis of certified reference materials; soil (S-7), uranium ore (S-8) and thorium ore (S-14) from the International Atomic Energy Agency (IAEA) and the Canadian rock sample (SY3) has been performed and results obtained compared with the certified values. Errors of orders of 5% and 10% have been realised on major and trace elements, respectively.

The results of repeatability of the EDXRF method performed on selected samples from Kerio Valley and Mrima Hill are also reported.

List of Tables .....	(vii)
Captions of Figures.....	(viii)

CHAPTER ONE

Introduction	
1.1. Aim of the Project study .....	2
1.2. Geology of Kerio Valley and Fluorite Mineralisation .....	2
1.3. Geology of Mrima Hill .....	4

CHAPTER TWO

Theory of Energy Dispersive x-ray Fluorescence Analysis	
2.1. Interaction of x-rays with matter .....	5
2.1.1. Attenuation and scatterings of x-rays .....	5
2.1.2. Photoelectric absorption effect .....	6
2.1.3. Incoherent (Compton) scattering .....	9
2.1.4. Coherent scattering (Rayleigh) .....	11
2.2. X-ray Fluorescence Radiation .....	12
2.2.1. Auger effect and Fluorescence Yield .....	14
2.3. Quantitative Analysis in EDXRF .....	15
2.3.1. Basic x ray intensity equation .....	15

	<u>PAGE</u>
2.3.2. Matrix effects .....	20
2.3.3. Correction methods for Matrix Effects .....	21
2.3.3.1 Empirical coefficient method .....	22
2.3.3.2 Lachance Traill - claisse Quintin (LTCQ) method .....	23
2.3.3.3 Rasberry and Heinrich method .....	24
2.3.3.4 Lucas - Tooths - Price method .....	24
2.3.4 Fundamental Parameter method .....	25
2.3.4.1 Matrix correction method for transparent sample analysis .....	27
2.4. Energy Dispersive x-ray Fluorescence Spectrometer .....	31

### CHAPTER THREE

#### Experimental Procedure

3.1. Kerio Valley Samples .....	34
3.2. Mrima Hill samples .....	37
3.3 Sample Preparations .....	39
3.4 Apparatus and Measurements .....	41
3.5 Calculation of Elemental concentrations ...	46
3.6 Accuracy of EDXRF by Fundamental Parameter method .....	49
3.7 Lower limits of Detections (LLD) .....	50
3.8 Repeatability of measurements .....	51

### CHAPTER FOUR

#### Results and Discussions

4.1. Accuracy of the method .....	52
-----------------------------------	----

	<u>PAGE</u>
4.1.1	Lower Limits of Detection ..... 52
4.1.2	Repeatability of Measurements ..... 53
4.1.3	Sources of Errors ..... 53
4.2.	Results of Kerio Valley samples ..... 54
4.3.	Results of Mrima Hill samples ..... 62

CHAPTER FIVE

Conclusions

5.1.	Results of Kerio Valley samples ..... 105
5.2.	Results of Mrima Hill samples ..... 108
	References ..... 110



LIST OF TABLES

		<u>PAGE</u>
Table 1.	Results of EDXRF Analysis of Certified Reference Materials (SY-3) .....	71
Table 2.	Results of EDXRF Analysis of certified Reference Materials Soil (S-7) .....	73
Table 3.	Results of EDXRF Analysis of Certified Reference Material - Uranium Ore (S-8)/IAEA .....	75
Table 4.	Results of EDXRF Analysis of Certified Reference Material - Thorium Ore (S-14) .....	76
Table 5.	Lower Limits of Detections for the elements analysed .....	77
Table 6.	Repeatability of measurements for Mrima Hill soil samples .....	78
Table 7.	Repeatability of measurements for Kerio Valley samples .....	79
Table 8.	Correlations of Uranium and fluorite ore constituents from Kerio Valley .....	80
Table 9.	Correlation of Thorium and some of soil constituents from Mrima Hills .....	81
Table 10.	Results of Elemental concentrations in soil samples from Mrima Hills .....	82
Table 11.	Results of Elemental concentrations in soil samples from Mrima Hills .....	87

CAPTIONS OF FIGURES

	<u>PAGE</u>
Fig. 2.1. Mass attenuation coefficients as function of the incident photo energy .....	8
Fig. 2.2. Incoherent (Compton) scattering .....	9
Fig. 2.3. Electron energy levels and characteristic x-ray emission lines in an atom .....	13
Fig. 2.4. Fluorescence Yields as a function of the atomic number Z .....	15
Fig. 2.5. Geometry of source, sample and the detector used in the derivation of the fluorescence intensity equation in EDXRF .....	16
Fig. 2.6. Presentation of experimental procedure for matrix absorption correction by measurements of transmitted x-ray intensities .....	28
Fig. 2.7. Functional block diagram of EDXRF system .....	31
Fig. 3.1. General locations of sampling sites from Kerio Valley .....	35
Fig. 3.2. General locations of sampling sites from Mrima Hill .....	38
Fig. 3.3. Direct sample excitation with annular cadmium 109 source .....	43

Fig. 3.4.	Typical spectrum of uranium bearing fluorite ore sample from Kerio Valley ..	44
Fig. 3.5.	Typical Spectrum of Mrima Hill soil sample .....	45
Fig. 3.6.	Typical matrix absorption correction curve for Kerio Valley fluorite samples .....	47
Fig. 3.7.	Typical matrix absorption correction curve for Mrima Hill soil samples .....	48
Fig. 4.1	Frequency Histogram distribution of potassium in fluorite samples .....	95
Fig. 4.2.	Frequency Histogram distribution of calcium in fluorite samples .....	95
Fig. 4.3.	Frequency Histogram distribution of titanium in fluorite samples .....	95
Fig. 4.4.	Frequency Histogram distribution of vanadium in fluorite samples .....	95
Fig. 4.5.	Frequency Histogram distribution of chromium in fluorite samples .....	96
Fig. 4.6.	Frequency Histogram distribution of manganese in fluorite samples .....	96
Fig. 4.7.	Frequency Histogram distribution of iron in fluorite samples .....	96
Fig. 4.8.	Frequency Histogram distribution of nickel in fluorite samples .....	96

Fig. 4.9.	Frequency Histogram distribution of Copper in fluorite samples .....	97
Fig. 4.10.	Frequency Histogram distribution of Zinc in fluorite samples .....	97
Fig. 4.11.	Frequency Histogram distribution of Rubidium in fluorite samples .....	97
Fig. 4.12.	Frequency Histogram distribution of Strontium in fluorite samples .....	97
Fig. 4.13.	Frequency Histogram distribution of Yttrium in fluorite samples .....	98
Fig. 4.14.	Frequency Histogram distribution of Zirconium in fluorite samples .....	98
Fig. 4.15.	Frequency Histogram distribution of Niobium in fluorite samples .....	98
Fig. 4.16.	Frequency Histogram distribution of Lead in fluorite samples .....	98
Fig. 4.17.	Frequency Histogram distribution of Thorium in fluorite samples .....	98
Fig. 4.18.	Frequency Histogram distribution of Uranium in fluorite samples .....	99
Fig. 4.19.	Frequency Histogram distribution of Calcium in Mrima Hill soil samples .....	99
Fig. 4.20.	Frequency Histogram distribution of Titanium in Mrima Hill soil samples .....	99
Fig. 4.21.	Frequency Histogram distribution of Vanadium in Mrima Hill soil samples .....	100
Fig. 4.22.	Frequency Histogram distribution of Manganese in Mrima Hill soil samples .....	100

Fig. 4.23.	Frequency Histogram distribution of Iron in Mrima Hill soil samples .....	100
Fig. 4.24.	Frequency Histogram distribution of Nickel in Mrima Hill soil samples .....	100
Fig. 4.25.	Frequency Histogram distribution of Copper in Mrima Hill soil samples .....	101
Fig. 4.26.	Frequency Histogram distribution of Zinc in Mrima Hill soil samples .....	101
Fig. 4.27.	Frequency Histogram distribution of Gallium in Mrima Hill soil samples .....	101
Fig. 4.28.	Frequency Histogram distribution of Selenium in Mrima Hill soil samples ....	101
Fig. 4.29.	Frequency Histogram distribution of Strontium in Mrima Hill soil samples ...	102
Fig. 4.30.	Frequency Histogram distribution of Yttrium in Mrima Hill soil samples .....	102
Fig. 4.31.	Frequency Histogram distribution of Zirconium in Mrima Hill soil samples ..	102
Fig. 4.32.	Frequency Histogram distribution of Niobium in Mrima Hill soil samples .....	102
Fig. 4.33.	Frequency Histogram distribution of Molybdenum in Mrima Hill soil samples ..	103
Fig. 4.34.	Frequency Histogram distribution of Barium in Mrima Hill soil samples .....	103
Fig. 4.35.	Frequency Histogram distribution of Cerium in Mrima Hill soil samples .....	103
Fig. 4.36.	Frequency Histogram distribution of Lead in Mrima Hill soil samples .....	103

Fig. 4.37.	Frequency Histogram distribution of Actinium in Mrima Hill soil samples ...	104
Fig. 4.38.	Frequency-Histogram distribution of Thorium in Mrima Hill soil samples ....	104

CHAPTER ONE

1.0. INTRODUCTION

The use of x-ray emission for elemental analysis became widely applicable in the 1950's and early 1960's [1]. Until late 1960's, most of the spectrometers used, were of wavelength dispersive type. More recently, energy dispersive spectrometers have become available in which Lithium drifted Silicon or pure Germanium detectors are used instead of Bragg crystal for x-ray energy selection. Radioisotope gamma or x-ray sources may be used as exciting radiation.

The energy dispersive x-ray fluorescence (.EDXRF) method exhibits the following exemplary features over other known analytical techniques as discussed in [2]:

- (i) Elemental analysis by use of characteristic x-ray method is relatively easy due to simplicity of the x-ray spectra.
- (ii) X-ray analysis is non-destructive.
- (iii) The analyte may be in various forms e.g. solids, liquids, powder, slurry etc.
- (iv) The requirements for sample preparations are frequently minimal.
- (v) Intrinsic capability of energy dispersive x-ray fluorescence method to analyse for a wide range of elements simultaneously.
- (vi) A wide range in concentrations of the analyte from several % down to less than 1ppm can be determined.

- (vii) Dependence on the use of prepared standards in evaluation of elemental concentrations is minimal.

#### 1.1. AIM OF THE PROJECT STUDY

The primary objective in this work is the application of energy dispersive x-ray fluorescence (EDXRF) method for multi-elemental analysis of geological samples from Kerio Valley and Mrima Hills. Emphasis is hereby made on the natural occurring radioactive elements in these samples. Concentrations of uranium and thorium are evaluated to ascertain any possibilities of their economic values.

#### 1.2. GEOLOGY OF KERIO VALLEY AND FLUORITE MINERALISATION

The Kenya Fluorspar Company mines from where some of the samples analysed were obtained, is situated at the head of Kerio Valley in the Elgeyo Marakwet district of the Rift Valley province.

The Kimwarer river, a tributary of the Kerio Valley river originates in the Escarpment headland to the south and flows past the mine site.

The following four main geological formations are observed in this area [3, 4]:

- (i) The Precambrian Basement system of rocks.
- (ii) Lower Miocene sediments.
- (iii) Upper Miocene volcanic rocks.
- (iv) The Quaternary and recent deposits.



The Precambrian rocks constitute mainly paragneisses varying in composition from hornblende gneisses through biotite gneisses to quartzofeldspathic gneisses. Quartzites, breccia, crystalline limestones (marble) are also present while biotite schists and amphibolites form the rest of the Precambrian rocks. The quartzofeldspathic gneisses, biotite schists and hornblende gneisses contain specks of galena (lead V). These rocks are exposed at the base of the Elgeyo escarpment.

The Lower Miocene sedimentary deposits unconformably overlay the Precambrian basement rocks in places separating the latter from the overlying Upper Miocene volcanics. The Lower Miocene sedimentary deposits consists of laminated red sandstones and grey to yellowish green shalley limestones. The Uasin Gishu phonolites and the Elgeyo basalts are the oldest volcanic rocks of the Upper Miocene age.

Quarternary and Recent deposits constitute the soils derived from the preceeding geological formations. They are mainly sandy to clay-loamy soils, highly eroded in places.

The fluorite mineralisation in this area is formed as an alteration of metamorphosed crystalline limestone [3]. In other places, it is found as a later stage in filling fissure deposits in some alkaline and acidic aqueous rocks [5].

The fluorite mineralisation in paragneisses has been ascribed to hydrothermal emanations consisting of fluorine which replaces the carbonate ( $\text{CO}_3^{2-}$ ) cation in the crystalline limestone (calcium carbonate) normally at low temperatures.

### 1.3 GEOLOGY OF MRIMA HILL

The Mrima Hill is situated approximately 80km south west of the main port of Mombasa in the Coast province of Kenya.

The Mrima Hill is composed of deeply weathered carbonatite rocks which form part of the alkaline igneous complex. The main intrusion is at Jombo Hill, 8km NW of Mrima where nepheline syenites, foyaites and melanocratic rocks of the ijolites series comprise the plutonic core of the complex. There are two hills at Kiruku and Nguluku formed by agglomeratic dykes and the area is crossed by a number of lamprophyre dykes according to Binge and Joubert [6] and Caswell [7].

The Mrima carbonatite is intruded into arenaceous Karoo sediments of the Duruma sandstone series which dip gently eastwards. On the eastern and southern margins of the intrusion, dips are occasionally reversed, this is indicated in the quarry on the south-west side where partially fenitized sediments dip into the hill. However, the geological structure of Mrima is masked by a deep soil and weathered rock cover, that can be up to several hundreds of meters thick in some places [6].

CHAPTER TWO

2.0. THEORY OF ENERGY DISPERSIVE X-RAY FLUORESCENCE ANALYSIS

In order to lay a foundation for energy dispersive x-ray fluorescence (EDXRF) method as a means of elemental analysis and to provide a background to some of the considerations in practical quantitative x-ray fluorescence analysis, a brief summary of the fundamentals involved are presented in this section. For a more comprehensive discussion on this section, reference is made to [1, 8, 9].

2.1. Interaction of X-rays with Matter

2.1.1 Attenuation and Scattering of X-rays

On passing through matter, x-ray photons interact with the atoms of the material through the processes of photoelectric absorption effect, incoherent and coherent scattering effects. The probabilities for these interactions are called cross sections.

The fraction of the photons that pass through the material after interaction is given by the exponential attenuation formula:

$$I = I_0 e^{-\mu\rho d} \text{-----} (2.1)$$

where

I is the intensity of the photon beam after transversing an absorbing material with density  $\rho$  expressed

in g/cm<sup>3</sup> and of thickness d.

$I_0$  is the initial intensity of the photon beam and  $\mu$  is the total mass attenuation coefficient, which is the sum of the scattering coefficients and the photoelectric absorption coefficient expressed in cm<sup>2</sup>/g. The product,  $\mu\rho$ , is the linear attenuation coefficient. For a composite material, the total attenuation coefficient  $\mu$  is replaced by the mean attenuation coefficient  $\bar{\mu}$ , calculated from the relationship:

$$\bar{\mu} = \sum_{i=1}^n W_i \mu_i \text{ ----- (2.2)}$$

where  $\mu_i$  and  $W_i$  are the individual mass attenuation coefficients and weight fractions, respectively.  $n$  is the number of components constituting the composite material.

### 2.1.2. Photoelectric absorption effect

In this process of interaction, the incident photon energy is completely absorbed by the electron. This results into ejection of electron from the atomic orbitals. For an electron to be ejected from the atom, the incident photon energy  $h\nu$  must be able to overcome its binding energy in a given shell.

The cross section for photoelectric absorption effect,  $\sigma^{ph}$  in an atom is given by the following expression:

$$\sigma^{\text{ph}} = \frac{aZ^5}{(h\nu)^3} \quad \text{-----} \quad (2.3)$$

where  $a$  is the proportionality constant.  $Z$  the atomic number of the atom.  $h\nu$  is the energy of the incident radiation. For practical purposes, a more convenient quantity is the mass photoelectric coefficient,  $\mu_{\text{ph}}$ . This gives the probability for photoelectric absorption per unit mass, usually per one gram of the absorbent. The mass absorption coefficient,  $\mu$  is obtained as the product of  $\sigma^{\text{ph}}$  value and the number of atoms per gram of the given element. Thus

$$\mu_{\text{ph}} = \frac{aZ^5 N}{(h\nu)^3 A} \quad \text{-----} \quad (2.4)$$

Where  $N$  and  $A$  are the Avogadro number and the atomic weight of the element, respectively.

As shown in the figure 2.1 (curve 1), the probability for this process exhibits characteristic discontinuities. At these discontinuities the radiation is strongly absorbed. The discontinuities are called the absorption edges and occur at the binding energies for the electron shells in consideration. In Iron for example, K absorption edge occurs at 7.1 KeV.

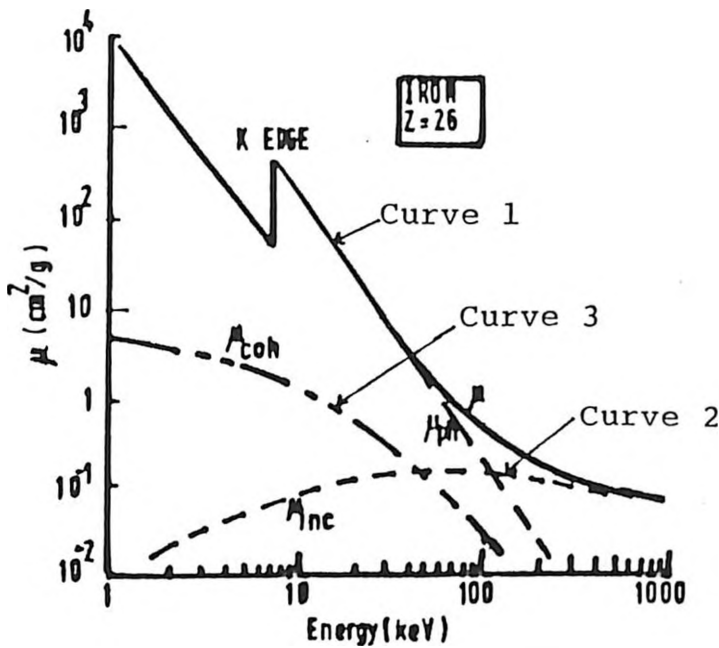


Fig.2.1. Mass attenuation coefficients as a function of the incident photon energy [1].

The maximum probability for the photoelectric effect occurs when the energy is just above the electron binding energy. The magnitude of a discontinuity is the absorption jump denoted by  $j_i$ , where  $i = K, L, M$ , depending on the electron shell in consideration. The absorption jump,  $j_K$  of element  $i$  for the K shell can be approximated by;

$$j_{ik} \approx \frac{\sigma_{\max}^{\text{ph}}}{\sigma_{\min}^{\text{ph}}} \text{-----} (2.5)$$

Photoelectric cross sections per one gram per atom for various elements of interest at various energies are available from tables [10].

### 2.1.3. Incoherent (Compton) Scattering

Besides the photoelectric absorption effect, the other mode of x-ray photons interaction with matter is through the process of incoherent or Compton scattering. The effect is best illustrated with the Fig. 2.2.

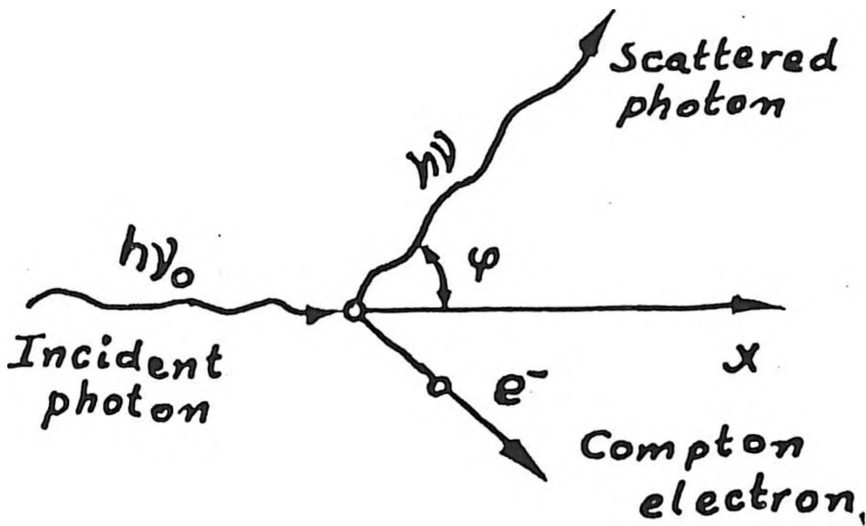


Fig.2.2. Incoherent (Compton) scattering [8].

From Fig. 2.2., it is observed that a photon of primary energy  $h\nu$  collides with a weakly bound electron assumed to be at rest. The interaction that results, is based on the principles of energy and momentum conservations, that is, part of the incident photon energy is converted into the kinetic energy of the struck electron with the original direction of the photon changing. The probability for compton scattering reaches its minimum value when the scattering angle,  $\psi = 90$ .

The energy  $h\nu$  of a Compton scattered photon depends both on the primary energy of the photon  $h\nu_0$  and the scattering angle  $\psi$ . The dependence is shown to be of the form:

$$h\nu = \frac{h\nu_0}{1 + h\nu_0 \left( \frac{1 - \cos\psi}{0.511} \right)} \quad \text{-----} \quad (2.6)$$

where  $h\nu$  and  $h\nu_0$  are energies given in MeV. 0.511 MeV is the electron rest mass.

The cross section for Compton scattering by an atom is given by

$$\sigma_a = \sigma_e Z \quad \text{-----} \quad (2.7)$$

where  $\sigma_e$  is the cross section due to Compton scattering by a single electron.  $Z$  the atomic number of the scatter. The mass absorption coefficient per one gram of element of atomic number  $Z$  due to Compton scattering would be:

$$\mu_{\text{incoh}} = \frac{\sigma_e Z N}{A} \quad \text{-----} \quad (2.8)$$

$A$  and  $N$  are the atomic weight and the Avogadro constant, respectively.

Incoherent (Compton) scattering is predominant in light elements and for photon energies markedly higher than the binding energies of all the electrons belonging to the atoms of the samples as indicated in Fig. 2:1 (curve 2).



2.1.4. Coherent Scattering (Rayleigh)

When the low energy photons are scattered by elements with higher atomic number, the probability for coherent scattering increases as more tightly bound atomic electrons are involved. Coherently scattered photons suffer no change in energy due to the fact that the mass of the atomic nucleus is much higher than that of the incident photon, the recoil of the nucleus is practically negligible.

The differential cross section for coherently scattered photons by a single atom, a, is of the form:

$$\left(\frac{d\xi}{d\Omega}\right)_a = k' \frac{(Z)^3}{h\nu_0} f(\psi) \text{ ----- (2.9)}$$

where k' is a constant.

f(ψ) is a function of the scattering angle. From the equation 2.9, the probability of coherent scattering increases rapidly as the atomic number of the scatter increases, Fig. 2.1 (curve 3). Similarly the concept of mass attenuation coefficient per one gram introduced earlier, now due to coherent scattering for a composite material is of the form;

$$\mu_{\text{coh}} = k'' \sum_{i=1}^n W_i \frac{Z_i^3}{A_i} \text{ ----- (2.10)}$$

where k'' is the constant depending on the geometry of measurement and energy of primary and secondary radiation.

$w_i$  is the weight fraction of element  $i$ ,  $Z_i$  and  $A_i$  are its atomic number and atomic weight, respectively.

## 2.2. X-ray Fluorescence Radiation

X-ray fluorescence radiation is a result of photoelectric effect after the atom has been excited with photons of sufficiently high energy. In the energy level from which the electron has been ejected, there is an empty place, "a hole". This process of ionisation, constitutes unstable system whose stability can however, be regained by transition of electrons from a higher level to the "hole". Each time an electron is transferred from a higher level to a lower energy level, the atom loses a certain amount of energy. This energy is emitted from the atom in the form of electromagnetic radiation called x-ray characteristic radiation.

From the principle of energy conservation, it follows that emission of characteristic x-rays phenomenon satisfies the condition:

$$(h\nu)_{j,i} = E_j - E_i \quad \text{-----} \quad (2.11)$$

where  $(h\nu)_{j,i}$  is the energy of the photon of characteristic radiation for the electron transition from level  $j$  to level  $i$ .  $E_j$  and  $E_i$  are electron binding energies in these levels.

All the lines that correspond to transitions that finalise at the K shell for example, constitute the K

spectrum or K series. In a similar way, one defines the L, M series as illustrated in the Fig. 2.3.

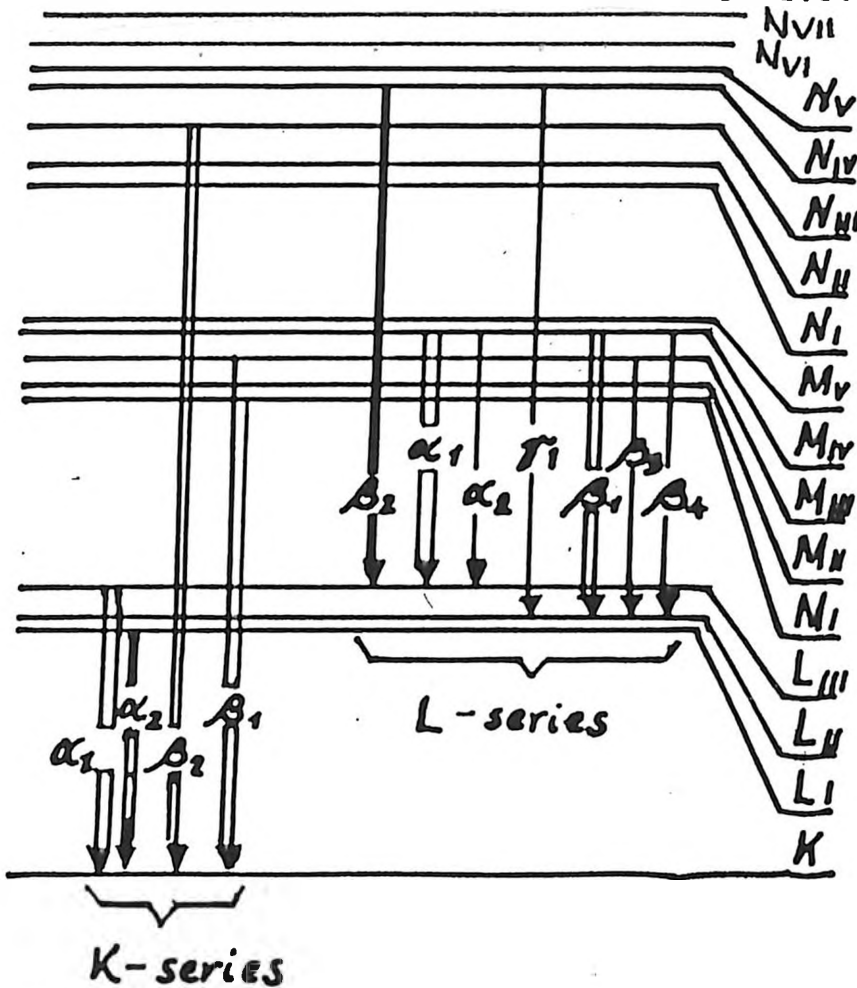


Fig.2.3. Electron Energy levels and characteristics X-ray emission lines in an atom [8]

The energy of x-ray characteristic radiation is a function of the atomic number  $Z$  according to Moseley law [11].

$$(\nu)_{j,i}^{1/2} = a(Z-\sigma) \quad \text{-----} \quad (2.12)$$

where  $\nu_{j,i}$  is the frequency of the characteristic x-rays.  $a$  is constant coefficient depending on the values of quantum numbers of energy levels involved.  $\sigma$  is the

screening constant. Moseley law is the basis for qualitative analysis.

### 2.2.1. Auger Effect and Fluorescence Yield

An excited atom when returning to its normal state does not always emit characteristic x-rays radiation. It may, instead emit an "Auger" electron. This only occurs if the liberated energy is higher than the binding energy of the electron in a given shell.

The probability of ejection of an Auger electron from, say level  $j$  depends on the energy difference;

$$(\Delta E)_{j,i} = (E_i - E_j) - E_j \quad \text{-----} \quad (2.13)$$

$E_i > E_j$

As the energy difference  $(\Delta E)_{j,i}$  increases, the probability of Auger effect decreases. It therefore follows that the effect increases with decreasing  $Z$  and is predominant in lighter elements, for  $Z$  smaller than 30. This effect is a competing process with respect to emission of characteristic x-rays radiation. It results in a decrease of the number of fluorescence photons emitted in a given time interval by the excited atoms.

The ratio of the number of fluorescent photons belonging to a given series to the number of all the atoms excited (vacancies) in this level within the same time interval is called the fluorescence yield  $\omega$ . The value of the fluorescence yield is always less than unity and increases with the atomic number  $Z$  (Fig. 2.4).

The fluorescence yield  $\omega$  is defined for each of the series ( $\omega_K, \omega_L, \omega_M$ ). The intensity of x-rays characteristic radiation arising in de-excited atoms of a given element is dependent of the excitation yield and the fluorescence yield  $\omega$ .

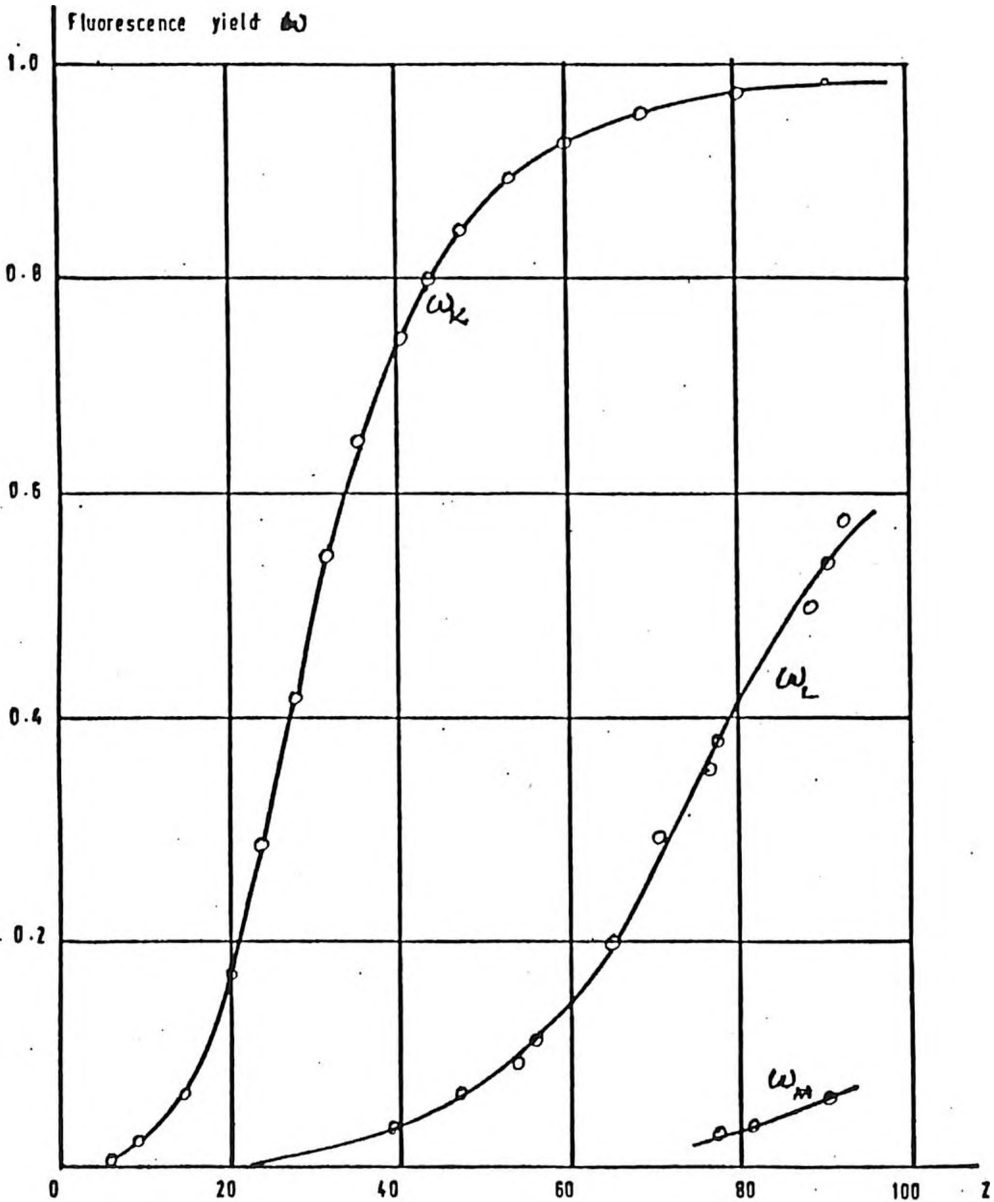


Fig.2.4. Fluorescence yields as a function of atomic number  $Z$ .

### 2.3 Quantitative Analysis in EDXRF

#### 2.3.1 Basic X-ray Intensity Equation

In x-ray fluorescence analysis, it is the intensities of the characteristic radiation from a sample

which is the basis of elemental quantitative analysis.

The energy spectrum consists of the characteristic x-rays lines and background contributions due to coherent and incoherent scatterings, the latter tend to interfere with quantitative analysis. The geometry of the excitation source in relation to the sample and the detector is shown in figure 2.5.

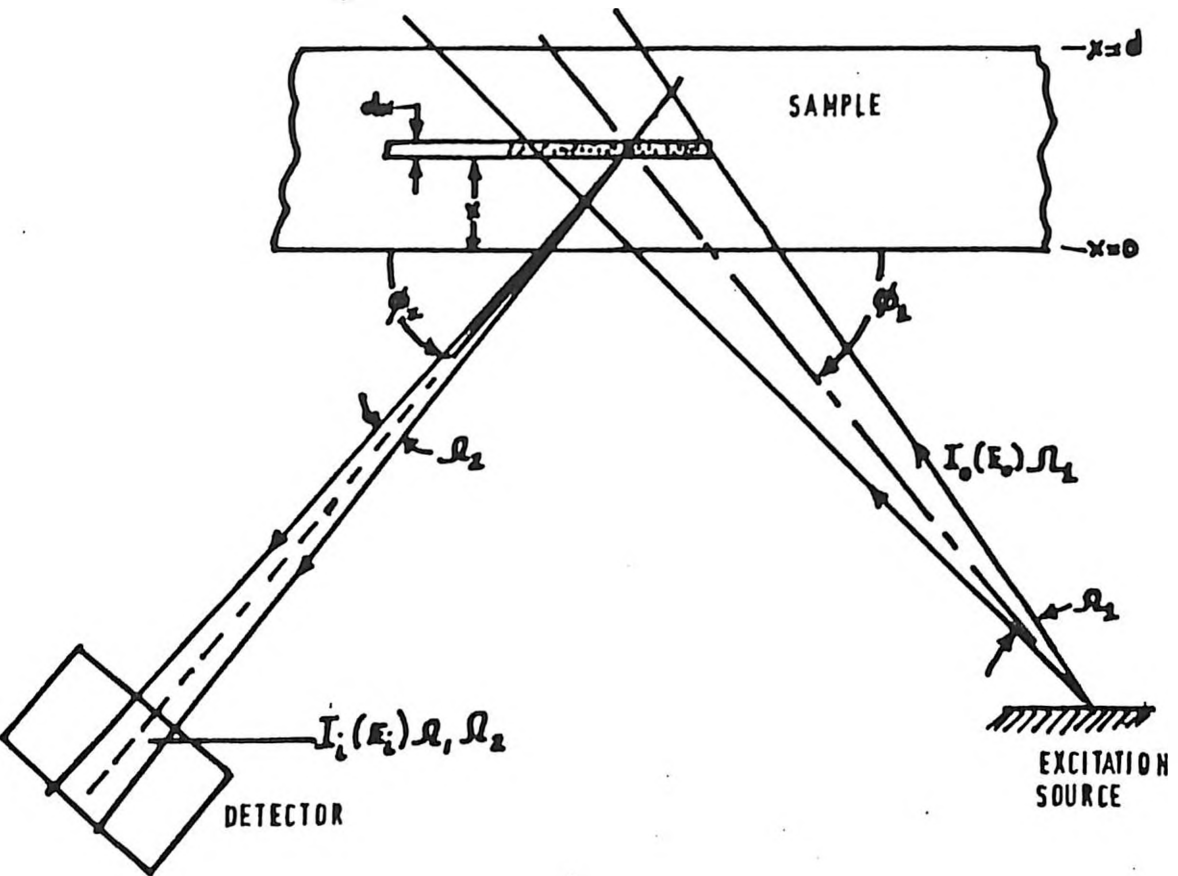


Fig.2.5. Geometry of source, sample and the detector used in the derivation of the fluorescence intensity equation in EDXRF [1].

The dependence of the intensity of fluorescence radiation of element  $i$  and its mass per unit area is according

to [12], given by;

$$I_i(E_i) = G_o \cdot K_i \cdot \epsilon(E_i) \cdot \rho_i d_i \cdot \frac{(1 - \exp(-a \rho d))}{a \rho d} \quad \text{---- (2.14a)}$$

where

$I_i(E_i)$  is the measured fluorescent intensity of element  $i$ .

$I_o(E_o)$  is the intensity of primary exciting radiation.

$G_o$  is the geometry constant which is also dependant on the source activity as is the case with radioisotope sources.

$$G_o = \frac{I_o(E_o) \Omega_1 \Omega_2}{\text{Sin } \phi_1} \quad \text{in which}$$

$\Omega_1$  is the solid angle of the incident primary radiation as seen by the sample.

$\Omega_2$  is the solid angle of the emergent secondary radiation as seen by the detector.

$K_i$  is the relative excitation efficiency given by;

$$K_i = \sigma_i^{\text{ph}}(E_o) \cdot (1 - 1/j_{is}) \cdot \omega_{is} \cdot f_s^i \quad \text{in which}$$

$\sigma_i^{\text{ph}}(E_o)$  is the photoelectric mass absorption coefficient of element  $i$  at energy  $E_o$ .

$\omega_{is}$  is the fluorescence yield for element  $i$  in shell "s".

$(1-f_{is})$  is the relative probability for photoelectric effect in shell "s".

$f_s^i$  is the ratio of the intensity of a given K or L line to the intensity of the whole series.

$\rho_i d_i$  is the mass per unit area of element  $i$  in the sample.

$d$  is the thickness of the sample and  $\rho$  its density.

$\epsilon(E_i)$  is the relative efficiency of the detector for photons of energy  $E$ .

$a = \mu(E_0) \csc\phi_1 + \mu(E_i) \csc\phi_2$ , in which  $\mu(E_0)$  and  $\mu(E_i)$  are the total mass absorption coefficients in the sample at primary and secondary energies.

$\phi_1$  is the incident angle of primary radiation with the sample.

$\phi_2$  is the emergent angle of secondary radiation with the sample.

In the derivation of equation 2.14a, the following assumptions were considered;

- (i) The excitation source is considered to be a point source.



- (ii) The sample is homogeneous.
- (iii) The primary radiation is monochromatic.
- (iv) The density of element  $i$ ,  $\rho_i$  in the sample is constant over the whole sample volume.
- (v) A fixed geometry is maintained during the intensity measurements of element  $i$  in the sample, thus  $\phi_1$  and  $\phi_2$  are constant and the detector is far from the sample.

The expression  $\frac{(1-\exp(-a\rho d))}{a\rho d}$  in equation 2.14a, is

called the absorption correction factor and accounts for the attenuation of the primary and secondary radiation in the sample.

Equation 2.14a can be simplified for use with thin and thick samples according to the following expressions;

- (i) Thin samples (from hundreds  $\mu\text{g}/\text{cm}^2$  to few  $\text{mg}/\text{cm}^2$ , depending on the element) such as film deposited (Mylar) samples, approximation on the exponential term,  $\exp(-a\rho d) \cong 1-a\rho d$ , with a relative error of 1% for  $a\rho d \ll 0.1$ , is assumed. Equation 2.14a then reduces to the form:

$$I_i(E_i) = G_o \cdot K_i \cdot \epsilon(E_i) \cdot \rho_i d_i \text{ ----- (2.14b)}$$

in which  $\rho_i d_i \leq \frac{0.134}{a\rho d}$

Thus for thin samples, the concentration in terms of the mass per unit area of element  $i$  is linearly dependent on the fluorescence radiation intensity.

(ii) A specimen is considered infinitely thick when increasing its thickness does not result in increase of intensity of fluorescence radiation. In such a case, approximation to  $\exp(-\rho d)$  in the equation 2.14a, asymptotically approaches zero, for  $\rho d \gg 1$ . Thus equation 2.14a then reduces to the form;

$$I_i(E_i) = \frac{G_o \cdot K_i \cdot \epsilon(E_i) \cdot \rho_i d_i}{\rho d} \text{ ----- (2.14c)}$$

in which  $\exp(-\rho d) < 0.01$ .

where  $\rho_i d_i \geq \frac{0.461}{\rho d}$  with relative error of 1%.

### 2.3.2. Matrix Effects.

Matrix effects in EDXRF method consist of the influence of variations of chemical composition of the sample on the fluorescence radiation intensity of the wanted element. They constitute the major sources of errors in EDXRF [8].

Two types of matrix effects in EDXRF are distinguished as absorption and enhancement,

(a) Absorption effect occurs when the variations in the matrix chemical composition result in changes of the mean absorption of the sample coefficients for both primary radiation and the fluoresced radiation of the wanted element. Influence of these variations on  $\mu_i(E_o)$  and  $\mu_i(E_i)$

are evident from the intensity equation, 2.14a, in which for fixed measurement conditions, the fluoresced radiation is a function of three variables;

$$I_i(E_i) = f(\rho_i d_i, \mu_i(E_0), \mu_i(E_i)) \text{ ----- (2.15)}$$

- (b) Enhancement effects consist of additional excitation of the atoms of the wanted element by the fluorescence radiation of some of the interelements. These effects constitute an ensemble of cascade processes, in which each one of them consists in excitation of the lighter atoms by the fluorescence radiation of the heavier atoms. The intensity of the wanted element will depend on the atomic numbers and the concentrations of the heavier elements in the sample.

Most matrix correction methods have been developed for absorption effects, since they are severe. Enhancement effects are regarded as minor, when analysing thin and diluted transparent samples, of the order or a few hundreds mg/cm<sup>2</sup> for most elements.

### 2.3.3. Correction Methods for Matrix Effects

Numerous approaches of eliminating, by correction for matrix effects in quantitative EDXRF are discussed in [13]. These approaches include:

- (i) Special sample preparation for addition or dilution method, thin-film methods and internal standard method.

- (ii) Standardisation to the scattered x-rays intensities and
- (iii) Mathematical correction methods.

For thick samples the following, mathematical correction methods are most often used ;

### 2.3.3.1 Empirical Coefficient Method.

The intensity  $I_i$  of the fluorescence radiation of element  $i$  excited in a complex material depends not only upon concentration  $w_i$  of this element but also upon  $w_j$  of other components of the sample material according to [8].

$$I_i = f(w_1, w_2, \dots, w_n) \text{ ----- (2.16)}$$

where  $n$  is the number of sample components.

For thick samples, therefore, the general expression for the concentration correction equation with empirical coefficients is given by;

$$w_i = R_i (w_i + \sum_{j \neq i}^n a_{ij} w_j) \text{ ----- (2.17)}$$

where

$$R_i = I_i / I_i^S$$

$w_i$  is the weight fraction of the  $i$ th element, fulfilling the condition;

$$w_i + \sum_{j \neq i}^n w_j = 1; I_i^S \text{ is the intensity of element}$$

$i$  in pure sample.

$a_{ij} = \bar{\mu}_j / \bar{\mu}_i$  is the factor responsible for absorption and enhancement effects of element  $j$  on element  $i$ , in which  $\bar{\mu}_j$  and  $\bar{\mu}_i$  are the mean mass absorption coefficients of element  $j$  and  $i$  for primary and secondary radiations in the sample. The influence coefficient factors  $a_{ij}$  corrects for both absorption and enhancement because the latter may be regarded as negative absorption.  $a_{ij}$  coefficients are obtained experimentally with data from a set of standard samples with known concentrations of elements of interest.

The principal weakness of the method, is its validity for application on limited elemental composition range in the sample matrix. This is difficult to predict before hand.

2.3.3.2 Lachance-Traill-Claisse-Quintin (LTCQ)  
Method [8, 9]

The principal problems encountered by equation 2.17, is the solution of sets of linear equations generated. An approach by Lachance and Traill considered the relationship between concentration  $w_i$  of the wanted element and those of the remaining elements concentrations  $w_j$ , such that;

$$w_i = 1 - \sum_{j \neq i}^n w_j \quad \text{and}$$

$$\beta_{ij} = a_{ij} - 1. \quad \text{Further modification by claisse}$$

and Quintin, introduced additional terms which contained

binary products of different interelement interactions with each other. These modifications transformed equation 2.17 to the general expression of the form:

$$w_i = R_i \left( 1 + \sum_{j \neq i}^n \beta_{ij} w_j + \sum_{j \neq i}^n \sum_{k \neq i}^n \beta_{ijk} w_j w_k \right) \text{----- (2.18)}$$

where  $\beta_{ij}$  and  $\beta_{ijk}$  are determined by means of binary standard samples containing different concentration ratios of the wanted elements.  $n$  is the number of the elements present in the sample.

### 2.3.3.3 Raspberry and Heinrich Method

This method for matrix correction, accounts for both absorption and enhancement effects. The basic equation according to [14] is given by;

$$w_i = R_i \left( 1 + \sum_{j \neq i}^n a_{ij} w_j + \sum_{j \neq i}^n \left( \frac{\beta_{ij} w_j}{1 + w_i} \right) \right) \text{----- (2.19)}$$

where  $a_{ij} = 0$ , if the influence of interelement  $j$  on  $i$  is mainly from enhancement effects and  $\beta_{ij} = 0$ , if absorption effects are predominant.

### 2.3.3.4 Lucas-Tooths-Price Method

This method unlike the other approaches mentioned earlier, uses measured relative intensities obtained from standard samples of known concentrations of the elements of interest. for matrix effects corrections.

The basic equation for this method is of the form:

$$w_i = a_o + R_i (a_{io} + \sum_{j \neq i}^n a_{ij} R_j) \text{ ----- (2.20)}$$

where  $a_o$  is related to measured background.  $a_{io}$  and  $a_{ij}$  depend on the chemical composition of the standard samples.

The method consists in calculating the concentrations of the wanted element from a single equation. It is applicable to analysis of materials in which the variations of the interelement concentrations are low of orders less than 10%. [14].

The correction coefficients,  $a_{ij}$  s are calculated by least squares fitting methods based on measurements of standard samples with known concentrations of the elements of interest.

#### 2.3.4 Fundamental Parameter Method

In this method, concentrations of the wanted elements in the sample are calculated using theoretical relationships of the fluorescence intensity,  $I_i$  of a given element to the individual concentrations of all the components that constitute the analysed sample.

Possibilities for using theoretical relationship for matrix effects correction were proposed by Criss and Birks [15]. The general expression for monoenergetic source of excitation according to [15] is of the form;

$$I_i = G_o \cdot K_i \cdot \rho_i \cdot d_i \cdot \sum_{j \neq i}^n F_{ij}(E_j) \{1 + \phi_{ij}(E_j, w_1, w_2, \dots, w_l, w_n)\} \text{----- (2.21)}$$

where

$F_{ij}(E_j)$  is the absorption function dependent upon the chemical compositions of the sample and represents the absorption matrix effects responsible for attenuation of radiation intensity,  $I_i$ .

$\phi_{ij}(E_j, E_i)$  is the enhancement function term and represents the enhancement of intensity,  $I_i$ , due to fluorescence radiation of all the interelements.  $G_o$  and  $K_i$  have the same meaning as in equation 2.14a.

In the application of FPM for quantitative analysis, prior knowledge of primary spectral distribution (for polyenergetic sources), mass absorption coefficients of all the elements characteristic lines for primary and secondary radiations in the sample, fluorescence yields, ratios of intensities of x-rays characteristic lines to the intensities of the whole series in consideration, their jump factors at the corresponding absorption edges and most notably the detection efficiencies at their corresponding characteristic line energies is essential.

Matrix absorption effects and analyte line excitation by matrix elements enter equation 2.21 explicitly for each sample to be analysed and requires few standards samples, no empirical coefficients are required for any sample matrix. However, the calculations



involved are complex and normally need a relatively high capacity memory computers with appropriate softwares. The method avoids in principle the limited compositional range of calibration methods.

Details on methods to solutions for obtaining concentrations of elements of interest for thick samples are also discussed in [15].

#### 2.3.4.1 Matrix Correction Method for Transparent Sample Analysis

Matrix absorption effects can be experimentally determined for uniform transparent samples (of orders of a few  $\text{mg}/\text{cm}^2$ ). The matrix effects due to absorption dominate over enhancements ones. The latter effects are considered negligible.

The technique used, involves transmission measurements of x-rays intensities from a multielement target located at a position adjacent to the back of the sample, with and without the sample of known mass per unit area as shown in Fig. 2.6a-c, according to [12, 15, 16].

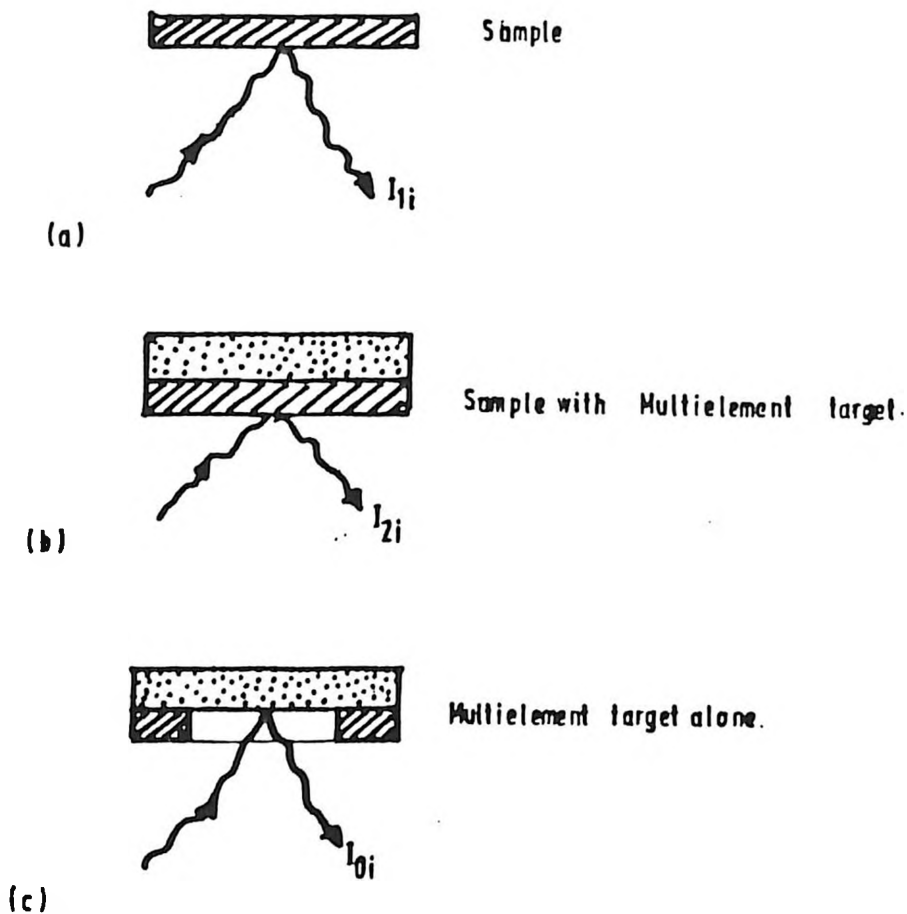


Fig.2.6a-c. Presentation of Experimental Procedure for Matrix absorption correction by Measurement of Transmitted X-ray intensities[12].

The correction factor  $(apd)_i$  for element  $i$  due to absorption of primary and fluorescence radiation transmitted through sample of thickness  $\rho d$  ( $g/cm^2$ ), according to [12], from the attenuation laws, is given by;

$$(apd)_i = \log_e \left( \frac{I_{0i}}{I_{2i} - I_{1i}} \right) \text{ ----- (2.22)}$$

Where  $I_{1i}$ ,  $I_{2i}$  and  $I_{0i}$  are net intensities of x-rays for element  $i$  in sample alone, sample with target, and target alone, respectively.  $(apd)_i$  embraces total mass absorption

coefficients of the element  $i$  for primary and fluorescence radiations, in which, (section 2.3.1),  $a$ , was given by;

$$a = \mu_i (E_0) \csc\phi_1 + \mu_i (E_i) \csc\phi_2$$

The multielement target is prepared from chemical compounds whose characteristic x-rays energies are within a range of interest. Values of  $(apd)_i$  for elements in the target, are obtained from relation 2.22 and plotted against their fluorescence x-rays energies on a log-log scale, from which  $apd$  values of elements of interest in the sample are then interpolated.

Concentrations of elements of interest in the sample are calculated by the following procedure;

- (i) The first estimate of concentration  $w_{i0}$  of the element  $i$ , in the sample is made from equation 2.14a in which the absorption correction factor,  $A_{corr} = ((1 - \exp(-apd))/apd)$  is approximated to 1. The uncorrected concentration,  $w_{i0} = \rho_i d_i / (\rho d)_s$ , is obtained, in which  $\rho_i d_i$  is the mass per unit area of element  $i$  and  $(\rho d)_s$  is the mass per unit area of the sample.
- (ii) Estimates of  $(apd)_i'$  are calculated by iteration of the approximate values obtained from log-log plot according to;

$$(apd)_i' = (apd)_i(0) \left\{ 1 - (1 - 1/j_{is}) w_i' \right\} \text{ ----- (2.23)}$$

in which  $(apd)_i(0)$  value is obtained from the presented curves on log-log scale.  $j_{is}$  is as already defined in section 2.3.1.

- (iii) (apd)  $w_i'$  from (ii) is in turn used to generate  $A'_{\text{corr}}$  factor.
- (iv) The new concentration estimates,  $w_i' = w_{i0}/A'_{\text{corr}}$  are substituted in equation 2.23. Steps (ii) and (iii) are repeated several times, until the difference of successive estimates of  $w_i'$  converges to less the required precision of iterations.

In cases of diluted transparent samples, the final corrected concentration  $w_i$  is calculated from;

$$\text{Final concentration, } w_i = w_i' \times \text{dilution factor} \dots (2.24)$$

in which,

$$\text{dilution factor} = \frac{\text{weight of sample} + \text{weight of dilutant}}{\text{Weight of sample.}}$$

## 2.4. Energy Dispersive X-ray Fluorescence Spectrometer

The energy dispersive x-ray fluorescence spectroscopy system consists of, apart from the excitation source and the sample, the x-ray detector, the pre-amplifier, the amplifier, the HV detector bias supply and the multi-channel analyser (MCA). A mini-computer and plotter are occasionally interfaced to the spectrometer to assist in acquisition and analysis of the spectra (Fig. 2.7).

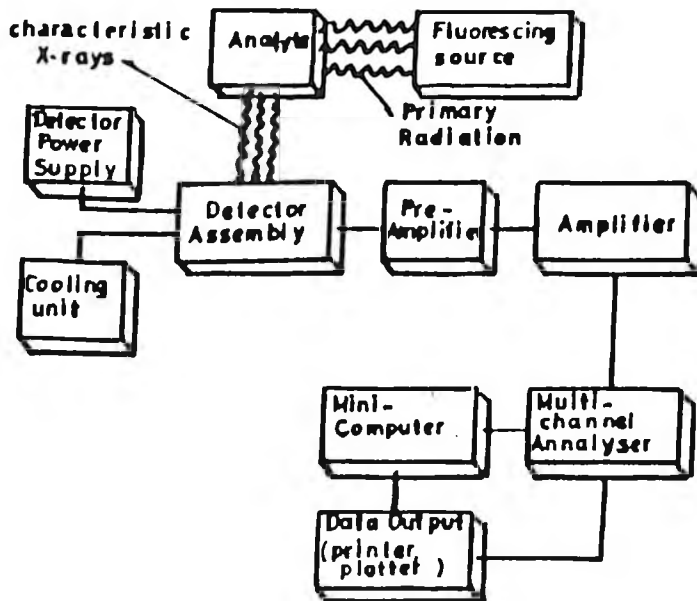


Fig. 2.7. Function block diagram of EDXRF system

Detectors used, are classified according to the nature of absorption of x-rays energy and to the secondary effects following absorption. Most often used detectors in EDXRF analysis include, solid-state detectors, proportional or scintillation detectors and operate on the principle of measuring the result of interaction of incident x-rays with the detector medium. The result produced is electron-ion pairs formations in the case of proportional counters, optical excitations in the case of scintillation counters and creation of electron-hole pairs in semiconductor detectors.

Effective operation of any detector for EDXRF applications requires high energy resolution, normally of the order of 150 - 250 eV (FWHM of Mn  $K_{\alpha}$  x-rays at 5.9 keV), to distinguish characteristic x-rays of adjacent lines.

The semi-conductor detector, such as lithium drifted silicon (Si(Li)), satisfactorily meets these criteria for practical purposes. The basic principle of operation of Si(Li) detector rests on production of a cloud of free electrons and holes as a result of x-rays photons interaction with the crystal electrons through the process of photoelectric effect. These free charges are swept away and collected on application of bias voltage. Assuming total x-rays absorption and total charge collection, the number of charges produced is proportional to the energy of the absorbed x-rays.

The energy resolution of a semi-conductor detector is determined by the electronic noises, mainly within the preamplifier and the statistical fluctuations in the number of electron-hole pairs generated by ionisation. The preamplifier and the detector assembly are mounted in the cooling system at liquid nitrogen temperature (77 K) to minimise electronic noises.

The preamplifier converts signals so produced in the detector medium into voltage pulses for convenience input to the main shaping amplifier. In addition, the preamplifier consists of cooled FET input stage to filter off extraneous noise contributions.

The shaping amplifier converts signals into 0 - 10V range, so that pulse height analysis can be performed and also filters off low and high frequencies in order to improve signal to noise ratio and energy resolution.

The signal has analog response up to the multi-channel analyser input. The multi-channel analyser measures heights of amplified output pulses and converts these amplitudes into an integer number in analog-digital converter (ADC). The number of times a pulse of same height has been detected is accumulated in the memory address to give a distribution of pulse heights. The pulse height distribution is converted to the x-ray energy spectrum by appropriate MCA calibration.

A more comprehensive discussion of EDXRF instrumentation is well documented in reference [1, 17].

## CHAPTER THREE

### 3.0 EXPERIMENTAL PROCEDURE

#### 3.1 Kerio Valley Samples

Radioactive fluorite samples were obtained from the precinct of Kenya Fluorspar Company on site basis as indicated on the map of sampling sites in Figure 3.1.

A portable Geiger Muller survey meter was used for assay of anomaly in radioactivity. The measured background radioactivity averaged 0.05mR/hr. Samples were collected from sites where radioactivity was three times the background level. Small bulk samples of approximately 500 g, considered to be representatives of radioactive fluorite ores, were obtained from these sites.

It was necessary to adopt the following precautions while sampling;

- (i) Cleanliness of the tools used was ensured against any possible contamination.
- (ii) Care was taken to obtain the hard and soft materials in proportion in which they occurred in the veins.
- (iii) Veins were sampled across the entire width and length.
- (iv) All the samples collected were labelled and stored in polythene bags that were in turn put in a shielded enclosure to minimise the radiation level.

Sample KV01 was obtained from the stream banks in Tumeiyo. The area has no fluorite mineralisation



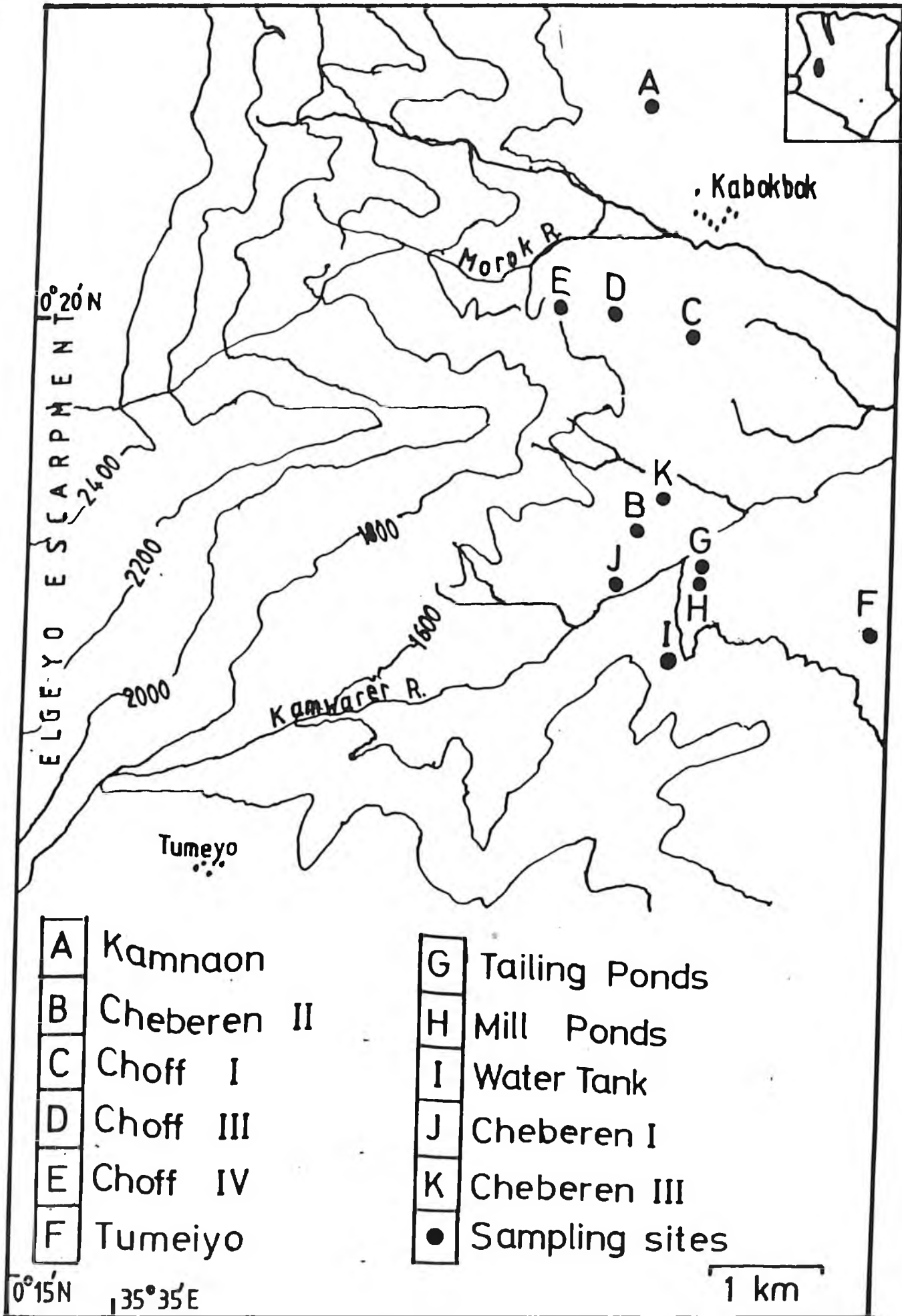


Fig.3.1. General locations of sampling sites from Kerio Valley.

but consists largely of sedimentary rocks that are partly silicified in places. Highest readings for radioactivity of the order of 0.5-0.8 mR/hr was registered from this area.

Kamnaon ore body is located in the northmost of the Fluorspar Company premises. The ore body consists of typical granular fine grained fluorite that range in colour from grey to brown or black and purple. A radioactivity of 0.4mR/hr was observed in this ore body. Eleven samples were collected from this site, within an area of four square kilometers and labelled KVO2 up to KVO12.

Sample KVO13 was obtained in the gully east of Kalwal road at a site ten meters west of sample KVO1 in the same locality.

In Cheberen ore body, the radioactivity readings on the whole was low. Samples KVO14 and KVO15 were collected from Cheberen I, while sample KVO16 was collected from Cheberen II, both from the same vein. The fluorite ores in these locations varied from purple to white with low radioactivity of order of 0.10mR/hr.

Samples KVO17 and KVO18 represent tailings and sample KVO19 is from the final mill concentrates. The radioactivity recorded, was minimal in these samples.

The Choff ore body constitutes fine grained white variety of fluorite ores in hill II and yellow-orange

variety in hill IV. Samples KVO20 and KVO21 were collected from the former hill while samples KVO22, KVO23 and KVO24 were obtained from the latter hill within an approximate area of about 2 - 3 square kilometers with radioactivity approximating 0.2mR/hr.

### 3.2 . Mrima Hill Samples

The sampling procedure described earlier was used in acquisition of bulk soil samples from this area. Thirty samples were collected from this area and labelled as MH01 to MH30. Figure 3.2 shows the general locations of sampling sites. Sampling mainly involved soil sediments from a depth of approximately 30 cm. Field sampling was started from an area formerly used as residential camp during previous excavations. Samples MH01, MH02, and MH03 were obtained from this area within an approximate area of one square kilometer. The radioactivity registered for these samples averaged 0.3mR/hr. The background activity had been estimated to be of the order of 0.1mR/hr prior to sampling. Samples MH04, MH05, and MH06 are soil samples obtained outside the pits at the old camp. Samples MH07, MH08, MH09 and MH10 constitute soils samples obtained from this site on eastern slopes of the hill. The radioactivity registered for this site, averaged 1mR/hr.

Samples MH11, MH12 and MH13 were obtained from an area south east of the old mine. The radioactivity registered for these samples approximated 1.5-2.0 mR/hr and cover an approximate area of one square kilometer.

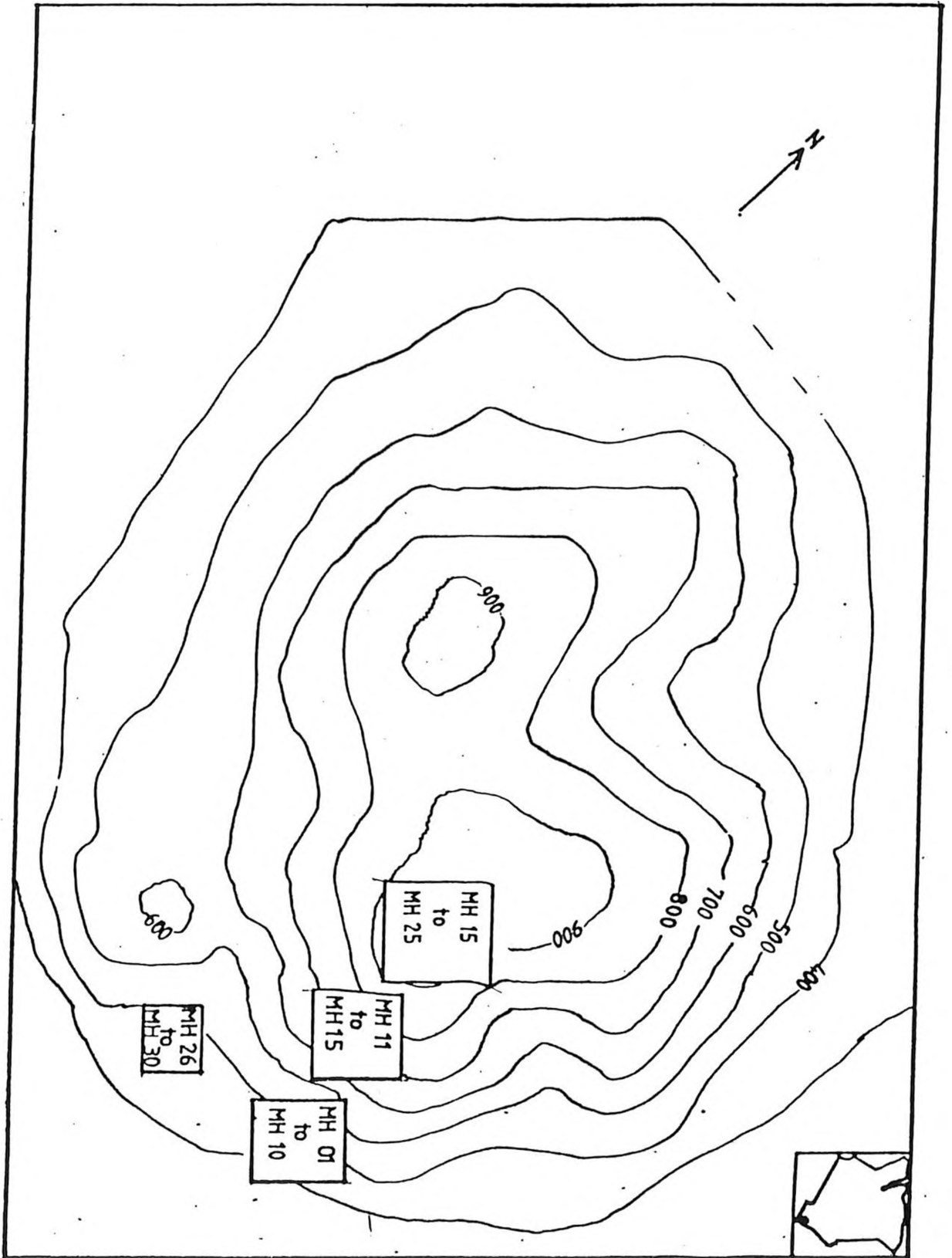


Fig.3.2. General locations of sampling sites from Mrima Hill.

Samples MH14 up to MH25 were obtained within the vicinity of the old mine located on the plateau of the hill. These samples were obtained from an area of approximately 0.5 - 1.0 square kilometers. The highest readings for radioactivity registered, was from these samples and averaged 2.5mR/hr.

Samples MH26 up to MH30 were obtained from a murram pit that had been recently excavated, situated on the eastern slope of the hill. The radioactivity was of the orders of 0.2 - 0.5mR/hr. Sample MH28 was an iron ore of relatively high grade.

### 3.3 Sample Preparations

Field samples obtained from these areas were mechanically ground in a Fritsch Pulverisette type 120 for thirty minutes to reduce particle size.

In order to obtain a representative of the pre-ground samples, a fraction was taken to facilitate further finer grinding to appropriate particle size and then homogenised for quantitative EDXRF. The criteria on which this fraction of the samples was obtained, was by coning and quartering [18] in the following way;

- (i) The ground sample was placed on a clean sheet of paper and mixed thoroughly by a plastic paddle.

- (ii) The sample was built into a cone on some vertical stick.
- (iii) The cone was then flattened radially and divided into four equal parts.
- (iv) The two opposite quarters were discarded while the other two quarters were further ground and sieved through 200 mesh (75 $\mu$ m). The fraction that remained was subject to further grinding and then sieved until none was left. The ground samples were oven dried at 100°C for 48 hours.

The procedure of coning and quartering was repeated for oven dried samples to obtain approximately 25g of the representative bulk samples. These were then stored in plastic vials and placed in dessicator for further pre-sample preparations as is required in quantitative analysis.

The powdered samples used for quantitative EDXRF, were further ground to smaller particle size in an agate mortar.

A measured amount of fine powder sample was then diluted in order to minimise the matrix effects, with cellulose in the ratio of 1:4 and homogenised. An approximate amount of orders of 500mg of diluted sample was pressed into a pellet of diameter 2.5cm with use of a hydraulic press at the pressure of 2 - 3 kilobars.

Determinations of mass per unit area ( $\rho d$ )<sub>s</sub> was obtained by weighing these pellets. For each sample five pellets were prepared and analysed.

### 3.4 Apparatus and Measurements

The energy dispersive x-ray fluorescence spectrometer used in this work consisted of:

- (i) Canberra series 40 multi-channel analyser (MCA).
- (ii) Spectroscopy amplifier Ortec type 571.
- (iii) High voltage bias supply, Ortec type 459.
- (iv) Liquid nitrogen level monitor, Ortec type 729A.
- (v) DEC Professional 350 series minicomputer with XRFA software is interfaced to the MCA for data acquisition and analysis.

The energy calibration of the MCA was performed with the use of Fe-55 and Cd-109 point sources; Fe-55 source emits Mn  $K\alpha$  lines at 5.9 keV while the latter emits Ag  $K\alpha$  characteristic x-rays at 22.1 keV enabling two point calibration of the MCA.

The Si(Li) Ortec detector used, was of the following characteristics; active diameter of 6mm, sensitive depth of 5mm and nominal beryllium window thickness of 0.025mm.

The detector was operated at a voltage of 1500V negative bias. The measured resolution prior to analysis was 210eV at full width half maximum (FWHM) at 5.9 keV of Mn  $K\alpha$  line and at pulse shaping time constant of 10 $\mu$ s as recommended by the manufacturers.

For quantitative EDXRF analysis, using FPM, accurate knowledge of the detector efficiency as a function of characteristic x-rays energies is essential. Numerous approaches for experimental determinations of

the detector efficiencies as a function of characteristic X-ray energies is well documented elsewhere [10,20].

In this work, the detector efficiency,  $\epsilon(E_i)$  values are those experimentally obtained by Murithii [12]. The source for sample excitation was annular Ammersham Cadmium 109 type C792 of activity of 0.93GBq as at 30/6/1982, with half life of 453 days.

The geometrical constant,  $G_0$  in equation 2.14a used, was  $2.07 \times 10^5$  counts per second experimentally determined on the 23/07/1983 by Lavi [21]. The geometrical constant,  $G_0$  at any one time ( $t_m$ ) in the course of the analysis was corrected for the decay of the source according to the following formula;

$$G_0(t_m) = G_0(t_0) \times 2^{-t/(T_{1/2})} \dots\dots\dots(3.1)$$

where  $G_0(t_0) = 2.07 \times 10^5$  as at 23/07/1983,  $t$  is the number of days so far elapsed from the predetermined  $G_0(t_0)$ .

Thus  $t = t_m - t_0$ .  $T_{1/2}$  is the half life of Cadmium 109 source.

The prepared transparent pellets of the samples, of orders of  $100\text{mg}/\text{cm}^2$  were irradiated with the Cadmium 109 excitation source in conformity to the geometry adopted as in Figure 3.3.



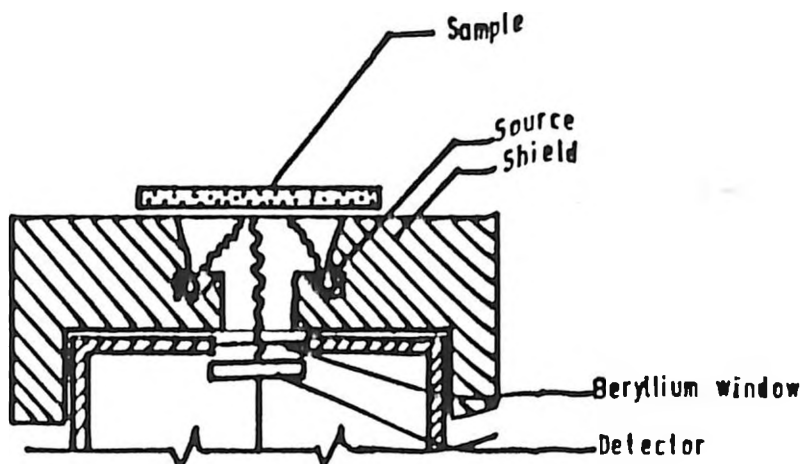


Fig.3.3. Direct samples excitation with annular Cadmium 109 sources [1]

The preset live counting time for spectra collection was 2000s for Kerio Valley samples and 1500s for the Mrima Hill samples. The resultant spectra were collected on the MCA in the pulse height analysis mode, then stored on magnetic floppy diskettes for quantitative analysis. Typical spectra for Kerio Valley fluorite ores and Mrima Hill soil samples are shown in the Figures 3.4 and 3.5, respectively.

The DEC minicomputer was used for spectra acquisition and processing. The program XRFA written for PDP11/45 systems of the type such as DEC Professional 350 series minicomputer is available at the Centre for Nuclear Sciences Techniques, University of Nairobi from the International Atomic Energy Agency. The program calculates backgrounds by fitting a polynomial function to the actual spectra. The net peak areas of the elements of interest present in the sample are calculated after spectrum deconvolution.

Fig. 3.4. Typical Spectrum of Uranium bearing fluorite ore sample from Kerio Valley

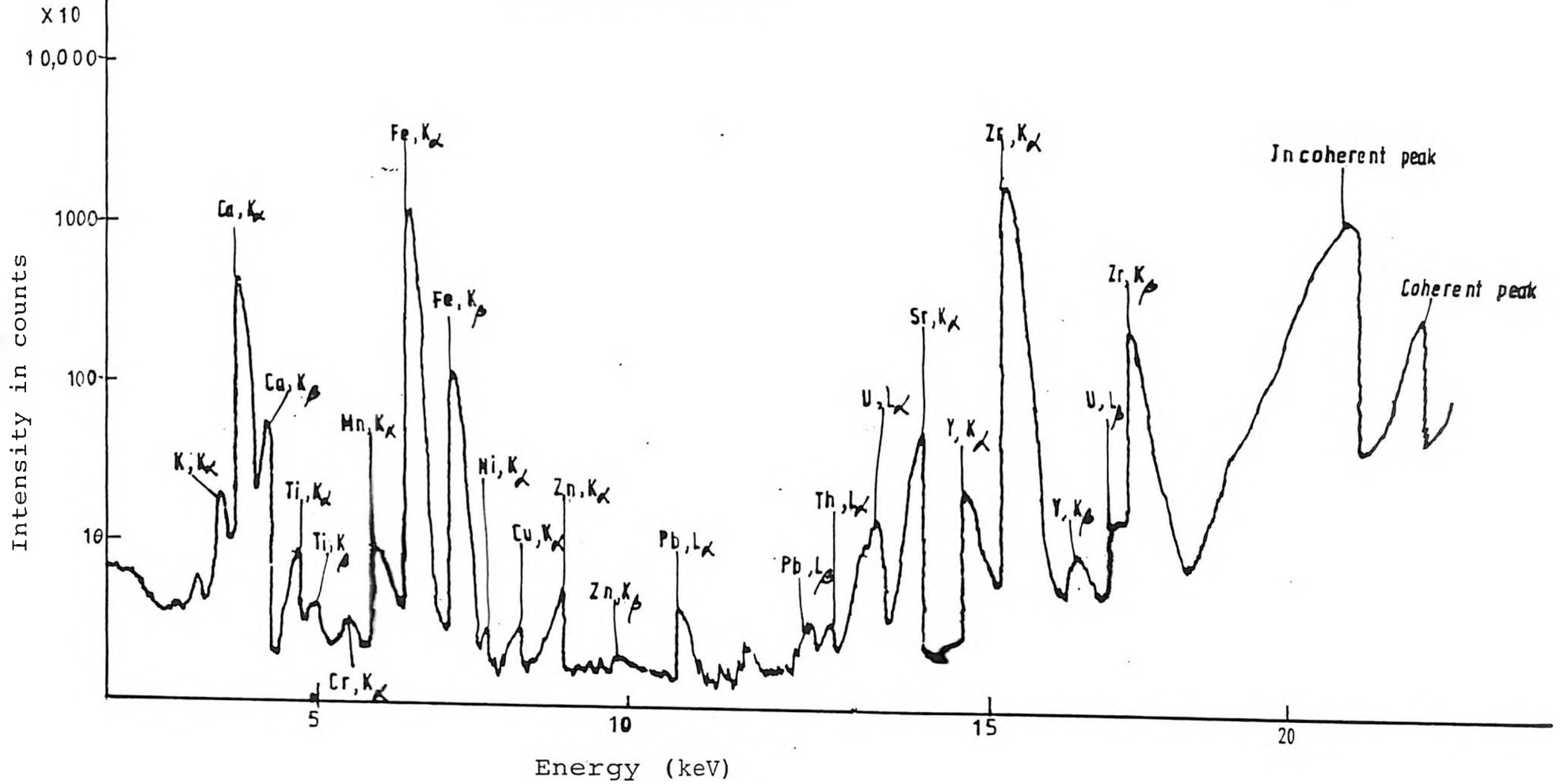
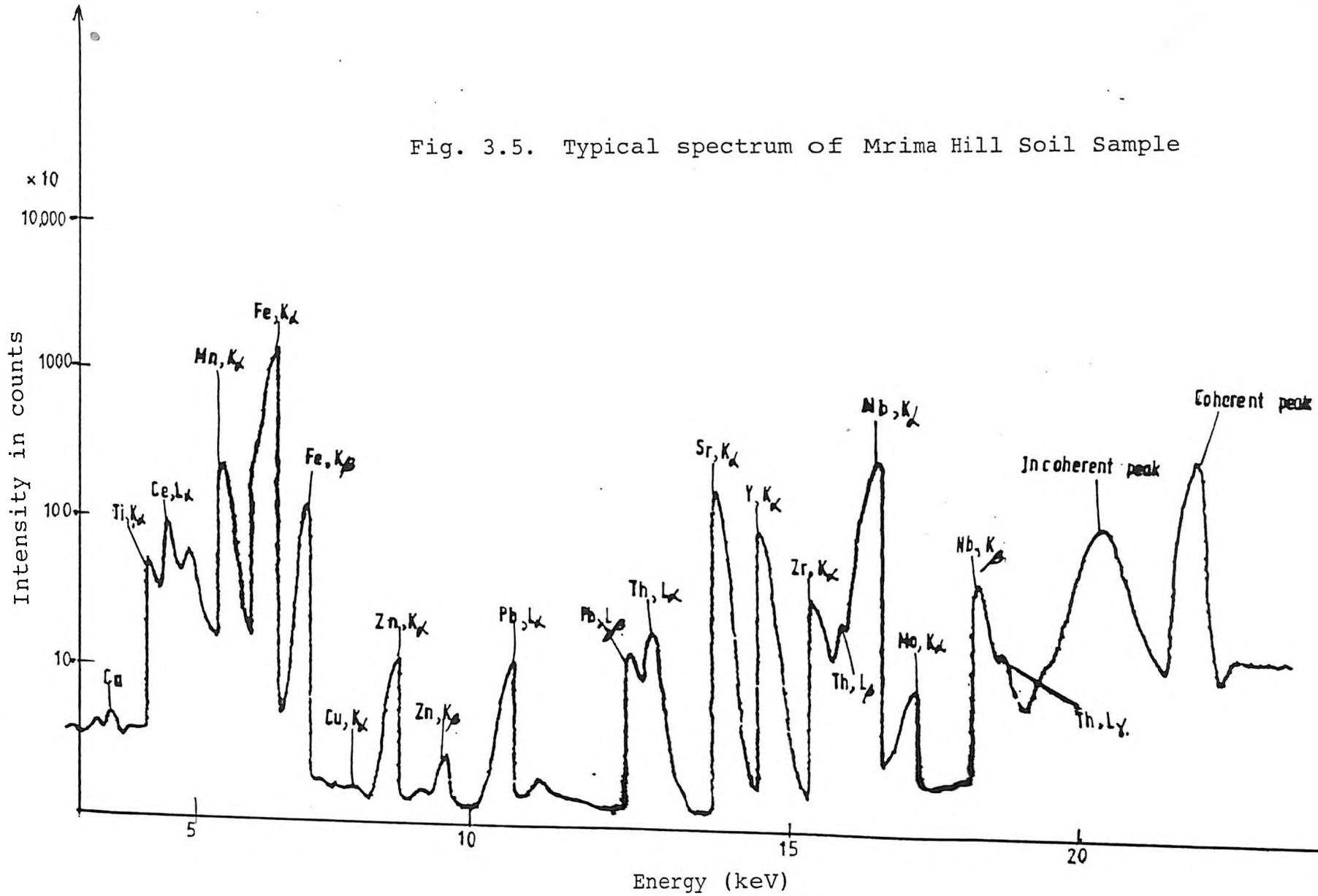


Fig. 3.5. Typical spectrum of Mrima Hill Soil Sample



For each specimen, three measurements were performed; sample alone, sample with multi-element target positioned on top of it and the target alone as described in section 2.3.4.1 .

The preset time for spectra collection for sample with multi-element target and target alone for the purposes of absorption correction measurements was 500 s.

The multi-element target used, is a thick pellet made of pure cellulose powder with admixtures of titanium, manganese, zinc, bromine and niobium compounds of high purity. The energies of characteristic x-rays of these elements covers the energy of the MCA calibration.

### 3.5 Calculations of Elemental Concentrations:

In computations of elemental concentrations values, the fundamental parameter method equation 2.14a was used. The use of this equation required measurements of intensities of the elements of interest in the sample and experimental determination of absorption correction factors.

After plotting  $apd$  values for the target elements against their characteristic energies, it was possible to approximate the absorption correction factors for the elements of interest in the sample. Typical plots of  $apd$  values versus characteristic energies for Kerio Valley fluorite and Mrima Hill soil sample are presented in Figures 3.6 and 3.7, respectively.

Fig.3.6. Typical matrix absorption correction curve for Kerio Valley fluorite ore samples.

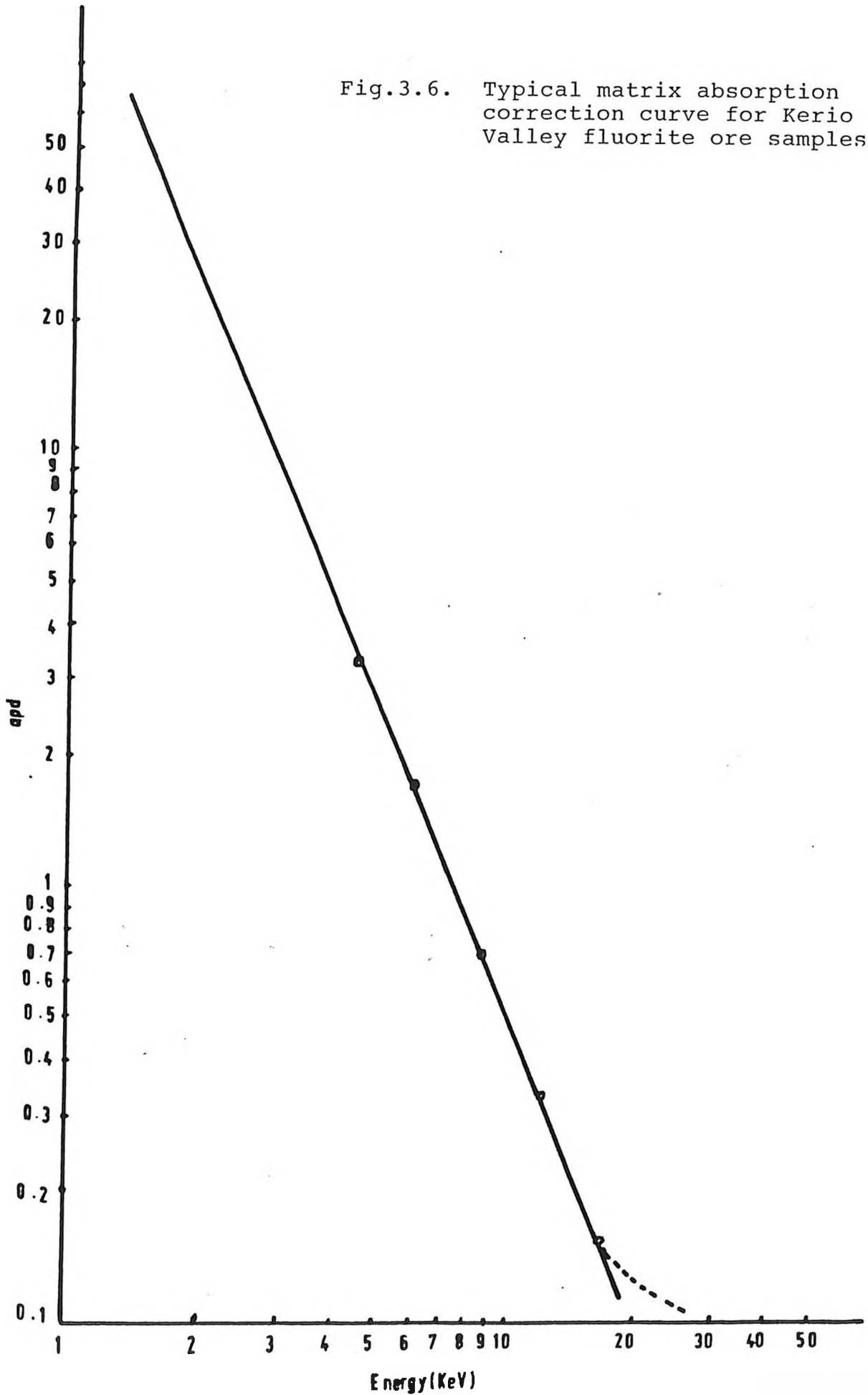
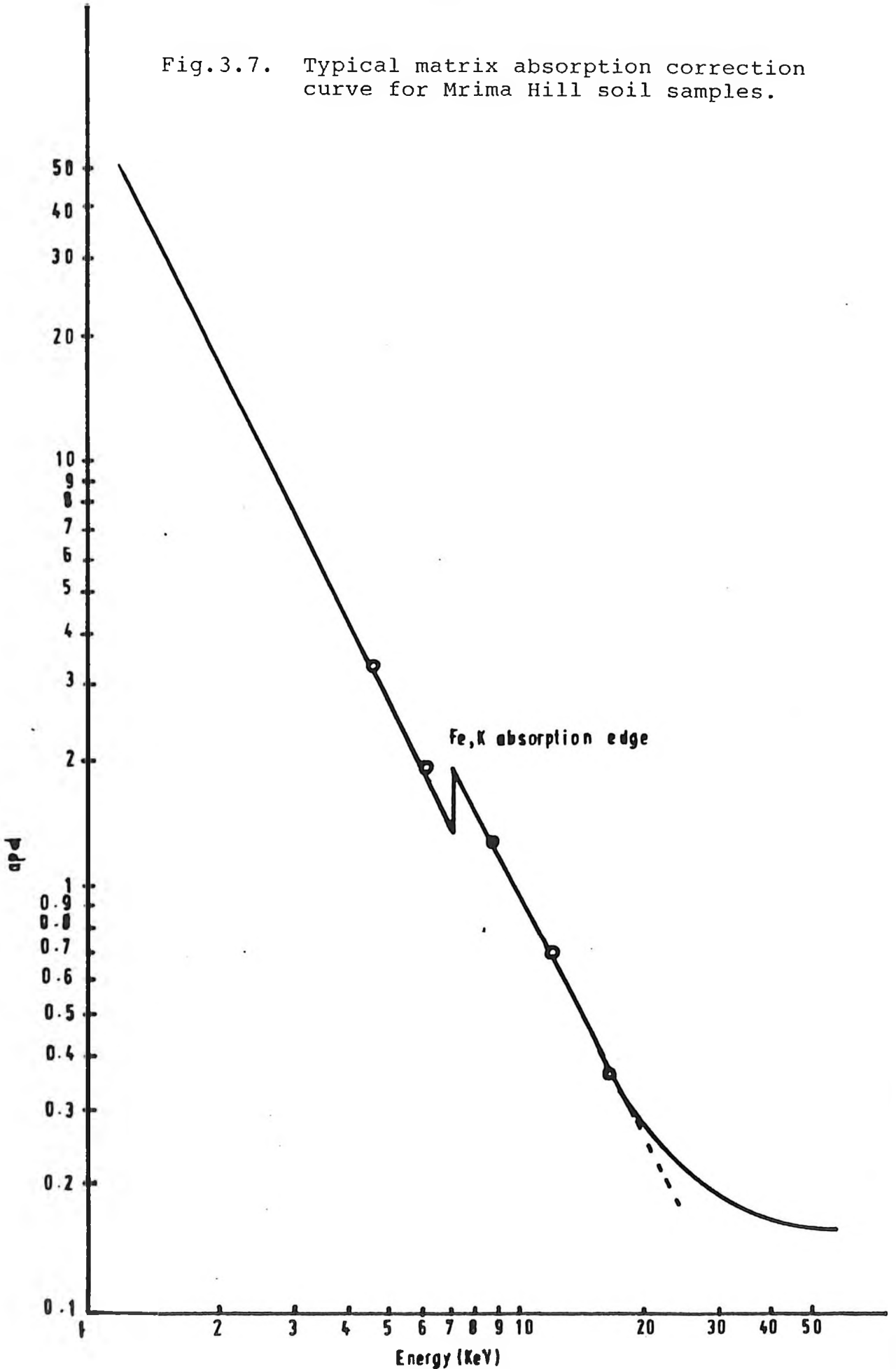


Fig.3.7. Typical matrix absorption correction curve for Mrima Hill soil samples.



### 3.6 Accuracy of EDXRF by Fundamental Parameter Method

The degree of agreement of measured concentration values obtained for a specimen being analysed, with "true" concentration values of e.g. certified reference material is accuracy of the analytical method.

For determination of accuracy for several elements by the EDXRF technique with the use of the fundamental parameter method (FPM), four certified reference materials were analysed. The reference materials used were soil (S-7) (IAEA), Uranium ore standard S-8 (IAEA), Thorium ore standard S-14 (IAEA) and the rock sample (SY-3) from Canada Centre for Mineral and Energy Technology.

Six samples were prepared from each of these certified reference materials and analysed. The mean concentrations of elements of interest were calculated. The obtained results follow the students t-distribution rather than the normal Gaussian, owing to the few number of repeated analysis. The calculated standard deviation was multiplied by the t-coefficient corresponding to 68.3% confidence limit level at five degrees of freedom [22].

The obtained concentration values of the elements of interest in these reference materials were compared with the certified values from the respective certificates. Relative errors were calculated using the following relationship [23];

$$\text{Error (\%)} = \left( \frac{\text{Mean concentration obtained from measurements} - \text{Concentration as stated in certified reference Materials certificate.}}{\text{Concentration as stated in certified reference Materials certificate.}} \right) \times 100$$

----- (3.2)

### 3.7 Lower limits of detection (LLD)

The presence of a given element in a sample was confirmed of, if the obtained concentration values was equal or higher than the experimentally determined lower limit of detection (LLD).

LLD is referred to as that minimum concentration equivalent to two standard deviations of the number of background counts. The LLD for the elements of interest, were then calculated from the following relationship derived according to [13];

$$\text{LLD} = 3/m \times \text{SQR}(I_b/T_b) \text{ ----- (3.3)}$$

where

m is the sensitivity expressed in count rate per unit concentration of element of interest.

$I_b$  is the background count rate.

$T_b$  is the background count time.

The sensitivity values are normally obtained from calibration curves of elements net peak count rates versus the corresponding concentrations. The concept of sensitivity



is most often applied to trace analysis in thin samples. However, for transparent samples used, the estimation of  $m$  was based on the concentration of elements obtained in low values of orders 100 - 1000 ppm, depending on the element [24].

### 3.8 Repeatability of measurements

The degree of mutual agreement between repeated measurements of the same sample by the same analytical method and by the same person involved in acquisition of the data, defines repeatability. In this sense, repeatability is taken to be the precision of measurements and its measure is the standard deviation obtained from repeated measurements made [8].

For determination of repeatability, two samples KV023 and MH006 were randomly chosen from the set of the samples analysed. Six pellets were prepared from each sample and analysed for the elements of interest.

## CHAPTER FOUR

### 4.0. RESULTS AND DISCUSSIONS

#### 4.1. Accuracy of the method

The accuracy of the method was carried out on sets of certified reference materials as already discussed in section 3.6. The results obtained were compared with the certified values from the respective certificates as shown in Tables 1 - 4.

Accuracies of order less than 5% or better were obtained for major constituents. For low concentrations, relative errors of the order of 2 - 10% were obtained for most of the elements. Discrepancies were noted in Soil (S-7) in the determination of Se and Br. The obtained relative errors are 50%, since the values of the concentrations obtained are on the threshold of the lower limit of detection. For other reference materials, acceptable accuracies were obtained for all the elements except for Ce and Pb in SY-3. The reported relative errors for these two elements can be attributed to interference of the  $K\alpha$  lines from elements of low Z in the sample for the former and probable error in the determination of the excitation detection efficiency ( $K_i$ ) for the latter.

##### 4.1.1 Lower Limit of Detection

For Z smaller than 26, the lower limit of detection for the elements of interest varies from

30ppm to 1000ppm as shown in Table 5. For Z greater than 26, but less than 42, the lower limit of detection values are within the range of 3ppm to 10ppm. For heavier elements like Ba, Ce and La, in which the  $L_{\alpha}$  lines were measured, the lower limit of detection values are within the range of 300ppm to 700ppm. The list of lower limit of detection values for all the elements determined are shown in Table 5.

#### 4.1.2 Repeatability of Measurements

The repeatability of measurements for the randomly chosen samples from Kerio Valley fluorite ores and Mrima Hill soils are presented in Table 6 and 7, respectively. The results are reported as the standard deviations relative to the means of the concentration and intensities values of the elements of interest. These values were calculated at 68.3% confidence limit and follow the students t-distribution with **five** degrees of freedom. The average standard deviations for most elements is of the order of 5-10%, an indication of high precision comparable to most workers [25].

#### 4.1.3 Sources of Errors

The basic equation 2.14a used, is an oversimplification of the true processes of x-rays interactions with matter that result in the characteristic x-rays intensities of the sample elements. Effects due to absorption are only considered while it is true that enhancement effects, which depend on the sample compositions, can cause additional uncertainties in determination of concentrations of the elements of interest are ignored for practical purposes.

Sources of errors in this respect were considered as from counting statistics, spectrum deconvolution for net peak area, equipment used,

sample preparation methods with possibilities of contaminations and possible inhomogeneity of analysed sample.

The application of EDXRF method with the use of Cadmium 109 source is noted to be limited to analysis of elements with Z greater than 18, but less than 42 with use of Ka lines. For heavier elements, use is made of the La lines. However, for the elements emitting La lines within the energy range up to 10 KeV, overlap of Ka lines can cause errors in determining the elements within the range of  $Z = 47$  to 74. The characteristic energies for these elements interfere with the Ka lines of low Z elements. In most cases the adjacent lines are so close that they cannot be distinguished. It is therefore difficult to get reliable analytical results for the light elements with Z smaller than 18 because fluorescence yields and the count rates are low, permitting high absorption of the fluorescence radiation of these elements within the detector window and the air path that separates it from the sample surface.

#### 4.2 Results of Kerio Valley Samples

Samples analysed from this area were predominantly fluorite ores. Fluorspar is the commercial name of the extract from the mineral fluorite ore with calcium as the major element in these samples [26].

The other minor and trace elements have been determined in the course of this work. The concentrations of all the elements are reported in Table 10 at 68.3% confidence limit level and are hereby presented in the increasing order of Z. Tables 1 to 11 herein referred to can be found on pages 77-94 while figures 4.1 to 4.38 are on pages 95-104 at the end of this section.

#### Potassium

The element occurs in all the samples collected from the area. Concentration values ranged from 1824ppm to 5.47% in samples KVO16 and KVO12, respectively. Frequency histogram distribution of this element is shown in Figure 4.1. The calculated mean of 1.60% was obtained for these samples. A correlation of 0.96 with rubidium was obtained as shown on the correlation matrix, Table 8.

#### Calcium

The element was detected in all the samples analysed. It occurs in low concentration of 3029ppm, only in sample KVO1, which was obtained from an area with no fluorite mineralisation. The highest obtained value was 39.84% in sample KVO3. The mean calcium content was 17.95%. The frequency histogram distribution of calcium is presented in Fig. 4.2. The element is weakly correlated to strontium and strongly, but negative correlation with thorium and rubidium, Table 8. Tailings from the fluorspar processing plant contain quite significant amounts of calcium of  $(5.10 \pm 0.55)\%$  and  $(10.47 \pm 0.47)\%$  in samples KVO17 and KVO18, respectively.

### Titanium

Only six samples would not yield the amount of titanium above the lower limit of detection. The reported concentrations for titanium in the fluorite ore samples varied from 443ppm to 8493ppm (Fig. 4.3), with a mean value of 2478ppm. Barium emits  $L\alpha$  characteristic X-ray lines of average energy of 4.4KeV, that partially overlap the titanium  $K\alpha$  lines. This could be the reason for relatively high errors due to counting statistics in analysis. However, high correlation coefficient values with vanadium, iron, nickel and zinc are obtained as shown in the correlation matrix, Table 8.

### Vanadium

The element could only be determined in twelve samples. Concentration values varied from 48.1ppm to 485ppm in these samples (Fig. 4.4) with a mean concentration value of 216ppm.

Correlation coefficients values of 0.74, 0.57 and 0.59 were obtained with titanium, thorium and rubidium respectively, Table 8.

### Chromium

Reported concentration range for chromium varied from 28.3ppm to 638ppm with calculated mean concentration of 186ppm. The mean value was calculated from fourteen samples which had the element in excess of the determined lower limit of detection. Figure 4.5 shows the frequency

distribution histogram for chromium in the samples. The element correlates weakly with nickel, copper and zinc, Table 8.

### Manganese

The element occurred in the eighteen samples of the twenty three analysed. The concentrations range varied from 25ppm to 984ppm, Fig. 4.6. The calculated mean concentration value in these samples is 358ppm. High correlation coefficient values were obtained with iron, nickel and zinc as reported on the correlation matrix, Table 8.

### Iron.

Concentrations of iron in the fluorite samples analysed varied from low concentration values of 1040ppm to 6.98%. The mean concentration value of the element is 1.637% as indicated on the frequency histogram distribution of this element in Fig. 4.7. The element was found to correlate with increasing order to manganese, nickel, titanium and zinc as shown on correlation matrix, Table 8.

### Nickel

The element was detected in most of the samples except KV13, KV15-16, KV20 and KV21. These samples were obtained from Tumeiyo, Cheberen Hills I and II and Choff II, respectively. The concentrations found are low in values

and varied from 10.9ppm to 163ppm. The calculated mean concentrations based on eighteen samples is 39.8ppm, Fig. 4.8.

The element is positively correlated with the following in increasing order; copper, manganese, thorium, titanium and zinc as shown in Table 8 of the correlation matrix.

#### Copper

The element was found to occur in low concentrations in all the samples analysed. The concentration values range from 30.3ppm to 97.5ppm. The calculated mean concentration for samples analysed was 59.8ppm. The element is evenly distributed in fluorite ore samples, Fig. 4.9, and correlates to the following elements in increasing order of the correlation coefficients; yttrium, lead, thorium, nickel, zinc and chromium, Table 8.

#### Zinc

Zinc occurs in all the samples with concentrations varying from 15.8ppm to 143ppm. The calculated mean concentration for the twenty three samples analysed was 58ppm. Fig. 4.10 shows the frequency distribution of this element. Zinc is shown to correlate positively with the following elements in the increasing order; lead, manganese, copper, titanium, iron and nickel as indicated on the correlation matrix, Table 8.



### Rubidium

Six samples did not show any measurable amount of the element. This was recognised in samples which had high calcium content. The measured concentrations values varied from 9.2ppm to 227ppm. The mean concentration, calculated on basis of seventeen samples is 82.7ppm.

The element correlates positively to the following in the increasing order; nickel, titanium, yttrium, vanadium, niobium, thorium and potassium, Table 8.

Fig. 4.11 shows the distribution of the element in the fluorite ore samples analysed.

### Strontium

Strontium occurs in all the samples analysed from the area. The concentrations values ranged from 41ppm to 2634ppm with a calculated mean concentration value of 855ppm. The element is evenly distributed in the concentration range of 200ppm to 1400ppm as shown in Fig. 4.12. The element correlates with zirconium, uranium and niobium but weakly with calcium as shown in Table 8.

### Yttrium

The element was found in twenty three samples in low concentration values varying from 3.5ppm to 441ppm.

The calculated mean concentration of the element was 74.7ppm. From the frequency distribution histogram in Fig. 4.13, it can be seen that concentration values for yttrium for most samples are below 120ppm. However, three samples (KVO1, KVO2, KVO8) have much higher content and also contain high concentrations of uranium, thorium, zirconium and niobium. High correlation values of yttrium with named elements is evidenced from the correlation matrix, Table 8.

#### Zirconium

The element is reported in all the samples analysed with varied concentrations from 11.5ppm to 2.37%. The calculated mean concentration of the element is 1959ppm. From the frequency distribution histogram (Fig. 4.14) of zirconium, it can be seen that most concentration values obtained are within 100ppm to 300ppm. In four samples, the concentrations ranged from 1000ppm to 5000ppm. These samples are fluorite with relatively high concentration values of uranium. Zirconium is positively correlated to the following elements in increasing order; uranium, strontium, yttrium and niobium as shown on the correlation matrix, Table 8.

#### Niobium

The element was detected in low concentrations in the thirteen samples. Concentration values varied from 10ppm to 255ppm. The calculated mean concentration of niobium in

these samples was 51.1ppm. The element is relatively evenly distributed in the concentration range of 20ppm to 300ppm as indicated on the frequency distribution in Fig. 4.15. Lower concentration values than average, correspond to samples with low calcium content. Tailing samples have the element content on the lower limit of detection threshold level. No measurable amount of niobium was reported in the milled fluospar ore samples, with high calcium content.

Niobium is positively correlated to the following elements in the increasing order; strontium, uranium, rubidium, thorium, zirconium and yttrium, as indicated on the correlation matrix, Table 8.

### Lead

Lead occurs in all the samples analysed except in sample KV13. Concentration values in these samples varies from 18.3ppm to 463ppm. The element averages 87ppm as indicated on the frequency histogram distribution in Fig. 4.16. Lead correlates with the following elements in the increasing order; copper, zinc, and thorium, Table 8.

### Thorium

Thorium occurred in seven samples in varying amounts of low concentration from 29ppm to 166ppm as shown in Fig. 4.17. The calculated mean concentration

is 81.0ppm in these samples. The element was found to correlate with the following elements in the increasing order; vanadium, copper, potassium, lead, nickel, niobium and yttrium as evidenced from the correlation matrix, Table 8.

#### Uranium

The element was detected in fourteen samples. The concentration values varied from 34ppm to 983ppm and averaged 208ppm for these samples. The distribution of the element is shown in Fig. 4.18. Samples with relatively high calcium content have extremely low concentration or none of the uranium, therefore negatively correlated to calcium. The highest amounts of the element are reported in samples KVO2 and KV12 with concentration values of 983ppm and 657ppm. These two samples have low calcium contents. Uranium is positively correlated to the following elements in the increasing order; zirconium, strontium, yttrium and niobium, Table 8.

#### 4.3. Results of Mrima Hill Samples

The samples collected from this area were soil sediments of carbonatite. The major constituent in these samples is iron despite the alkaline nature associated with their origin. Other elements, have been determined in the course of analysis. The results of their concentrations values are reported in Table 11. Following is a list of the occurrence and distributions of these elements in the soil samples analysed:-

### Calcium

The element occurs in traces in all the samples analysed with the exception of sample MH11. The element is mostly within the concentration range of 2000ppm to 8000ppm with a calculated mean value of 4497ppm (Fig. 4.19). Sample MH04 exhibits exceptional high value of the element with reported concentration value of 1.29% and the corresponding relatively high concentration value of iron. From the Table 11 of results, the trend is high values of calcium correspond to relatively high values of iron.

### Titanium

The element is one of the major constituents in Mrima Hill samples as shown in Table 11. It is unevenly distributed in the concentration range of 1.00% to 9.00% with a calculated mean concentration value of 4.69% (Fig. 4.20).

The occurrence of titanium in these samples, is positively correlated to the following elements in increasing order; barium, vanadium and cerium (Table 9).

### Vanadium

Vanadium occurs in all the samples as a major constituent. Figure 4.21 shows that the element is unevenly distributed in the concentration range of 0.5% to 4.00% with calculated mean concentration value of 1.867%. High concentration values of the element

correspond to low iron, manganese, strontium and niobium contents, therefore poor correlation values with these elements were obtained. However, the element correlates positively in increasing order, with the following elements; thorium, barium, titanium, and cerium (Table 9).

### Manganese

This element is also a major constituent in the Mrima Hill soil samples as evidenced from the Table 11 of results. The concentrations of the element varied from 3556ppm in sample MH30 to 17.05% in sample MH09, The former correspond to murram soil sample, rich in iron but difficient of manganese. The concentration distribution of the element in the samples is shown in Fig. 4.22 together with the calculated mean value of 6.32%. The element is weakly correlated to the following elements in increasing order; barium, titanium, cerium and iron, Table 9.

### Iron

The element was detected in all the samples analysed. It is a major constituent in the soils at the concentration range of 5% to 30%, Fig. 4.23. Sample MH12 has higher concentration value of 39.09%. This sample has corresponding higher than average values of copper and zinc.

The calculated mean value of iron in the soil samples was found to be 21.25%. The element correlates

weakly with manganese and thorium with correlation coefficients of 0.53 and 0.55, respectively (Table 9).

### Nickel

From the data obtained during the course of analysis of Mrima Hill samples, it is not possible, to conclude the existence of the element in the area. Of the 30 samples analysed, the presence of the element was found only in four samples (MHO2, MHO4, MH27 and MH30). The concentrations of the element varied from 13.9ppm to 28.5ppm as seen from Fig. 4.24.

### Copper

The element occurs only in low concentrations in all the samples. Reported concentrations values varied from 10.9ppm to 92.6ppm. Concentration distribution of the element is shown in Fig. 4.25, together with the calculated mean value of 33.1ppm. Sample MH30 indicates exceptionally high value of 92.6ppm. This sample has lower than average concentrations values of manganese, iron and zinc but also with the highest concentration value of niobium.

### Zinc

The concentration of this element in the samples is in traces. The values of concentrations varied from 644ppm to 371ppm, (Fig. 4.26), with calculated mean of 1815ppm.

High values of the element correspond to relatively high than average, concentration values of copper, iron and manganese.

### Gallium

The element was detected in all the samples except sample MH12. This sample as shown in Table 11, has the highest contents of iron. Gallium is relatively evenly distributed within concentration range of 10ppm to 60ppm as indicated in the Fig. 4.27, with calculated mean of 44.3ppm. Four samples (MH16, MH18, MH25 and MH26) however, have higher contents of gallium within concentration range of 70ppm to 220ppm. Sample MH26 also has the highest reported concentrations values of lead and niobium.

### Selenium

The element was detected and analysed for in all the samples except sample MH12. The reported concentration range varied from 3.00ppm to 40ppm (Fig. 4.28). The calculated mean concentration is 12.1ppm. The element is correlated to cerium and weakly to lead in these samples Table 9.

### Strontium

The element occurs in all the samples analysed as minor constituent. The concentration range in which it occurs is 1457ppm to 6923ppm. Frequency distribution histogram of the element in these samples (Fig. 4.29) is



bimodal. The concentration range of 1000ppm to 3500ppm corresponds to low iron content and the range of 4000ppm to 7000ppm is the converse. The calculated mean concentration of the element is 4076ppm. The element is weakly correlated only to niobium with a correlation coefficient of 0.41 (Table 9).

#### Yttrium

The element occurs in all the samples analysed. The concentration range is within 200ppm (sample MHO6) and 3780ppm (sample MH25). The frequency distribution of the element in the samples is shown in Fig. 4.30. The calculated mean concentration of the element is 1031ppm.

#### Zirconium

The reported concentration of this element in the samples are within 94ppm to 720ppm (Fig. 4.31). The highest zirconium content (sample MH22) corresponds to the highest reported value of niobium as shown in Table 11. The calculated mean concentration of zirconium in the samples is 251ppm. A correlation coefficient of 0.64 was obtained with niobium, Table 9.

#### Niobium

All the samples analysed, indicated that niobium is a minor constituent within the concentration range of 1000ppm to 9000ppm (Fig.4.32). The anomaly only occurs in

sample MH30 where a concentration value of 2.24% was obtained. The mean concentration in the distribution range, was 4068ppm. The element is correlated, in increasing order, to the following elements; strontium and zirconium, Table 9.

#### Molybdenum

In all the samples analysed, concentrations values of molybdenum are low and varied from 23.5ppm to 646ppm. The low concentration values correspond to relatively lower than average the iron content. The frequency distribution of the element shown in Fig. 4.33 indicates that the element is relatively evenly distributed in the concentration range of 50ppm to 500ppm with a calculated mean value of 245ppm. The element is correlated to cerium and thorium, Table 9 .

#### Barium

The element exists as a major constituent. Concentrations values of the element were found to vary from 2821ppm to 5.18%.

Figure 4.34 shows the frequency distribution of the element in the samples with a calculated mean of 2.62%. The element was found to be positively correlated, in increasing order to the following elements; vanadium, cerium and titanium as shown on the correlation matrix, Table 9.

### Cerium

Obtained concentration values for this element varied from 8976ppm to 18.11%. The element is a major constituent in the samples and occurs in all the samples analysed. The higher concentrations values of the element in the samples correspond to relatively lower than average iron contents. High correlation coefficients of 0.66, 0.92, 0.96 were obtained with barium, titanium and vanadium, respectively (Table 9). The distribution of the element in these samples is shown in Fig. 4.35 with a calculated mean concentration value of 8.70%.

### Lead

The element occurs in low concentrations in all the samples analysed from Mrima Hill. The reported concentrations values are mostly within the range of 500ppm to 3000ppm as shown in Fig. 4.36. Four samples (MH12, MH16, MH18 and MH26) obtained from the summit of the hill, show higher contents of this element. The calculated mean concentration value of the element is 2032ppm. Lead is weakly correlated in increasing order to the following elements; titanium, vanadium and thorium (Table 9).

### Actinium

The element was detected in twenty three samples of the thirty samples analysed. The concentrations of the element was found to vary from 71.8ppm in sample

MH15 to 825ppm in sample MH26. Actinium is relatively evenly distributed in the concentration range of 100 ppm to 300ppm with a calculated mean concentration value of 234ppm as shown in Fig. 4.37. Four samples (MH12, MH16, MH18 and MH26) have the element content higher than 350ppm with corresponding higher than average the contents of lead.

### Thorium

The element was detected and analysed for in all the samples. It occurs in low concentration range of 95.2ppm to 1470ppm as shown in Table 11. The element is evenly distributed in concentration range of 100ppm to 1100ppm with a calculated mean concentration value of 763ppm (Fig. 4.38). In six samples, higher concentrations values of the element were obtained within range of 1200ppm of 1500ppm. Sample MH12 had the element content of 3341ppm. This sample has also the highest obtained values of lead and actinium.

Thorium is weakly correlated to the following elements in the increasing order; lead, iron, vanadium and cerium, Table 9. The occurrence of thorium is usually associated with monazite minerals and is mainly responsible for the high radioactivity of the soils.

TABLE 1

RESULTS OF EDXRF ANALYSIS OF CERTIFIED REFERENCE MATERIALS (SY-3)  
 (Concentration Values are in ppm unless otherwise stated)

ELEMENT	EXPERIMENTALLY OBTAINED VALUES (EDXRF)		CERTIFIED REFERENCE VALUES		RELATIVE ERROR (%)
	RANGE	MEAN CONCENTRATION	RECOMMENDED CONCENTRATION	RANGE	
MAJOR AND MINOR CONSTITUENTS					
K	3.00% - 3.45%	(3.197 ± 0.191)%	3.520%	3.05% - 4.12%	-9.2%
Ca	5.03% - 5.84%	(5.36 ± 0.15)%	5.904%	5.636%-6.029%	-9.2%
Fe	4.34% - 4.77%	(4.598 ± 0.754)%	4.526%	4.403%-4.725%	+1.59%
TRACE CONSTITUENTS					
Ti	724 - 1490	795 ± 160	900*	720 - 1740	-11.7%
Mn	2033 - 2388	2240 ± 123	2556	2246 - 2866	-12.4%
Cu	15.6 - 26.0	22.0 ± 7.0	17.0*	12.0 - 34.0	+29.4%
Zn	256 - 285	268 ± 14	250	256 - 259	+7.2%
Ga	15.2 - 22.7	22.0 ± 5.0	28.0*	25.6 - 36.0	-21.0%
Rb	160 - 264	205 ± 8	210	188 - 213	-2.4%

TABLE 1

RESULTS OF EDXRF ANALYSIS OF CERTIFIED REFERENCE MATERIALS (SY-3)  
 (Concentration Values are in ppm unless otherwise stated)

ELEMENT	EXPERIMENTALLY OBTAINED VALUES (EDXRF)		CERTIFIED REFERENCE VALUES		RELATIVE ERROR (%)
	RANGE	MEAN CONCENTRATION	RECOMMENDED CONCENTRATION	RANGE	
MAJOR AND MINOR CONSTITUENTS					
K	3.00% - 3.45%	(3.197 ± 0.191)%	3.520%	3.05% - 4.12%	-9.2%
Ca	5.03% - 5.84%	(5.36 ± 0.15)%	5.904%	5.636%-6.029%	-9.2%
Fe	4.34% - 4.77%	(4.598 ± 0.754)%	4.526%	4.403%-4.725%	+1.59%
TRACE CONSTITUENTS					
Ti	724 - 1490	795 ± 160	900*	720 - 1740	-11.7%
Mn	2033 - 2388	2240 ± 123	2556	2246 - 2866	-12.4%
Cu	15.6 - 26.0	22.0 ± 7.0	17.0*	12.0 - 34.0	+29.4%
Zn	256 - 285	268 ± 14	250	256 - 259	+7.2%
Ga	15.2 - 22.7	22.0 ± 5.0	28.0*	25.6 - 36.0	-21.0%
Rb	160 - 264	205 ± 8	210	188 - 213	-2.4%

TABLE 1 (CONTD.)

Sr	275 - 314	300 ± 11	300	250 - 472	0%
Y	661 - 727	699 ± 11	740	610 - 880	-5.5%
Zr	272 - 371	312 ± 14	340	295 - 392	-5.3%
Nb	107 - 122	115 ± 13	145*	93.8 - 195	-17.3%
Ia	1099 - 1784	1528 ± 373	1400*	<1530	+9.1%
Ce	1236 - 1628	1454 ± 404	2000*	950 - 2640	-27%
Pb	110 - 210	183 ± 12	130	110 - 214	+38%
Th	933 - 1016	979 ± 21	980	850 - 1180	-0.1%
U	589 - 663	626 ± 20	640	540 - 863	+2.2%

\* Non certified values

TABLE 2

RESULTS OF EDXRF ANALYSIS OF CERTIFIED REFERENCE MATERIAL SOIL (S-7)  
 (Concentration values are in ppm unless otherwise stated)

ELEMENT	EXPERIMENTALLY OBTAINED VALUES (EDXRF)		CERTIFIED REFERENCE VALUES		RELATIVE ERROR (%)
	RANGE	MEAN CONCENTRATION	RECOMMENDED CONCENTRATION	RANGE	
MAJOR AND MINOR CONSTITUENTS					
K	1.42% - 1.61%	(1.49 ± 0.43)%	1.21%*	1.13% - 1.27%	+23%
Ca	18.40% - 19.76%	(18.93 ± 1.66)%	16.30%*	15.7% - 17.4%	+16%
Fe	3.02% - 3.21%	(3.11 ± 0.44)	2.59%*	2.54% - 2.67%	+20%
TRACE CONSTITUENTS					
Ti	2803 - 3051	2943 ± 310	3000*	2600 - 3700	-2.0%
Cr	26.0 - 77.0	42.0 ± 28.0	60.0	39.0 - 74.0	-30%
Mn	688 - 745	723 ± 100	631	604 - 650	+14%
Cu	25.0 - 36.0	31.5 ± 8.0	11.0 *	9.0 - 13.0	>100%
Zn	122 - 136	130 ± 12	104	101 - 113	+25%
Ga	7.3 - 14.0	9.7 ± 3.0	10.0 *	9.0 - 13.0	-3%



TABLE 2 (CONTD.)

Se	2.4 - 5.4	3.0 ± 1.0	2.0*	2.0 - 8.0	+50%
Br	9.0 - 13.0	10.5 ± 3.0	7.0*	3.0 - 10.0	+50%
Rb	47.0 - 57.0	51.3 ± 6.0	51.0	47.0 - 56.0	+0.6%
Sr	113 - 120	115 ± 13	108	103 - 114	+6.5%
Y	16.0 - 20.0	18.3 ± 5.0	21.0	15.0 - 27.0	-13%
Zr	181 - 204	190 ± 16	185	180 - 201	+2.7%
Nb	7.0 - 11.0	10.0 ± 3.0	12.0*	7.0 - 17.0	-20%
Pb	63.7 - 118	91.0 ± 25.7	60.0*	55.0 - 71.0	±51%

\* Non-certified values

TABLE 3

RESULTS OF EDXRF ANALYSIS OF CERTIFIED REFERENCE MATERIAL - URANIUM ORE (S-8)/IAEA  
 (Concentration values in ppm, unless otherwise stated)

ELEMENT	EXPERIMENTALLY OBTAINED VALUES (EDXRF)		CERTIFIED REFERENCE VALUES		RELATIVE ERROR (%)
	RANGE	MEAN CONCENTRATION	RECOMMENDED CONCENTRATION	RANGE	
MAJOR AND MINOR CONSTITUENTS					
K	2.69% - 2.97%	(2.82 ± 0.18)%	3.00%*	-	-4%
Ca	5183 - 5705	5460 ± 707	5574*	-	- 2%
Fe	1.69% - 1.79%	(1.74 ± 0.06)%	<1.3%*	-	-
TRACE CONSTITUENTS					
Ti	592 - 658	634 ± 89	600*	-	+5.7%
Cr	26.0 - 30.0	28.0 ± 18.0	<50*	-	-
Mn	148 - 196	172 ± 55	<300*	-	-
Co	129 - 161	145 ± 86	<150*	-	-
Rb	301 - 382	331 ± 14	<450*	-	-
Sr	35 - 41	38.0 ± 3.0	<45*	-	-
Zr	50 - 65	57 ± 3	*	-	-
U	1077 - 1248	1185 ± 25	1162	-	2%

\* Non certified values

TABLE 4

RESULTS OF EDXRF ANALYSIS OF CERTIFIED REFERENCE MATERIAL - THORIUM ORE (S-14/IAEA)  
 (Concentration Values in ppm, unless otherwise stated)

ELEMENT	EXPERIMENTALLY OBTAINED VALUES (EDXRF)		CERTIFIED REFERENCE VALUES		RELATIVE ERROR (%)
	RANGE	MEAN CONCENTRATION	RECOMMENDED CONCENTRATION	RANGE	
MAJOR AND MINOR CONSTITUENTS					
Ca	20.12% - 22.42%	(21.06 ± 0.93)%	21.43%*	-	-1.7%
Fe	1.06% - 1.59%	(1.25 ± 0.23)%	1.40%*	-	-10.7%
Ba	10.08% - 17.59%	(12.39 ± 3.35)%	14.33%*	-	13.5%
Ce	3.88% - 4.40%	(4.18 ± 0.23)%	**	-	-
TRACE CONSTITUENTS					
Mn	5988 - 6368	6215 ± 141	**	-	-
Cu	28 - 56	41.1 ± 8.0	**	-	-
Zn	147 - 194	164 ± 16	**	-	-
Sr	8098 - 8999	8600 ± 332	**	-	-
Y	295 - 341	319 ± 14	**	-	-
Zr	108 - 177	152 ± 28	**	-	-
Pb	189 - 263	231 ± 27	**	-	-
Th	505 - 653	609.9 ± 57	610	570 - 660	<0.1%
U	BDL	BDL	29	26 - 31	-

\* Non-certified values.

\*\* Values not stated in the certificate.

TABLE 5:

LOWER LIMIT OF DETECTION FOR THE ELEMENTS ANALYSIS

ELEMENT	LOWER LIMIT OF DETECTION (LLD) - ppm
K	834
Ca	414
Ti	84
V	46.5
Cr	25
Mn	22
Fe	29.2
Ni	9.4
Cu	8.5
Zn	8.3
Ga	7.0
Se	2.2
Br	2.3
Rb	4.6
Sr	4.0
Y	2.7
Zr	3.2
Nb	6.4
Mo	11.1
Ba	279
La	736
Ce	537
Pb	18
Th	27.6
U	29.1

TABLE 6

REPEATABILITY OF MEASUREMENTS FOR MRIMA HILL SAMPLES  
 (Concentration values are in ppm, unless otherwise  
 stated, while intensity values are in counts/sec.)

ELEMENT	CONCENTRATION RANGE	DETERMINED MEAN OF SIX		ST. DEV. REL *MEAN CONCENTRATION	*ST. DEV. REV MEAN INTENSITY
		CONCENTRATION	INTENSITY		
Ca	915 - 1294	116	0.134	76	0.011
Ti	2.43% - 2.79%	2.60%	7.269	0.095	0.210
V	7042 - 8829	7938	3.360	353	0.172
Mn	3.81% - 4.44%	4.13%	35.961	0.13	1.351
Fe	6.75% - 7.66%	7.28%	87.538	0.18	3.4602
Cu	10.0 - 21.5	17.4	0.046	2.5	0.005
Zn	611 - 701	644	1.911	16.0	0.106
Ga	13.7 - 24.7	18.4	0.047	3.8	0.014
Se	2.3 - 3.8	3.00	0.017	0.36	0.002
Sr	1272 - 1557	1457	14.750	50	0.980
Y	174 - 225	201	2.368	10	0.184
Zr	140 - 182	163	1.951	8	0.116
Nb	868 - 1114	1008	12.953	42	0.998
Mo	211 - 276	244	3.601	12	0.316
Ba	1.21% - 1.85%	1.39	1.220	0.12	0.065
Ce	4.52% - 5.92%	5.25	6.774	0.27	0.314
Pb	649 - 775	699	1.614	25	0.089
Ac	23.4 - 123	66.8	0.243	12.1	0.074
Th	184 - 266	233	0.932	16	0.091

\* Rel. St. Dev. computed at 68.3% confidence level at five degrees of freedom.

TABLE 7

REPEATABILITY OF MEASUREMENTS FOR KERIO VALLEY SAMPLES  
 (Concentration values are in ppm, unless otherwise stated, while the  
 intensity values are in counts/sec).

ELEMENT	CONCEN. RANGE	DETERMINED MEAN OF SIX		*ST. DEV. REL MEAN CONCEN.	*ST. DEV. REL MEAN INTENSITY
		CONCEN.	INTENSITY		
K	1.650% - 1.915%	1.81%	1.014	0.103	0.097
Ca	23.55% - 27.68%	25.54%	35.163	0.78	1.336
Ti	410 - 510	443	0.134	17	0.005
Mn	22.0 - 30.8	25.0	0.022	1.8	0.014
Fe	3880 - 4530	4293	6.550	361	0.511
Ni	9.0 - 14.0	12.8	0.022	0.632	0.567
Cu	43.5 - 48.5	46.7	0.157	2.4	0.005
Zn	18.7 - 25.8	22.6	0.097	3.4	0.007
Rb	53.0 - 66.3	59.1	0.710	6.7	0.091
Sr	1160 - 1570	1317	17.500	74	0.163
Y	69.3 - 92.0	80.4	1.187	5.5	0.106
Zr	3950 - 5160	4500	74.103	221	4.406
Pb	26.7 - 31.7	29.3	0.096	2.5	0.004
U	190 - 250	222	1.386	25	0.135

\* Rel St. Dev. computed at 68.3% confidence level for five degrees of freedom

TABLE 8

## CORRELATION OF URANIUM AND FLUORITE ORE CONSTITUTENTS FROM KERIO VALLEY

	U	K	Ca	Ti	V	Mn	Fe	Ni	Cu	Zn	Pb	Th	Rb	Sr	Y	Zr	Nb
U	1																
K	0.18	1															
Ca	-0.19	-0.68	1														
Ti	-0.21	0.51	-0.47	1													
V	-0.17	0.53	-0.57	0.74	1												
Mn	0.12	0.44	-0.41	0.39	-0.12	1											
Fe	-0.19	0.44	-0.53	0.87	0.43	0.71	1										
Ni	0.12	0.49	-0.39	0.85	0.41	0.61	0.82	1									
Cu	0.42	0.29	-0.13	0.05	-0.05	0.26	0.35	0.59	1								
Zn	-0.14	0.47	-0.47	0.79	0.43	0.59	0.88	0.92	0.61	1							
Pb	-0.18	0.41	-0.27	0.24	0.22	0.08	0.25	0.34	0.51	0.56	1						
Th	0.33	0.61	-0.92	0.40	0.57	-0.75	0.04	0.69	0.53	0.38	0.67	1					
Rb	0.49	0.96	-0.77	0.55	0.59	0.40	0.45	0.50	0.09	0.44	0.34	0.95	1				
Sr	0.63	-0.40	0.47	-0.41	-0.32	-0.55	-0.55	-0.28	-0.06	-0.48	-0.37	0.38	-0.58	1			
Y	0.70	0.45	-0.40	0.10	0.44	-0.12	0.17	0.33	0.50	0.34	0.45	0.89	0.59	0.30	1		
Zr	0.53	0.17	-0.23	-0.25	-0.20	-0.18	-0.09	0.04	-0.37	-0.04	-0.04	0.46	0.34	0.58	0.80	1	
Nb	0.71	0.22	-0.32	-0.03	0.34	-0.24	-0.07	0.22	0.40	0.06	0.20	0.82	0.76	0.69	0.91	0.86	1
Cr	0.15	-0.08	0.17	-0.38	0.18	0.31	0.35	0.54	0.68	0.48	0.22	-0.18	0.14	-0.12	0.04	-0.09	-0.18

TABLE 9

## CORRELATION OF THORIUM AND SOME OF SOIL CONSTITUENTS FROM MRIMA HILLS

	Th	Ti	V	Mn	Fe	Sr	Zr	Nb	Ba	Ce	Pb
Th	1										
Ti	0.37	1									
V	0.57	0.89	1								
Mn	0.03	0.47	0.29	1							
Fe	0.53	0.21	0.17	0.55	1						
Sr	-0.05	0.15	0.10	-0.15	0.09	1					
Zr	-0.34	-0.37	-0.44	-0.46	-0.12	0.15	1				
Nb	-0.07	-0.07	0.02	-0.34	-0.02	0.41	0.64	1			
Ba	0.25	0.69	0.65	0.43	0.19	0.10	-0.38	-0.05	1		
Ce	0.63	0.92	0.96	0.48	0.09	0.08	-0.43	0.01	0.66	1	
Pb	0.47	0.34	0.36	-0.17	0.26	0.21	0.21	0.16	-0.11	0.22	1



TABLE 10: RESULTS OF ELEMENTAL CONCENTRATIONS OF FLUORITE ORES  
SAMPLES FROM KERIO VALLEY\*

FIELD SAMPLING LOCATIONS					
	TUMEIYO SEDIMENTARY ROCKS - PARTLY SILICAFIED	KAMNAON I (WEATHERED GNEISS	KAMNAON I (YELLOW- FLUORITE)	KAMNAON I (SHIMO LA BAHATI (PURPLE FLUORITE)	KAMNAON I (YELLOW-PURPLE FLUORITE)
LABORATORY SAMPLE NUMBER					
ELEMENT	KV01	KV02	KV03	KV04	KV06
K	(4.82±0.19)%	(1.66±0.11)%	8175±487	(2.25±0.16)%	5833±971
Ca	3029±146	(6.38±0.71)%	(39.84±1.54)%	(18.54±1.02)%	(29.13±1.51)%
Ti	6253±109	1112±177	2626±366	4269±234	457±53
V	485±74	BDL	BDL	441±66	48.1±10.5
Cr	BDL	134±17	638±68	114±16	250±29
Mn	206±24	129±14	244±29	304±29	210±25
Fe	(3.29±0.18)%	(1.00±0.07)%	(1.00±0.12)%	(2.74±0.25)%	(1.44±0.11)%
Ni	90.3±15.7	49.6±7.1	28.9±4.8	42.2±8.4	53.9±12.1
Cu	75.8±11.2	95.5±8.7	85.1±9.5	51.5±6.7	87.9±9.1
Zn	143±20	51.6±8.7	37.8±5.1	78.5±10.1	78.5±11.6
Rb	205±4	BDL	9.2±4.9	72.8±7.1	32.7±7.1
Sr	319±16	2634±191	1280±179	771±89	740±53
Y	326±41	441±45	33.4±7.1	34.3±7.3	31.8±7.5
Zr	228±16	(2.37±0.25)%	234±22	281±11	33.1±4.8
Nb	107±7	255±38	14.3±4.6	13.1±4.8	BDL
Pb	463±45	75.0±11.5	28.1±16.1	36.6±15.5	83.0±14.5
Th	161±15	146±21	BDL	29±10	34.7±7.1
U	35.7±12.0	983±78	BDL	45.3±12.5	34.0±14.0

\* Concentration values used in ppm. unless otherwise stated.

BDL - Below Detection limit

TABLE 10 (CONTD..)

FIELD SAMPLING LOCATIONS					
	KAMNAON I (PURPLE FLUORITE)	KAMNAON I (PURPLE FLUORITE)	KAMNAON I WEATHERED GNEISS -MAIN ROAD	KAMNAON I (BIOTITE GNEISS)	KAMNAON I (YELLOW-PURPLE ORE)
LABORATORY SAMPLE NUMBER					
ELEMENT	KV07	KV08	KV09	KV10	KV11
K	8733±1050	(1.89±0.31)%	(1.08±0.16)%	(2.94±0.44)%	2510±352
Ca	(15.85±1.34)%	(21.14±1.67)%	4237±205	(5.23±0.51)%	(39.11±1.44)%
Ti	800±136	810±140	3820±113	8493±430	513±33
V	83.1±10.3	116±11	75.3±8.1	381±25	BDL
Cr	263±45	118±26	142±16.4	413±21	137±15
Mn	463±36	310±53	590±33	915±85	96.1±28
Fe	(1.04±0.05)%	(2.28±0.21)%	(5.44±0.49)%	(6.98±0.55)%	3450±147
Ni	30.7±7.2	20±8	57.7±14.1	163±28	27.7±8.1
Cu	97.0±10.1	68.7±7.1	71.7±6.1	88.3±9.2	69.3±6.8
Zn	92.1±15.1	76.4±16.0	117±12	197±12	40.8±12.5
Rb	33.1±14.0	82.8±5.0	67±11	150±13	9.3±4.2
Sr	377±32	647±60	41.0±5.7	380±10	968±31
Y	65.3±6.4	210±26	31.7±5.1	87.7±8.0	18.7±3.5
Zr	70.3±12.7	7377±301	135±97	267±15	138±37
Nb	22.2±3.5	47.1±10.7	15.8±4.9	39.3±6.0	BDL
Pb	403±76	103±17	101±18	82.1±12.3	119±25
Th	BDL	39.3±7	BDL	BDL	BDL
U	40±13	603±56	35±14	BDL	36±13

TABLE 10 (CONTD..)

FIELD SAMPLING LOCATIONS					
	KAMNAON I (PEGMATITE QUARTZ)	TUMEIYO (SEDIMENTARY ROCK)	CHEBEREN I (VEIN I)	CHEBEREN I (VEIN III)	CHEBEREN II (VEIN I)
LABORATORY SAMPLE					
ELEMENT	KV12	KV13	KV14	KV15	KV16
K	(5.47±0.42)%	(3.53±0.10)%	(1.74±0.51)%	6410±398	1824±310
Ca	(1.06±0.12)%	6675±409	(30.03±1.79)%	(26.13±1.81)%	(27.80±0.51)%
Ti	1997±60	5040±169	764±117	BDL	BDL
V	214±19	BDL	62.7±7.1	BDL	202±14
Cr	BDL	170±18	131±14	BDL	BDL
Mn	593±38	984±74	626±74	BDL	BDL
Fe	(1.03±0.01)%	(3.84±0.11)%	8891±182	3626±228	3735±201
Ni	49.3±13	BDL	19.7±5	BDL	BDL
Cu	83.7±7.1	42.3±15	74.0±8.1	30.3±5.9	30.3±8.7
Zn	47.7±15	71.0±10.8	57±15	20±7	25.4±6
Rb	227±12	166±10	24.6±5.8	BDL	BDL
Sr	410±40	89.9±11	791±73	1204±91	1099±38
Y	103±6	47.1±7.8	36.8±8.5	3.5±1.5	5.7±1.5
Zr	5868±174	259±25	160±13	66.5±8.3	23.5±6.6
Nb	35.4±7.2	76.2±12.1	14.4±5.0	BDL	BDL
Pb	73.7±16.3	BDL	67.5±15.0	18.7±7.5	18.3±8.1
Th	123±18	BDL	BDL	BDL	BDL
U	657±75	BDL	BDL	BDL	BDL

TABLE 10 (CONTD..)

FIELD SAMPLING LOCATIONS					
FLUORSPAR TAILINGS (POND)		MILLED FLUOSPAR (FACTORY PLANT)	CHOFF II (WHITE ORE)	CHOFF II (WHITE ORE)	
LABORATORY SAMPLE NUMBER					
ELEMENT	KV17	KV18	KV19	KV20	KV21
K	(1.22±0.22)%	8987±850	3473±757	3260±450	4055±605
Ca	(5.10±0.55)%	(10.47±0.78)%	(33.97±1.01)%	(26.47±1.34)%	(27.45±1.32)%
Ti	2290±118	1670±60	BDL	BDL	BDL
V	427±35	BDL	BDL	BDL	BDL
Cr	33.1±15.3	BDL	BDL	BDL	BDL
Mn	333±38	237±29	BDL	BDL	BDL
Fe	(1.74±0.09)%	(1.53±0.11)%	1117±147	1160±255	1040±240
Ni	10.9±3.4	12.0±2.5	13.7±2.7	BDL	BDL
Cu	39.4±9.1	47.5±9.2	36.4±7.5	35.9±7.1	39.0±7.7
Zn	35.5±8.0	33.4±8.1	19.8±4.6	15.8±6.0	20.4±9.3
Rb	51.7±8.4	46.3±7.1	BDL	BDL	BDL
Sr	394±14	533±15	2017±113	1020±70	950±48
Y	41.1±5.1	14.3±2.9	11.5±2.9	11.1±2.8	18.0±2.4
Zr	160±17	220±30	20.8±4.8	26.4±4.9	11.5±2.4
Nb	10.0±1.4	14.7±1.2	BDL	BDL	BDL
Pb	25.5±4.3	40.3±6.0	18.4±4.7	18.3±4.3	21.5±4.8
Th	BDL	BDL	BDL	BDL	BDL
U	39.3±14.5	37.0±15.1	BDL	BDL	BDL

TABLE 10 (CONTD..)

FIELD SAMPLING LOCATIONS			
CHOFF IV (QUARTZ)		CHOFF IV YELLOW-ORANGE ORE	CHOFF IV (YELLOW-ORANGE)
LABORATORY SAMPLE			
ELEMENT	KV 22	KV23	KV24
K	(2.38±0.12)%	(1.81±0.14)%	7840±658
Ca	6435±301	(25.54±0.27)%	(21.57±0.61)%
Ti	762±130	443±58	BDL
V	BDL	BDL	52±15
Cr	36.5±14.3	BDL	28.3±13.3
Mn	63.5±5.1	25±15	110±14
Fe	6795±135	4293±359	8850±157
Ni	15.0±2.8	12.8±2.1	18.8±3.7
Cu	33.9±9.5	46.7±7.4	44.1±6.8
Zn	24.2±8.0	22.6±6.4	27.6±7.3
Rb	135±17	59.1±7.6	34.0±10.8
Sr	665±35	1317±121	1015±135
Y	37.4±4.9	80.4±11.0	27.7±4.4
Zr	1095±71	4500±250	188±14
Nb	BDL	BDL	BDL
Pb	65.8±15.0	29.3±13.0	28.3±16.4
Th	BDL	34.0±9.0	BDL
U	50.4±14	222±25	101±12

TABLE 11

## RESULTS OF ELEMENTAL CONCENTRATIONS IN SOIL SAMPLES FROM MRIMA HILLS\*

ELEMENT	LABORATORY SAMPLE NUMBERS				
	MHO1	MHO2	MHO3	MHO4	MHO5
Ca	3392 ± 833	2934 ± 600	5159 ± 1389	(1.29 ± 0.14)%	3170 ± 291
Ti	(1.44 ± 0.39)%	(1.26 ± 0.15)%	(1.38 ± 0.43)%	(1.48 ± 0.18)%	(1.77 ± 0.23)%
V	2847 ± 738	2035 ± 360	1896 ± 0.69)%	2760 ± 662	5085 ± 386
Mn	(3.19 ± 0.96)%	(3.82 ± 0.63)%	(2.78 ± 0.69)%	(5.98 ± 0.28)%	(5.76 ± 0.71)%
Fe	(17.80 ± 3.61)%	(15.97 ± 1.69)%	(12.24 ± 2.02)%	(23.51 ± 1.08)%	(12.72 ± 1.62)%
Ni	BDL	21.2 ± 3.2	BDL	19.2 ± 6	BDL
Cu	27.5 ± 7.3	68.0 ± 6.2	50.0 ± 9.5	15.7 ± 3.7	18.8 ± 2.6
Zn	1189 ± 234	912 ± 102	985 ± 232	2623 ± 150	1465 ± 178
Ga	33.4 ± 7.9	16.6 ± 2.4	7.3 ± 4.1	20.7 ± 9.5	17.6 ± 4.4
Se	5.7 ± 2.9	5.9 ± 3.1	3.95 ± 2.5	2.5 ± 1.5	5.1 ± 2.8
Sr	4885 ± 909	2830 ± 206	3188 ± 647	2069 ± 152	2353 ± 291
Y	449 ± 75	422 ± 79	431 ± 80	599 ± 42	423 ± 43
Zr	326 ± 44	277 ± 66	435 ± 117	278 ± 40	313 ± 16
Nb	2886 ± 490	1499 ± 171	2102 ± 342	3560 ± 101	1618 ± 215

TABLE 11 (CONTD.)

	MHO1	MHO2	MHO3	MHO4	MHO5
Mo	162 ± 47	72.7 ± 12.7	23.5 ± 7.1	111.2 ± 17.6	264 ± 23
Ba	8362 ± 360	8059 ± 993	5841 ± 636	6280 ± 1421	(1.02 ± 0.17) %
Ce	(1.51 ± 0.49) %	(1.16 ± 0.26) %	8976 ± 596	(1.69 ± 0.14)	(2.97 ± 0.38) %
Pb	844 ± 91	427 ± 104	373 ± 61	434 ± 101	781 ± 115
Ac	38.4 ± 11	BDL	BDL	BDL	50.0 ± 7.3
Th	258 ± 44	95.2 ± 20	121 ± 25	144 ± 22	366 ± 41

\* Concentration values are in ppm, unless otherwise stated

TABLE 11 (CONTD.)

ELEMENT	LABORATORY SAMPLE NUMBER				
	MHO6	MHO7	MHO8	MHO9	MH10
Ca	1116 ± 148	6443 ± 484	4090 ± 1119	3045 ± 890	3684 ± 709
Ti	(2.60 ± 0.17)%	(4.16 ± 0.39)%	(3.91 ± 0.14)%	(8.60 ± 0.10)%	(5.93 ± 0.18)%
V	7838 ± 691	(1.39 ± 0.15)%	(1.41 ± 0.07)%	(2.84 ± 0.13)%	(2.02 ± 0.05)%
Mn	(4.13 ± 0.25)%	(10.60 ± 0.92)%	(9.19 ± 0.21)%	(17.05 ± 0.34)%	(11.33 ± 0.29)%
Fe	(7.28 ± 0.35)%	(24.34 ± 1.51)%	(24.18 ± 0.52)	(17.88 ± 0.51)%	(22.54 ± 0.76)%
Ni	BDL	BDL	BDL	BDL	BDL
Cu	17.4 ± 4.5	23.8 ± 5.9	15.3 ± 3.8	24.4 ± 8.7	10.9 ± 3.2
Zn	644 ± 32	3401 ± 156	3071 ± 137	1657 ± 33	2460 ± 123
Ga	18.4 ± 3.7	76.4 ± 20.5	42.0 ± 8.9	48.5 ± 13.6	45.9 ± 12.2
Se	2.97 ± 1.5	4.65 ± 1.8	4.5 ± 1.3	22.0 ± 3.9	18.2 ± 5.7
Sr	1457 ± 100	6494 ± 429	4060 ± 183	1958 ± 44	2858 ± 131
Y	201 ± 20	1891 ± 94	1318 ± 62	430 ± 29	436 ± 19
Zr	163 ± 17	294 ± 47	339 ± 23	201 ± 17	217 ± 36
Nb	1008 ± 83	6888 ± 312	5622 ± 295	1331 ± 87	1401 ± 46
Mo	244 ± 23	269 ± 26	304 ± 16	366 ± 22	229 ± 17



TABLE 11 (CONTD.)

	MHO6	MHO7	MHO8	MHO9	MH10
Ba	(1.39 ± 0.23) %	(2.62 ± 0.37) %	(2.58 ± 0.26) %	(5.01 ± 0.44) %	(3.68 ± 0.34) %
Ce	(5.25 ± 0.53) %	(7.53 ± 0.85) %	(7.37 ± 0.10) %	(18.11 ± 0.40) %	(12.57 ± 0.53) %
Pb	699 ± 50	1054 ± 59	1270 ± 66	2141 ± 104	2448 ± 128
Ac	66.8 ± 21.4	BDL	BDL	133 ± 43	206 ± 38
Th	233 ± 32	385 ± 42	477 ± 43	667 ± 39	913 ± 68

TABLE 11 (CONTD.)

ELEMENT	LABORATORY SAMPLE NUMBER				
	MH11	MH12	MH13	MH14	MH15
Ca	BDL	9673 ± 1028	1424 ± 206	1859 ± 177	1441 ± 284
Ti	(6.14 ± 0.89)%	(3.75 ± 0.13)%	(4.74 ± 0.27)%	(5.18 ± 0.34)%	(4.61 ± 0.48)%
V	(2.43 ± 0.59)%	BDL	(2.15 ± 0.65)%	(2.19 ± 0.22)%	(2.35 ± 0.30)%
Mn	(10.09 ± 1.39)%	(2.97 ± 0.11)%	(6.16 ± 0.37)%	(3.35 ± 0.16)%	(7.47 ± 0.61)%
Fe	(21.90 ± 3.32)%	(39.09 ± 0.53)%	(17.93 ± 1.48)%	(22.27 ± 1.03)%	(15.15 ± 1.14)%
Ni	BDL	BDL	BDL	BDL	BDL
Cu	36.1 ± 9.4	51.5 ± 6.4	19.5 ± 4.0	23.0 ± 5.2	19.6 ± 9.0
Zn	1953 ± 149	2661 ± 82	1483 ± 62	948 ± 46	1117 ± 40
Ga	32.9 ± 11.9	BDL	35.2 ± 11.4	27.0 ± 8.8	36.9 ± 11.0
Se	17.2 ± 3.1	BDL	13.4 ± 2.2	19.0 ± 7.0	6.5 ± 1.0
Sr	1965 ± 239	2935 ± 83	2063 ± 63	3419 ± 85	6735 ± 422
Y	486 ± 73	1335 ± 107	654 ± 26	766 ± 17	1130 ± 51
Zr	200 ± 50	234 ± 54	158 ± 51	149 ± 14	127 ± 2
Nb	1290 ± 137	976 ± 58	2492 ± 88	4007 ± 137	5099 ± 304
Mo	286 ± 27	203 ± 17	355 ± 15	161 ± 16	298 ± 19
Ba	BDL	(2.78 ± 0.18)%	BDL	BDL	(4.56 ± 0.94)%
Ce	(9.88 ± 1.31)%	(1.90 ± 0.02)%	(8.04 ± 1.94)%	(10.63 ± 1.26)%	(10.40 ± 0.53)%
Pb	1688 ± 217	5552 ± 217	1761 ± 81	1518 ± 119	1451 ± 82
Ac	191 ± 36	673 ± 67	149 ± 78	172 ± 43	71.8 ± 28.0
Th	545 ± 49	3341 ± 96	729 ± 59	795 ± 61	1066 ± 74

TABLE 11 (CONTD.)

ELEMENT	LABORATORY SAMPLE NUMBER				
	MH16	MH17	MH18	MH19	MH20
Ca	4571 ± 401	6056 ± 715	5837 ± 665	4240 ± 707	5055 ± 631
Ti	(5.71 ± 0.36)%	(6.46 ± 0.49)%	(6.32 ± 0.25)%	(5.62 ± 0.43)%	(5.50 ± 0.24)%
V	(2.46 ± 0.09)%	(3.04 ± 0.09)%	(2.78 ± 0.08)%	(2.65 ± 0.14)%	(2.22 ± 0.12)%
Mn	(8.96 ± 0.19)%	(8.53 ± 0.22)%	(4.02 ± 0.07)%	(7.06 ± 0.22)%	(8.25 ± 0.24)%
Fe	(24.54 ± 0.57)%	(28.85 ± 0.77)%	(27.92 ± 0.49)%	(28.01 ± 0.87)%	(28.50 ± 0.81)%
Ni	BDL	BDL	BDL	BDL	BDL
Cu	31.5 ± 11.4	30.8 ± 8.5	36.9 ± 7.6	18.6 ± 4.3	49.7 ± 5.4
Zn	1232 ± 62	1981 ± 70	1237 ± 29	2044 ± 113	2149 ± 70
Ga	75.3 ± 15.0	55 ± 14	91.2 ± 14.0	6.5 ± 2.0	53.2 ± 14.0
Se	40 ± 5	14.4 ± 5.0	15.1 ± 1.6	14.4 ± 2.6	13.1 ± 4.5
Sr	4879 ± 146	3212 ± 197	5398 ± 271	2329 ± 150	6866 ± 314
Y	1193 ± 40	1177 ± 78	1122 ± 54	925 ± 45	1127 ± 38
Zr	159 ± 30	153 ± 17	177 ± 33	144 ± 17	134 ± 24
Nb	5471 ± 259	3854 ± 250	5541 ± 357	1801 ± 122	5983 ± 307
Mo	646 ± 25	426 ± 39	297 ± 26	250 ± 32	401 ± 33
Ba	BDL	(1.74 ± 0.24)%	9388 ± 1990	(3.53 ± 0.50)%	(2.82 ± 0.17)%
Ce	(13.47 ± 0.72)%	(14.51 ± 0.67)%	(12.87 ± 0.42)%	(11.65 ± 0.67)%	(9.63 ± 0.38)%
Pb	3565 ± 94	2866 ± 147	4199 ± 135	1246 ± 52	1544 ± 47
Ac	394 ± 63	270 ± 39	401 ± 26	170 ± 45	154 ± 36
Th	1470 ± 80	1463 ± 110	1078 ± 45	836 ± 52	1250 ± 75

TABLE 11 (CONTD.)

ELEMENT	LABORATORY SAMPLE NUMBER				
	MH21	MH22	MH23	MH24	MH25
Ca	4679 ± 1118	1206 ± 145	3029 ± 779	3805 ± 776	3778 ± 1128
Ti	(4.85 ± 0.68)%	(5.26 ± 0.23)%	(7.01 ± 0.32)%	(6.64 ± 0.33)%	(7.79 ± 0.29)%
V	(1.60 ± 0.23)%	(2.59 ± 0.60)%	(3.84 ± 0.70)%	(3.54 ± 0.13)%	(4.05 ± 0.08)%
Mn	(10.47 ± 1.14)%	(5.19 ± 0.06)%	(7.05 ± 0.13)%	(7.05 ± 0.45)%	(1.91 ± 0.07)%
Fe	(22.43 ± 1.79)%	(15.39 ± 0.27)%	(15.83 ± 0.19)%	(26.09 ± 1.09)%	(10.01 ± 0.28)%
Ni	BDL	BDL	BDL	BDL	BDL
Cu	14.6 ± 6.3	25.9 ± 8.1	18.3 ± 8.0	20.4 ± 5.1	32.9 ± 10.4
Zn	2014 ± 187	1292 ± 50	1680 ± 83	1215 ± 78	956 ± 42
Ga	38.6 ± 6.4	19.8 ± 7.0	51.7 ± 14.2	23.9 ± 1.8	85.8 ± 18.2
Se	6.8 ± 3.0	19.1 ± 5.1	15.9 ± 4.5	20.8 ± 5.4	21.1 ± 8.7
Sr	5947 ± 372	3025 ± 102	4921 ± 203	1956 ± 181	6923 ± 233
Y	1238 ± 103	1362 ± 39	2031 ± 84	1409 ± 141	3781 ± 112
Zr	141 ± 37	94 ± 11	115 ± 31	145 ± 21	306 ± 28
Nb	4145 ± 263	2908 ± 112	1698 ± 83	2441 ± 302	7862 ± 454
Mo	453 ± 27	91 ± 12	70.4 ± 10.4	55.0 ± 7.0	30.8 ± 10
Ba	(3.19 ± 0.32)%	(5.18 ± 0.97)%	(2.77 ± 0.48)%	(4.56 ± 0.25)%	(4.68 ± 0.12)%
Ce	(9.49 ± 0.35)%	(11.36 ± 0.74)%	(16.10 ± 0.65)%	(15.62 ± 0.76)%	(18.32 ± 0.60)%
Pb	1026 ± 57	2018 ± 65	2381 ± 109	1566 ± 118	3526 ± 124
Ac	78.3 ± 23	144 ± 43	235 ± 46	207 ± 44	296 ± 53
Th	549 ± 25	1211 ± 53	816 ± 35	1464 ± 51	1206 ± 41

TABLE 11 (CONTD.)

ELEMENT	LABORATORY SAMPLE NUMBER				
	MH26	MH27	MH28	MH29	MH30
Ca	7638 ± 474	5401 ± 403	3147 ± 236	7612 ± 390	4020 ± 164
Ti	(4.81 ± 0.25)%	(4.57 ± 0.30)%	(4.12 ± 0.25)%	(6.41 ± 0.26)%	(2.69 ± 0.55)%
V	(1.48 ± 0.05)%	(1.06 ± 0.06)%	(1.02 ± 0.29)%	(1.55 ± 0.08)%	(1.28 ± 0.21)%
Mn	(2.20 ± 0.17)%	(4.15 ± 0.16)%	(5.23 ± 0.23)%	(5.44 ± 0.09)%	3556 ± 474
Fe	(19.94 ± 0.79)%	(26.41 ± 0.99)%	(24.91 ± 1.47)%	(24.27 ± 1.17)%	(19.66 ± 1.54)%
Ni	BDL	28.5 ± 9.1	BDL	BDL	13.9 ± 6.7
Cu	45.3 ± 16.0	37.0 ± 7.0	61.5 ± 12.5	56.5 ± 17.0	92.6 ± 15.0
Zn	2348 ± 81	3719 ± 96	2142 ± 40	2621 ± 44	1255 ± 58
Ga	220 ± 22	25.6 ± 3.7	19.5 ± 2.6	24.6 ± 7.1	36.4 ± 5.2
Se	19 ± 9	3.1 ± 2.2	3.5 ± 2.7	9.6 ± 3.3	3.5 ± 2.9
Sr	5721 ± 553	5733 ± 212	6427 ± 780	5040 ± 151	4641 ± 182
Y	1363 ± 109	741 ± 45	472 ± 66	1013 ± 20	1015 ± 45
Zr	599 ± 36	355 ± 31	139 ± 23	425 ± 36	720 ± 29
Nb	8339 ± 231	2782 ± 103	2375 ± 105	2666 ± 80	(2.24 ± 0.07)%
Mo	115 ± 14	277 ± 12	457 ± 25	285 ± 19	155 ± 11
Ba	2821 ± 664	(2.85 ± 0.35)%	(2.72 ± 0.99)%	(4.06 ± 0.16)%	(2.37 ± 0.13)%
Ce	(6.48 ± 0.43)%	(5.13 ± 0.29)%	(3.79 ± 0.32)%	(7.51 ± 0.78)%	(5.18 ± 0.69)%
Pb	9495 ± 333	1065 ± 50	1318 ± 148	1296 ± 96	1321 ± 88
Ac	825 ± 107	BDL	BDL	BDL	BDL
Th	457 ± 46	185 ± 28	97.8 ± 12.0	244 ± 14	437 ± 33

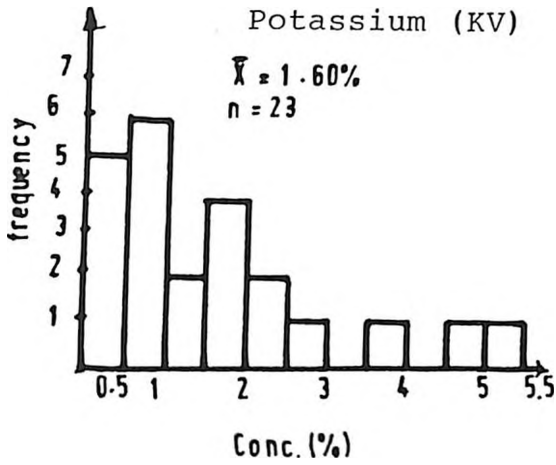


Fig.4.1. Frequency Histogram Distribution of Potassium in fluorite ore samples.

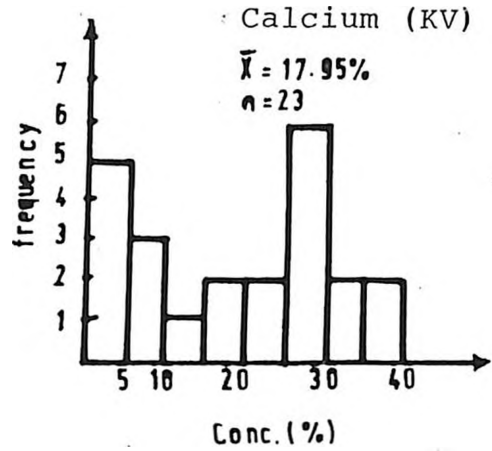


Fig.4.2. Frequency Histogram Distribution of Calcium in fluorite ore samples.

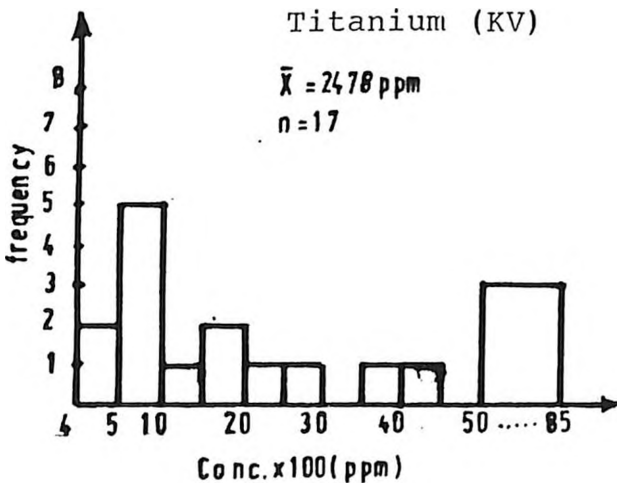


Fig.4.3. Frequency Histogram Distribution of Titanium in fluorite ore samples

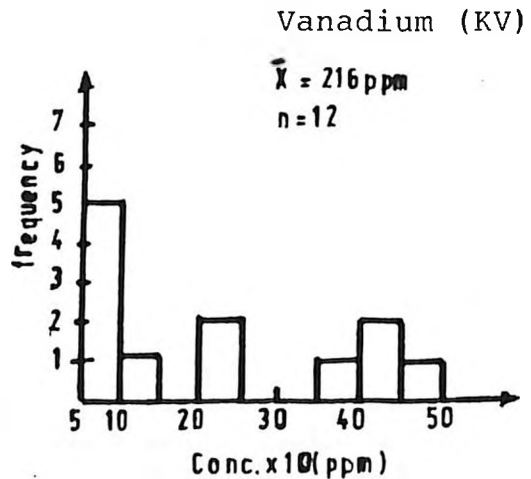


Fig.4.4. Frequency Histogram Distribution of Vanadium in fluorite ore samples

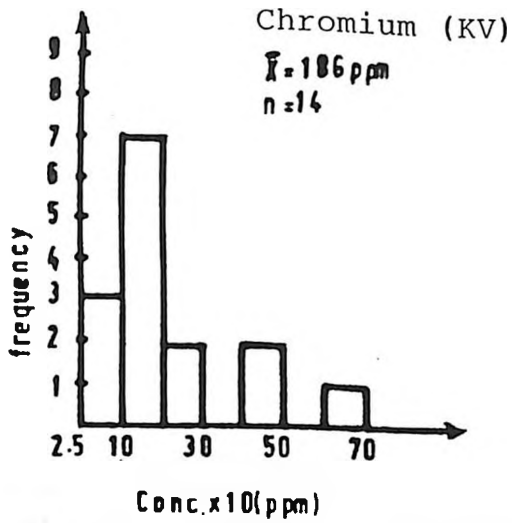


Fig.4.5. Frequency Histogram distribution of chromium in fluorite samples .

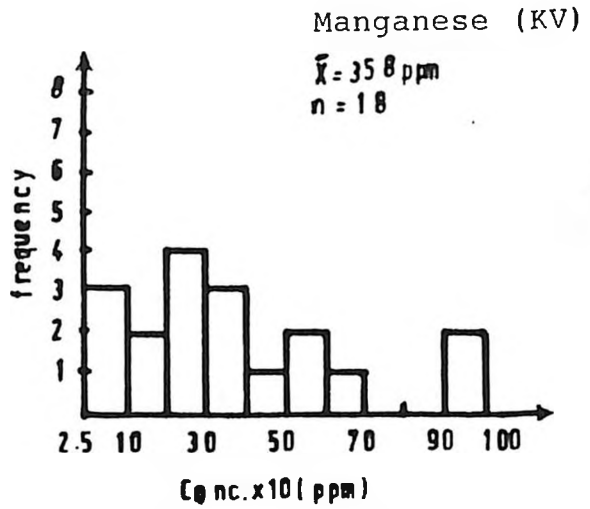


Fig.4.6. Frequency Histogram distribution of Manganese in fluorite samples

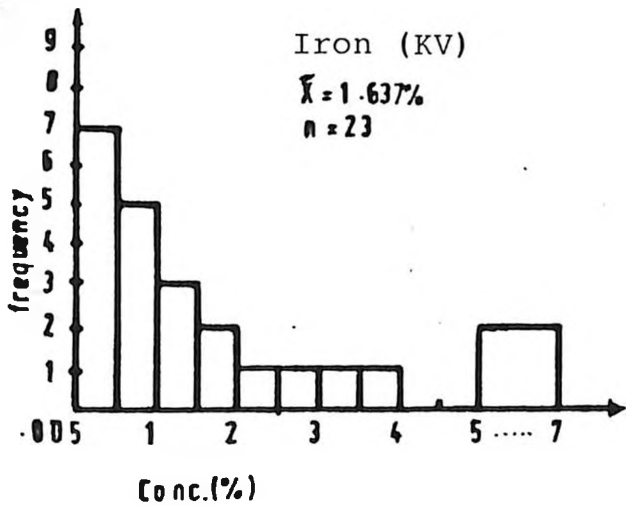


Fig.4.7. Frequency Histogram distribution of Iron in fluorite samples

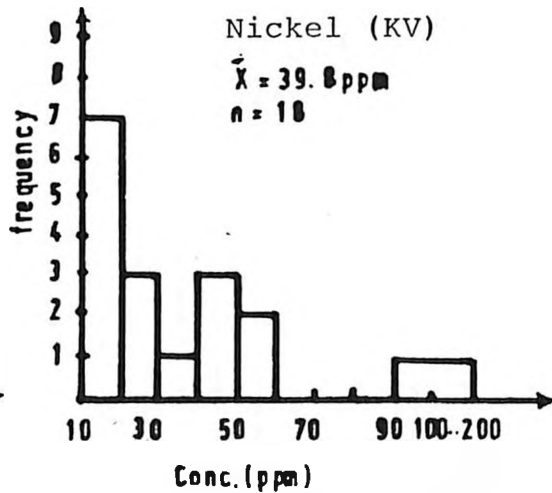


Fig.4.8. Frequency Histogram distribution of Nickel in fluorite samples.

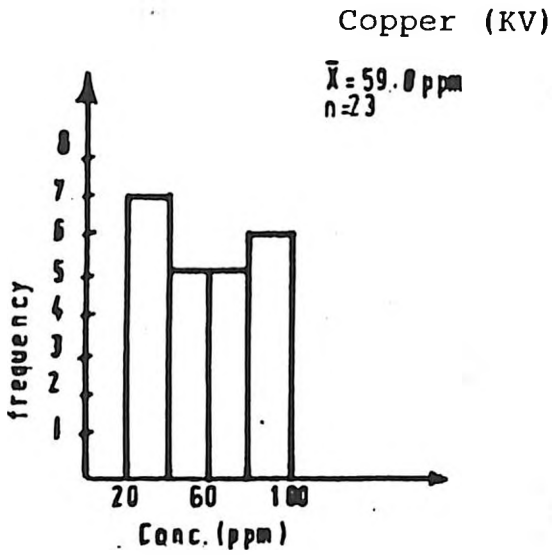


Fig.4.9. Frequency Histogram Distribution of Copper in fluorite samples.

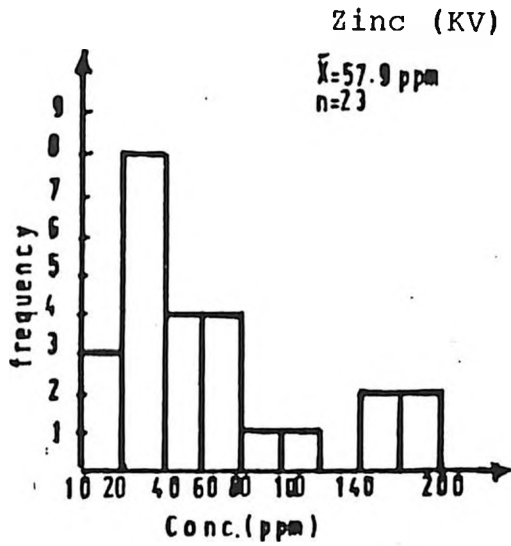


Fig.4.10. Frequency Histogram Distribution of Zinc in fluorite samples.

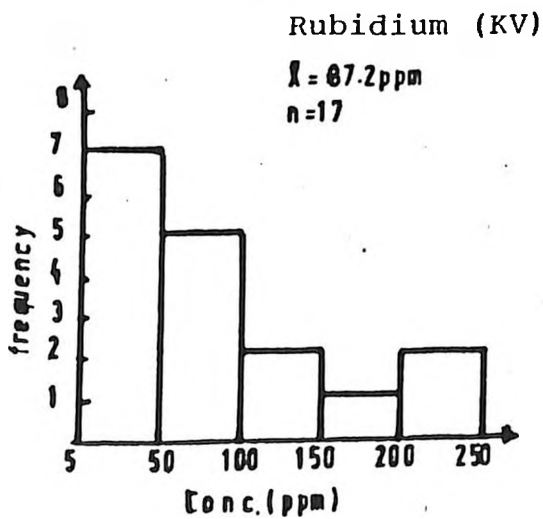


Fig.4.11. Frequency Histogram Distribution of Rubidium in fluorite samples

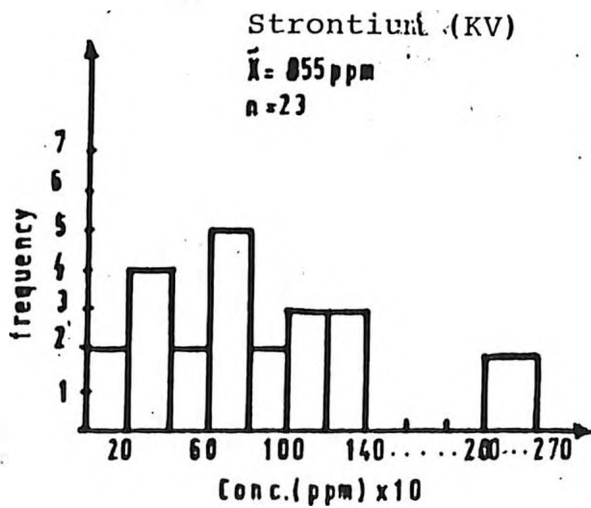


Fig.4.12. Frequency Distribution Histogram of strontium in fluorite samples.



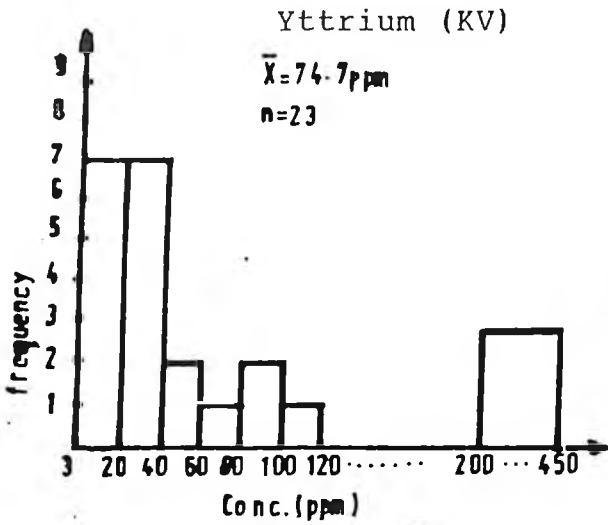


Fig.4.13. Frequency Histogram Distribution of Yttrium in fluorite samples

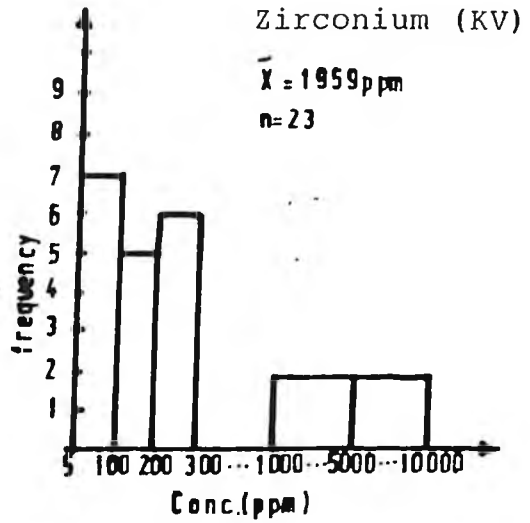


Fig.4.14. Frequency Histogram Distribution of Zirconium in fluorite samples.

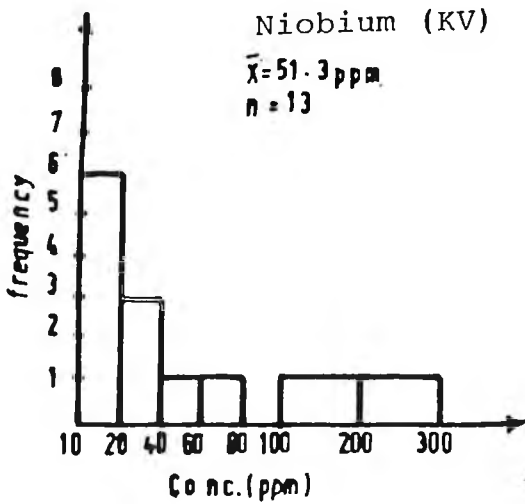


Fig.4.15. Frequency Histogram Distribution of Niobium in fluorite samples

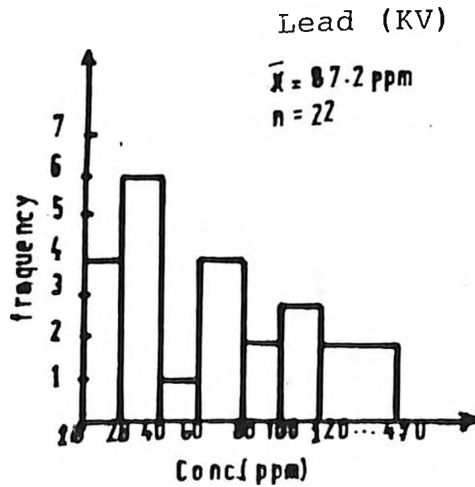


Fig.4.16. Frequency Histogram Distribution of Lead in fluorite samples.

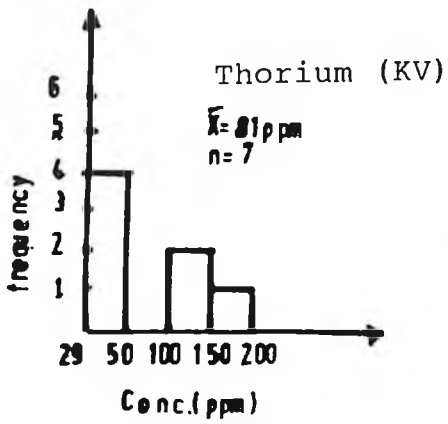


Fig.4.17. Frequency Histogram Distribution of Thorium in fluorite samples

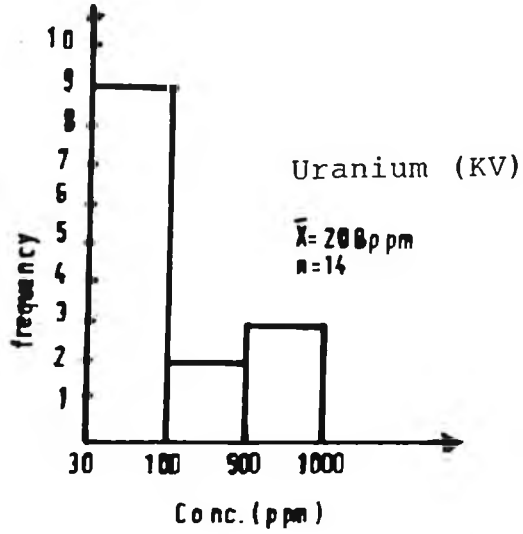


Fig.4.18. Frequency Histogram Distribution of Uranium in fluorite samples

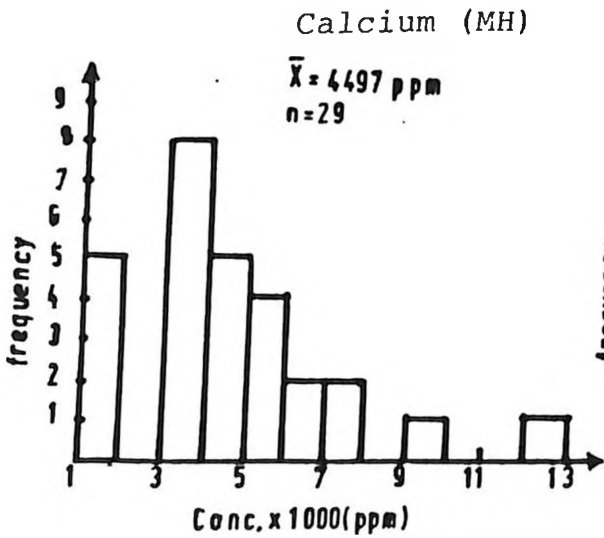


Fig.4.19. Frequency Histogram Distribution of Calcium in Mrima Hill soil samples

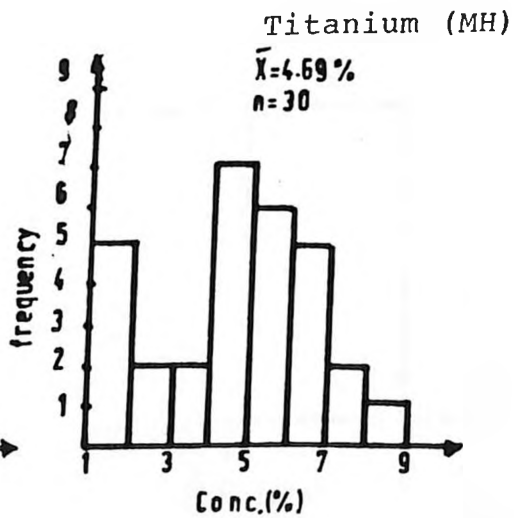


Fig.4.20. Frequency Histogram Distribution of Titanium in Mrima Hill soil samples

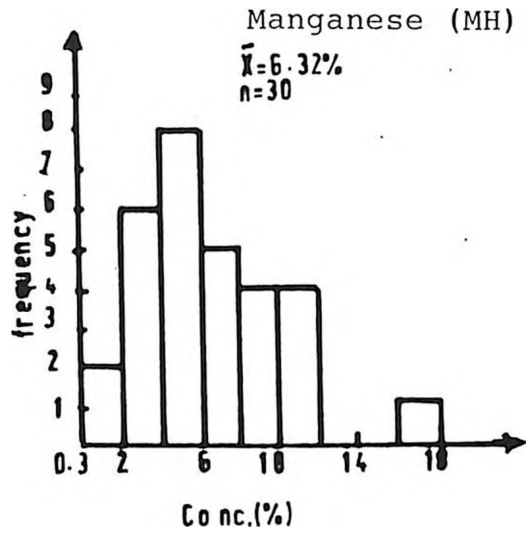
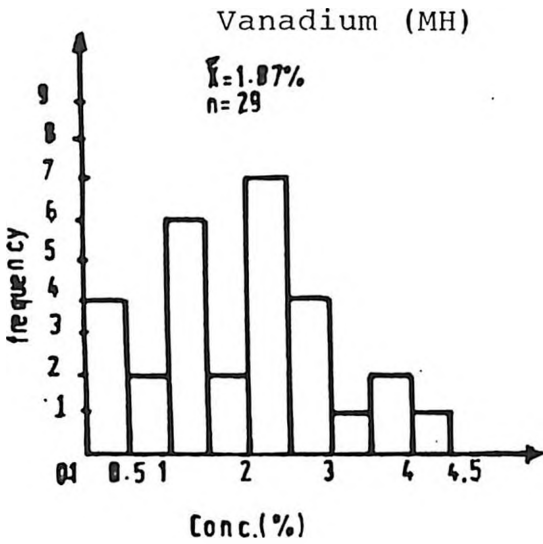


Fig.4.21. Frequency Histogram Distribution of Vanadium in Mrima Hill Soil samples

Fig.4.22. Frequency Histogram Distribution of Manganese in Mrima Hill soil samples.

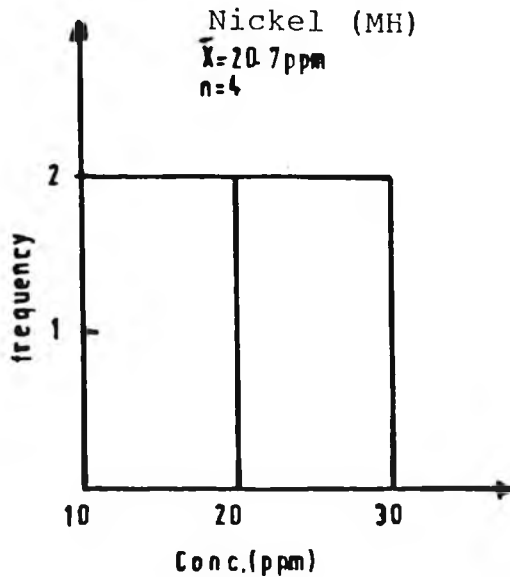
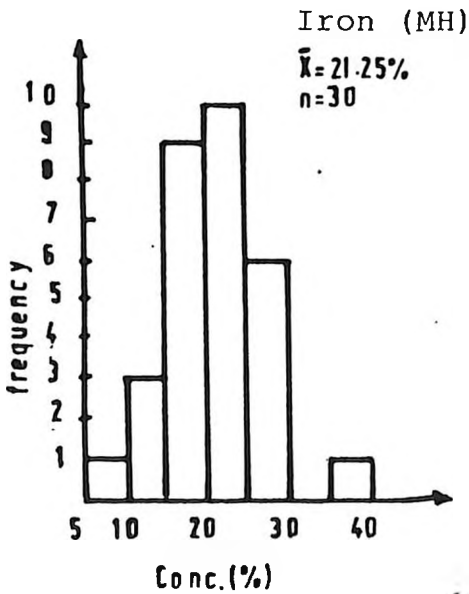


Fig.4.23. Frequency Histogram Distribution of Iron in Mrima Hill soil samples

Fig.4.24. Frequency Histogram Distribution of Nickel in Mrima Hill soil samples.

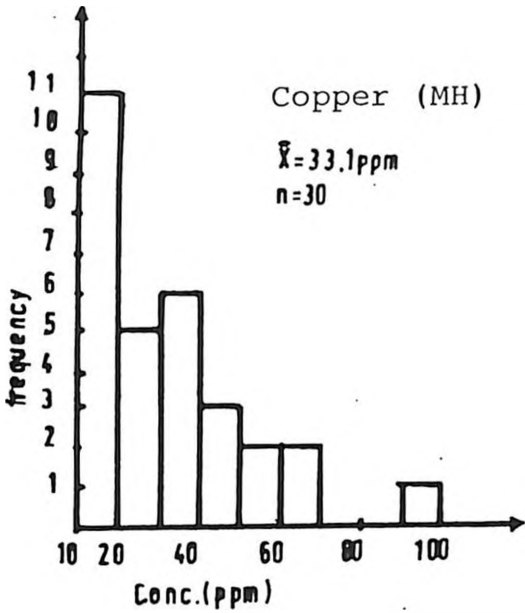


Fig.4.25. Frequency Histogram Distribution of copper in Mrima Hill Soil samples

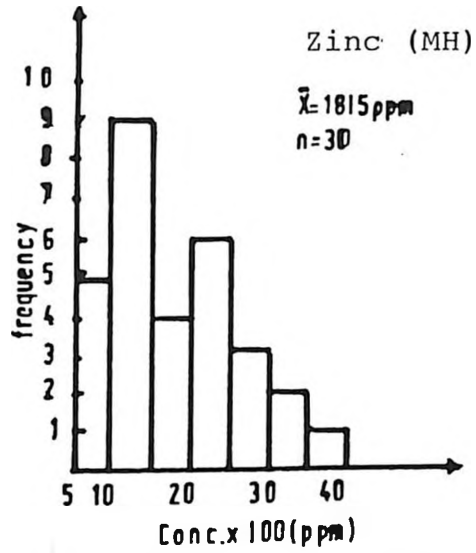


Fig.4.26. Frequency Histogram Distribution of Zinc in Mrima Hill soil samples.

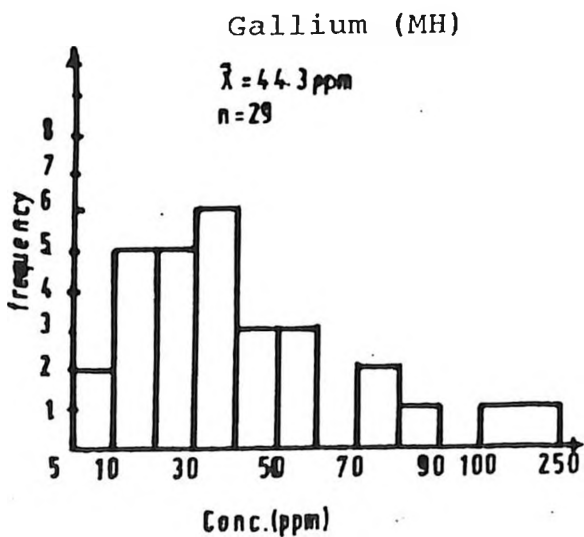


Fig.4.27. Frequency Histogram Distribution of Gallium in Mrima Hill soil samples

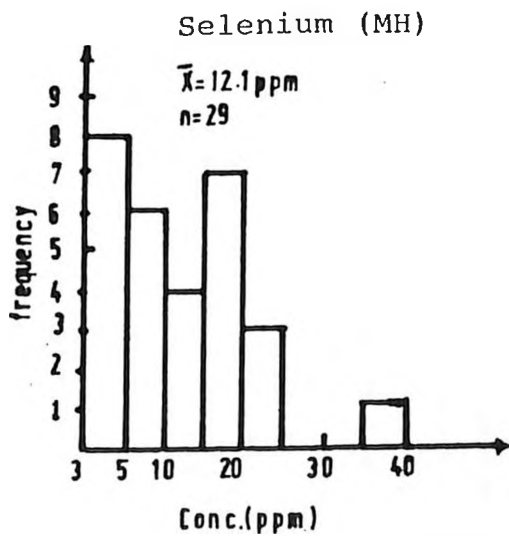


Fig.4.28. Frequency Histogram Distribution of selenium in Mrima Hill soil samples

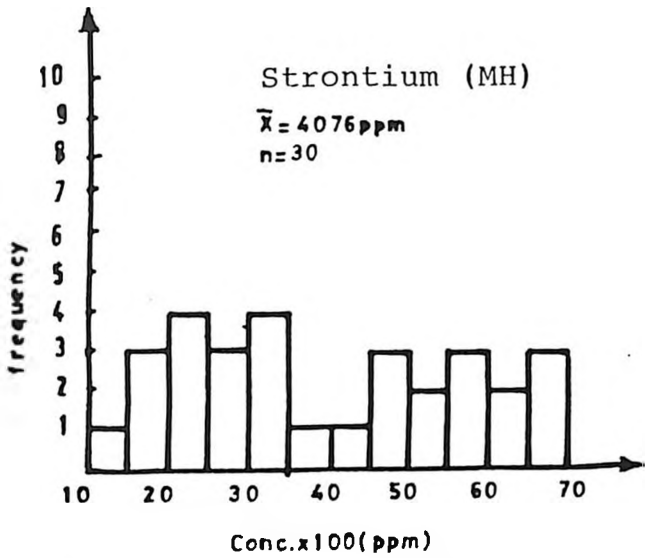


Fig. 4.29. Frequency Histogram Distribution of strontium in Mrima Hill soil samples

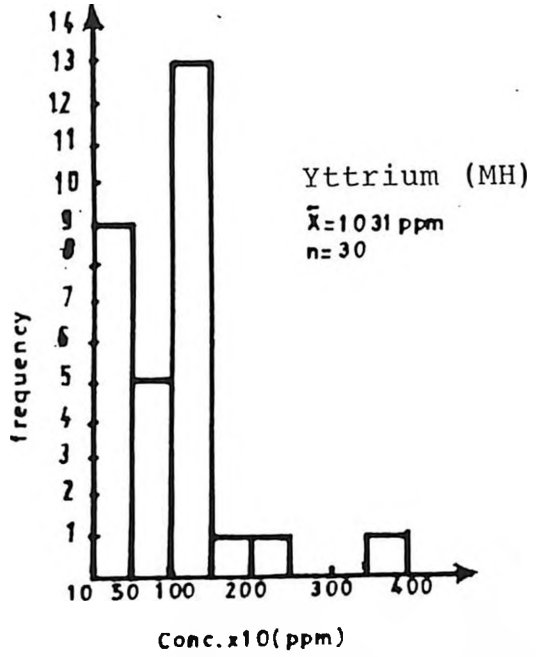


Fig. 4.30. Frequency Histogram Distribution of Yttrium in Mrima Hill soil samples.

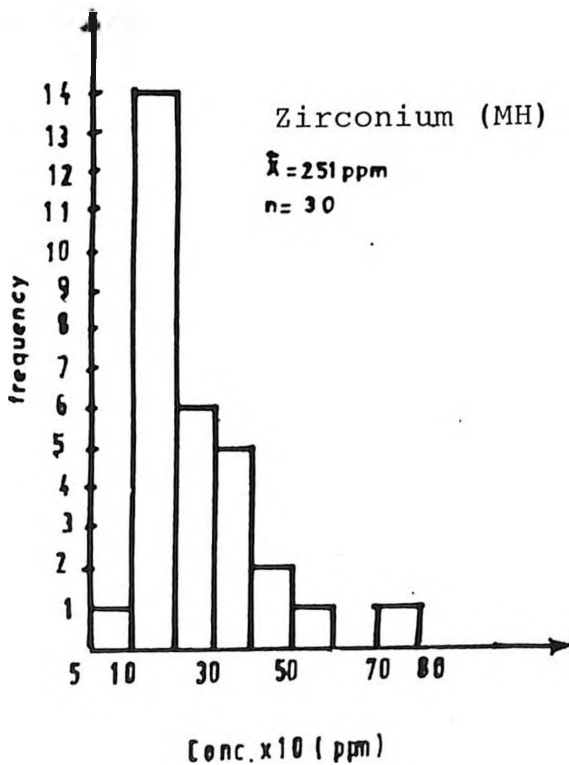


Fig. 4.31. Frequency Histogram Distribution of Zirconium in Mrima Hill soil samples

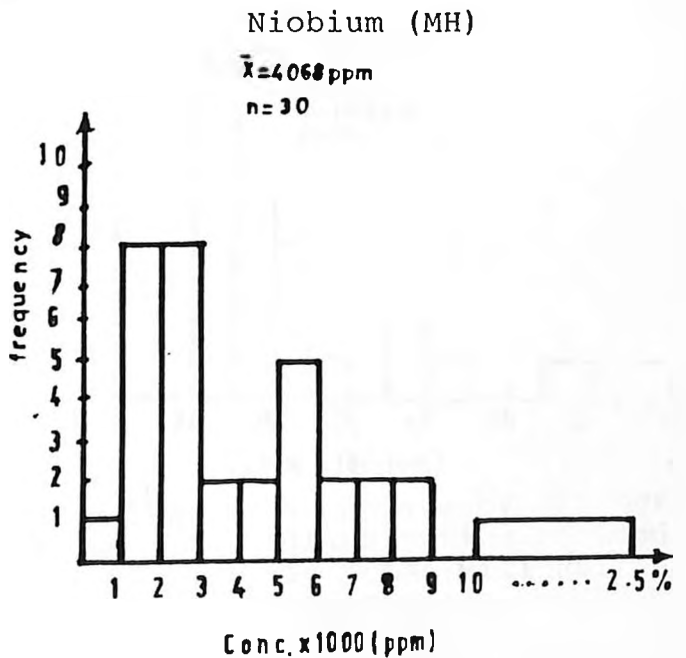


Fig. 4.32. Frequency Histogram Distribution of Niobium in Mrima Hill soil samples.

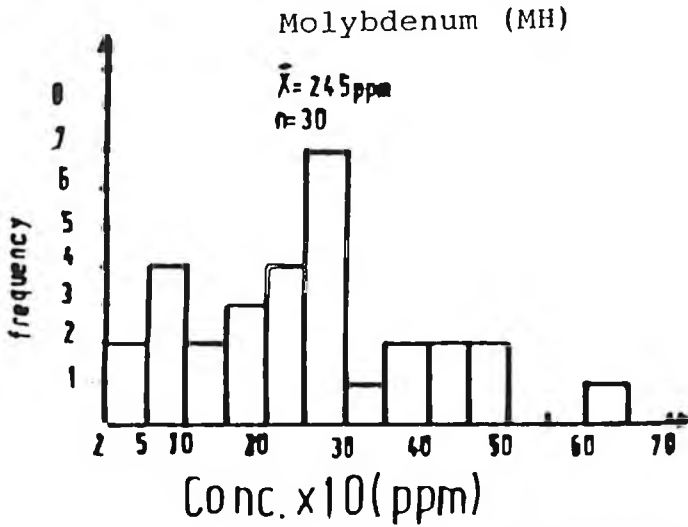


Fig. 4.33. Frequency Histogram Distribution of Molybdenum in Mrima Hill soil samples

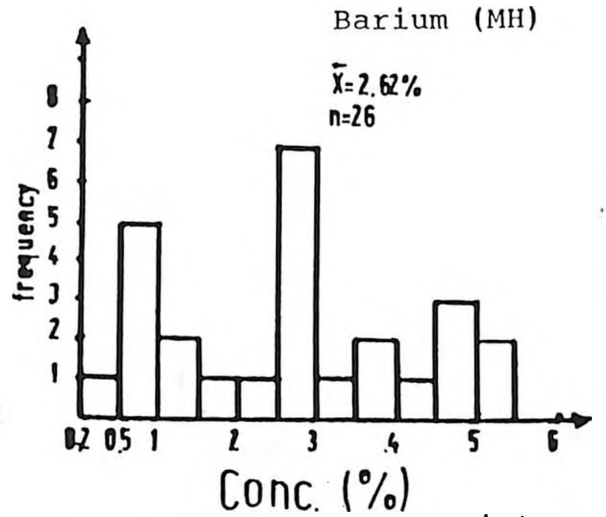


Fig. 4.34. Frequency Histogram Distribution of Barium in Mrima Hill soil samples

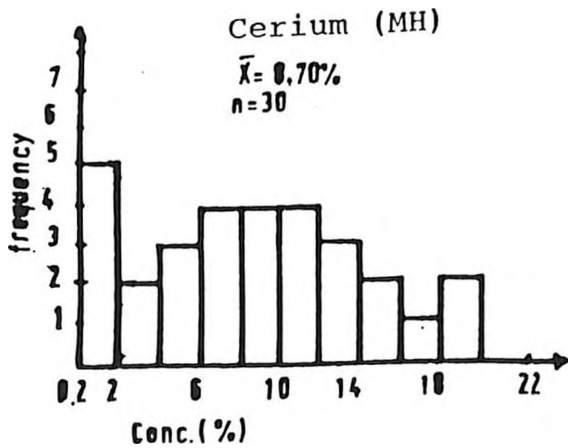


Fig. 4.35. Frequency Histogram Distribution of cerium in Mrima Hill soil samples

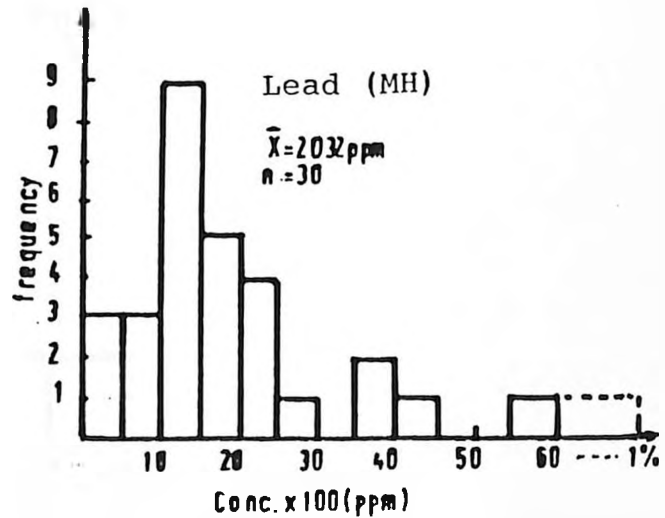


Fig. 4.36. Frequency Histogram Distribution of Lead in Mrima Hill soil samples

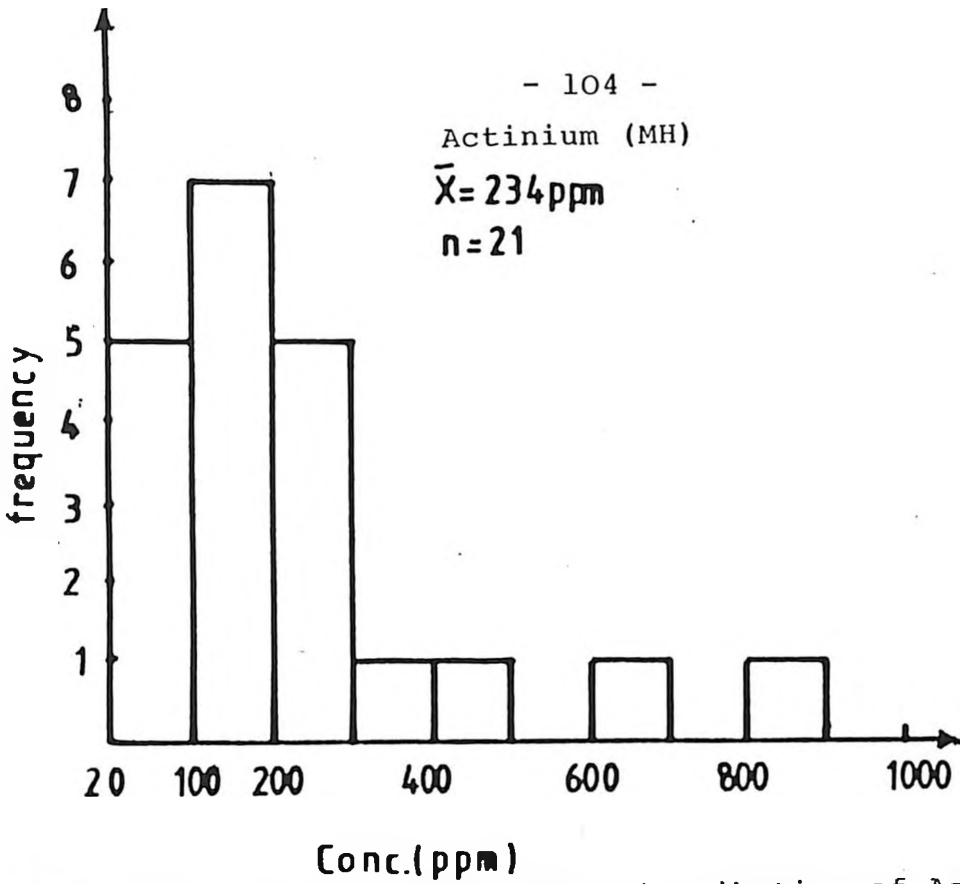


Fig.4.37. Frequency Histogram Distribution of Actinium in Mrima Hill soil samples.

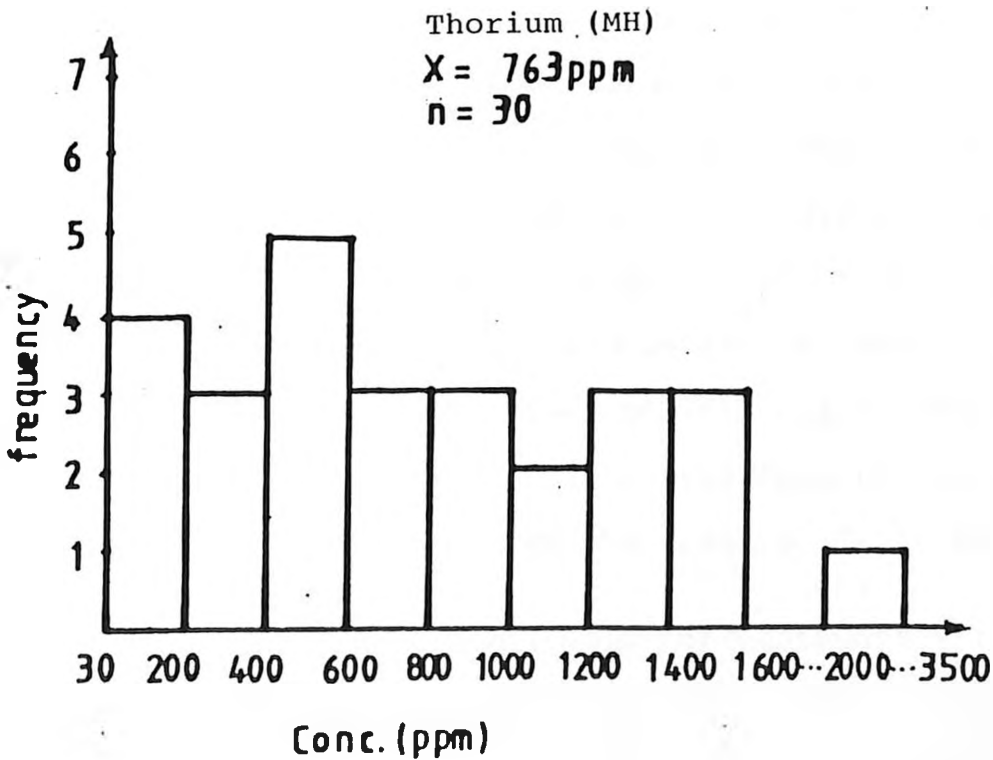


Fig.4.38. Frequency Histogram distribution of Thorium in Mrima Hill soil samples.

## CHAPTER FIVE

### 5.0. CONCLUSIONS:

#### General

This work has demonstrated the potential usefulness of quantitative EDXRF method in elemental analysis of geological samples. Other methods need the sample to be in solution form, thus making the analytical procedure long and more susceptible to possible contamination during preparations and are not multi-elemental. On the contrary, EDXRF method is multi-elemental.

However, the method is not free from errors and has limitations in its applications as earlier discussed.

#### 5.1. Results of Kerio Valley Samples

The presence of uranium has been established in various ore bodies in Kerio Valley fluorite samples within the concentration range of 34ppm to 983ppm. The amount of uranium in low grade uranium ore which could be exploitable is within the concentration range of 100ppm to 300ppm, [27]. However, the element is non uniformly distributed in the crystalline structure of the purple fluorite ore as shown from the results, Table 10, [28].

The area is favourable for sedimentary accumulation of uranium, as acidic volcanic rocks and sandstones are regarded the potential sources [29]. The presence of uranium investigated in the samples can be attributed



to the processes of reduction and oxidation given the previous volcanic activity of the area [30, 31]. The latter represents a state in which uranium exists as an oxide while in the former, the element is dissolved and possibly not found. The uranium bearing rocks could have been formed by crystallisation of magma in a two stage process. The early crystallisation of magma can be considered as responsible for the formation of iron, magnesium, chromium and calcium minerals, while the later stage for minerals containing sodium, potassium, silicon, uranium, copper and zinc. As the magma crystallises, there is removal of some of the elements mentioned in the first stage. It is possible that uranium may be concentrated in the silicious rocks present in the second phase and separated from the volcanics by the process of oxidation [31]. Uranium may not be associated with fluorine as both occur concurrently in this phase. The results of this work has shown that uranium is not linked to high grade fluorite ore. It is possible, that the reported uranium in the fluorite ores, is a result of transportation from the other areas within Kerio Valley not covered during the present survey.

Muruga [32] and Lavi [21] have reported higher concentration values of uranium contrary to the results presented in this survey, although they took samples from the same ore bodies. In Kamnaon ore body (Shimo La Bahati), concentration values on the average greater than 2000ppm

were reported by Muruga. Since no certified reference materials were analysed by him, the results cannot be possibly fully relied on.

Detailed work by the competent authorities need be undertaken in the entire Kerio Valley area to determine and establish any possible mineralisation, like uraninite, pitchblende or any of the uranium bearing minerals mentioned elsewhere in the literature [33]. The following are possible guide lines for further work:

- (i) This area is dissected by numerous streams, from which stream sediments and water samples could be obtained for geochemical analysis and correlations between uranium content and the conductivity of water to be established. This would enable uranium to be traced upstream towards a possible potential source. This method has been successfully applied in Sumatra and Thailand [33]. It offers the advantage over the radiometric measurements, since large areas can be monitored.
- (ii) Several elements associated with uranium can be used as path finders for uranium minerals exploration. Characteristic elements and important minerals in uranium deposits are comprehensively discussed in the proceedings of IAEA working group on Uranium Exploration [34].

## 5.2. Results of Mrima Hill Samples

The high radioactivity in this area is mainly due to thorium since it occurs in all the soil samples collected and analysed with a calculated mean of 763ppm. An attempt was made to deduce the presence of monazite mineral  $(\text{Ce, La, Th})\text{PO}_4$ , [35], in the Mrima Hill samples, since cerium and thorium were determined. However, it was not possible to establish the presence of phosphorus in these samples due to strong interference from zirconium L lines. Survey work by Binge et al. [6] have, however, positively identified the mineral in Mrima Hill area.

A need for detailed contour mapping of the radioactivity level in the area and its impact on the environment is worth future attention. Also further survey work should be undertaken to establish whether the occurrence of thorium can be of economic value.

The concentrations of such elements like cerium, barium, lead, niobium and iron in the samples is quite worth future attention of relevant authorities for possibilities of economic exploitation. Also of notable importance is the possible presence of rare earths elements like praseodymium, neodymium, samarium and dysprosium. A qualitative analysis of the samples indicated the presence of these elements, in low concentrations. Quantitative analysis for these elements with the Cadmium 109 source is possible only by the use

of  $L_{\alpha}$  lines. The characteristic emission lines of these elements interfere with low Z elements lines like vanadium, manganese and iron. It was practically impossible to quantitatively determine these elements in the presence of high concentrations of the above mentioned elements.

However, the previous survey work in the area (Binge et al. 1966) has quantified these elements. Their work involved the analysis of core drilled samples at various depths.

REFERENCES

1. Ron Jenkins, R.W. Gould, Dale Gedcke, " Quantitative X-ray Spectrometry", Marcel Decker Inc., (1981) pp 161-203
2. Woldseth, R.: X-ray Energy Spectroscopy, Kevex Corporation (1973)
3. Aljabri, S.S : " Some notes on the geology of fluorite mineralisation in Kerio Valley", Kenya Fluorspar Company, Unpublished, (1986)
4. Unesco, Report of the First Unesco Regional Training Programme in Mining geology, 16th Sep-14th Nov 1981, David Haworth and Nayan Bhatt, publication consultants, (1983) pp4-26
5. Nyambok, I.O. Gachiri, S.J. Geology of the fluorite Deposits in Kerio Valley, Kenya, Economic Geology Vol. 70, 1975, pp 299-307.
6. Binge, F.W. and Joubert, P. "The Mrima Hill Niobium Deposit, Coast Province, Kenya", Ministry of Natural Resources, Mines and Geological Department (1966), pp2-51.
7. Caswell, P.V. "Geology of the Mombasa-Kwale area Report No. 24", Geol. Survey, Kenya (1953).
8. Dziunikowaski, B. 'Energy Dispersive X-ray Fluorescence Analysis,' Institute of Physics and Nuclear Techniques

- Technical University of Mining and Metallurgy  
Cracow, Poland (1984), pp19-261.

9. Tertian, R. and Claisse, 'Principles of Quantitative X-ray Fluorescence Analysis', Heyden and Son Ltd (1982).
10. Storm, E. and Israel, H.I., 'Nuclear data Tables A7,' (1970)
11. Sparks, C.J. 'X-ray Fluorescence Analysis', Oak Ridge National Laboratory Report, ORNL-37830 (1982).
12. Muriithi, A.K. 'Multi-element Analysis of Solid and Liquid samples by X-ray Fluorescence Analysis', M.Sc. unpublished, U.O.N. (1982).
13. Bertin, P.E. 'Principles and Practice of X-ray Spectrometric Analysis', Plenum Press, New York (1975) pp529-545.
14. Herglotz and Birks 'X-ray Spectrometry', Practical Spectrometry Series Vol.2, Marcel Decker Inc (1978) pp241-276
15. Sparks, C.J. 'Rapid Quantitative X-ray Fluorescence using Fundamental Parameter method', Advances

in X-ray Analysis' Gould, R.W. et al Ed.  
Plenum Press N.Y. 19 (1975).

16. Giaugue, R.D. et al 'Determination of trace elements in light element matrices by X-ray fluorescence spectrometry with incoherent scattered radiation as an internal standard', Anal Chem, April '79, pp511-516.
17. Knoll, G.F. 'Radiation Detection and Measurements', John Wiley and Sons. N.Y. (1979) pp 235-351
18. Valkovic, V. 'Sample Preparation Techniques in trace element Analysis by X-ray Emission Spectrometry', IAEA TECDOC 300, Institute Ruder Boskovic Zagreb, Croatia, Yugoslavia (1983) pp112
19. Espen, P. Van and Adams, F., 'Calibration of Tube Excited Energy Dispersive X-ray Spectrometers with thin Film Standards and with Fundamental Constants', X-ray Spectrometry, Vol. 10, No.2., 1981 pp64-68.
20. Cohen, D.D. 'A radially dependent photopeak efficiency model for Si (Li) detectors'

Nuclear Instruments and Methods 178 (1980)  
pp481-490.

21. Lavi, M.M. 'A practical approach to Quantitative Analysis in X-ray fluorescence Analysis'  
M.Sc. thesis unpublished U.O.N. (1984)
22. Selby, S.M. Ed: 'Standard Mathematical Tables,  
14th Edition', Chemical Rubber Company  
(1985), pp269.
23. BS 5497: Part 1: 1979, 'Precision of test methods',  
British Standards Institution (1979).
24. Holynska, B. 'Personal Communication, IAEA Expert,  
Centre for Nuclear Science Techniques,  
U.O.N. (1987).
25. Fabbi, B.P. 'X-ray fluorescence analysis of Geological  
samples', X-ray spectrometry Vol.2, Ed.  
Herglotz and Birks, Marcel Decker (1978)  
pp297-353.
26. Jones, G.M. 'Kenya Fluorspar', Mining Magazine,  
December 1982 pp536-543.



UNIVERSITY OF NAIROBI  
LIBRARY

27. Choppin, G.R. and Rydberg, J. Eds: " Theory and Application of Nuclear Chemistry ", Pergamon Press (1985) pp235-236.
28. Staatz, M.H and Osterwald, F.W. " Uranium in the fluospar Deposits of Thomas range, Utah, U.S.A ", IAEA proceedings, Sept 1985, Vol.5, pp275-278.
29. Hambleton-Jones and Toens P.D. " Alkaline rocks and the occurrence of Uranium ", unpublished paper submitted to the International Geological congress, Paris: July 1980.
30. Bohse et al. " On the behaviour of Uranium during Crystallisation of magmas- with special emphasis on alkaline magmas ", IAEA preceedings of a Symposium on Formation of Uranium Ore Deposits , 6-10th May 1974, pp 49-60.
31. Sinabantu, S. " Personal communication , Department of Geology, University of Makerere", (1987).
32. Muruga, Kabaruu. " Report on Radiometric survey in Kerio Valley at the Kenya Fluospar Company,

19th-26th March 1981', Mines and Geological Department - internal report.

33. Hahn, L. 'Techniques of Uranium Exploration in Tropical rain Forests as applied in Sumatra and other Tropical areas', Uranium Exploration in Wet Tropical Environments IAEA proceedings of an advisory Group meeting Vienna, 16-19 November 1981, pp1-13.
34. IAEA, 'Working Group Reports on Uranium Exploration in Wet Tropical Environments' - Proceedings of an advisory Group meeting Vienna, 16-19th November 1981, pp137-159.
35. Deer, W.A., Howie, R.A., & Zussman, S., 'An Introduction to the Rock Forming Minerals', Longman Group Ltd. (1966) pp510-513.